Optical studies of GaAs:C grown at low temperature and of localized vibrations in normal GaAs:C

by

Sathon Vijarnwannaluk

Dissertation submitted to the Faculty of the Virginia Polytechnic Institute and State University in partial fulfillment of the requirements for the degree of

DOCTOR OF PHILOSOPHY

In

PHYSICS

R. Zallen, Chairman

M. Di Ventra

J. R. Heflin

G. Indebetouw

A. L. Ritter

April 25, 2002

Blacksburg, Virginia

Keywords: gallium arsenide, GaAs, GaAs:C, LT-GaAs, carbon-doped, infrared, Raman, photoluminescence, localized vibrational mode.

Optical studies of GaAs:C grown at low temperature

and of localized vibrations in normal GaAs:C

by

Sathon Vijarnwannluk

Abstract

Optical studies of heavily-doped GaAs:C grown at low temperature by molecular beam epitaxy (LT-GaAs:C) were performed using room-temperature photoluminescence, infrared transmission, and Raman scattering measurements. Infrared transmittance experiments were used to investigate the absorption band corresponding to the localized vibrational mode (LVM) of substitutional carbon (C_{As}, a carbon atom occupying an arsenic site) in LT-GaAs:C. The integrated absorption of the LVM band shows a linear increase with increasing growth temperature in the range 200-300 C and reveals that only a fraction of the carbons occupy arsenic sites. Hall effect, Raman, and photoluminescence measurements carried out as a function of growth temperature T_{growth} reveal a crossover from LT-GaAs:C behavior (highly resistive, nonluminescent) to normal GaAs:C behavior (p-type conducting, luminescent) at a T_{growth} of about 370 C. For T_{growth} of 400 C and higher, most of the carbon atoms occupy arsenic sites and are activated as acceptors. In photoluminescence, this is seen by the appearance (above the crossover T_{growth}) of bandgap luminescence with lineshape consistent with a deep distribution of valenceband holes. In Raman scattering, the crossover is seen by the replacement of the longitudinal-optical (LO) phonon line by the coupled phonon-plasmon line associated with the free-hole plasmon. Thus the special properties characteristic of LT-GaAs:C require T_{growth} lower than 400 C. Within this low-T_{growth} range, extrapolation to zero of the strength of

the LVM infrared band suggests that no carbons occupy arsenic sites for T_{growth} lower that 150 C. with decreasing T_{growth} the linewidth of the LVM band increases, reflecting increased disorder.

LT-GaAs is known to contain arsenic-antisite defects, arsenic atoms sitting at sites where galliums should be (As_{Ga}). These defects are largely responsible for the nonradiative recombination processes which quench photoluminescence in LT-GaAs. Detailed Raman measurements were carried on an undoped LT-GaAs film grown at 240 C. The small shift of the LO phonon line was analyzed to yield an estimate of $2\times10^{20}cm^{-3}$ for the concentration of As_{Ga} antisite defects.

The LO Raman line in LT-GaAs:C was studied as a function of the growth temperature and the total carbon concentration [C]. As T_{growth} decreases, the LO line broadens, becomes weaker and asymmetric, and its peak position shifts upward. The shift in position and the lineshape asymmetry are strongly correlated, suggesting a disorder mechanism. As [C] increases, the LO line similarly shifts upward, become asymmetric, and weakens. These effects correlate with ([C]-[C_{As}]), where [C_{As}] is estimated from the LVM infrared absorption, and are attributed to the disorder associated with the presence of interstitial carbon.

One LT-GaAs:C sample was air-annealed at 600 C and then investigated by Raman, infrared, and photoluminescence. The Raman spectrum revealed the presence of a thin film of crystalline arsenic. Although bandgap luminescence was absent, indicating that the LT-GaAs:C maintained its LT characteristics, infrared reflectivity revealed a shallow plasmon dip suggesting that a very thin near-surface layer of normal GaAs:C had formed.

Infrared transmission and photoluminescence measurements were also carried out on heavily-doped GaAs:C films grown by molecular beam epitaxy at the standard 600 C temperature. The infrared results reveal, for dopings under 5×10^{19} cm^{-3}, a linear relation between doping concentration and the integrated optical absorption of the carbon LVM band. At higher dopings, the LVM integrated absorption saturates. Formation of C_{As}-C_{As} clusters is proposed as the mechanism of the saturation. The photoluminescence spectra were successfully analyzed with a simple model assuming thermalization of photoelectrons to the bottom of the conduction band and indirect-transition recombination with holes populating the degenerately doped valence band. The analysis yields the bandgap reduction and the Fermi-level-depth increase at high doping.

For Kai

Acknowledgements

I would like to express my sincere gratitude to Professor Richard Zallen. His guidance and encouragement helped me gain confidence in my work. Without his help, this work could not have been accomplished. I have learned a lot from him including physics, English, and perspective on life.

I would like to thank the committee members for their time, support, and valuable suggestions for this dissertation.

I would like to thank the following people for their contribution to this dissertation: Dr. W. K. (Amy) Liu for the GaAs:C and LT-GaAs:C samples, valuable information, and suggestions; Prof. Mark Holtz and Dr. Moon Suk Seon of Texas Tech for useful discussions of GaAs:C and its Raman spectra; Ming-Liang Hsieh of Imperial College, London and Chris Froud of Renishaw corporation for photoluminescence measurements; Dr. Wantana Songprakob and Dr. Jing Ling for their contribution in data acquisition and for many useful discussions.

I would also like to thank Christa Thomas and Diane Walker Green for all their support and encouragement; also I would like to thank the faculty and staff of the Physics Department, Virginia Tech, for their support.

Finally, I would like to thank the Royal Thai government for their financial support, and my family and friends for their endless support and understanding.

Contents

List of Tables

List of Figures

Chapter 1. General overview

1.1 Introduction

For decades, gallium arsenide has been the topic of intense scientific studies. This is largely because it is a direct-bandgap semiconductor and is thus an efficient photoemitter and photodetector [1]. With different dopant impurities, GaAs can be n-type or p-type with a wide range of extrinsic carrier concentrations. There are several techniques to obtain the doping concentration in GaAs. Hall-effect measurements give the total free-carrier concentration, which may approximate the doping concentration. Secondary ion mass spectrometry gives the total impurity concentration of an impurity species in the semiconductor, whether or not the impurity atoms substitute for host atoms as desired (and so act as donors or acceptors), or the impurity atoms sit instead at interstitial sites (and are electrically inactive). Optical measurements provide a nondestructive way of measuring the optical absorption associated with impurity atoms at substitutional sites. By determining the strength of the absorption line for samples with known substitutional impurity concentrations, the optical-absorption/impurity-concentration conversion factor can be determined. Once this conversion factor is known, it can be used to find the substitutional impurity concentration of other samples from optical absorption measurements. Details of this optical probe of impurity concentration are discussed later in chapter 2

Photoluminescence and Raman-scattering experiments are also widely used to study the optical, electronic, and structural properties of semiconductors. From photoluminescence spectra, one can extract the bandgap energy and the Fermi level, as will be described in a later chapter. Raman measurements yield structural information

and can detect the presence or absence of charge carriers. Infrared, Raman scattering, and photoluminescence techniques are used in this dissertation to investigate GaAs materials that are highly doped with carbon (GaAs:C).

In one focus of this dissertation, infrared transmission measurements were used to study the localized-vibrational-mode (LVM) infrared absorption band associated with the carbon impurity in GaAs:C. Carbon substitutes for arsenic in GaAs:C, forming a C_{As} acceptor. The appropriate conversion factors for going from optical absorption to C_{As} concentration, $[C_{As}]$ was studied at much higher concentrations than previously reported. At very high $[C_{As}]$, the LVM absorption strength was found to saturate

The same set of heavily doped GaAs:C samples were also investigated by photoluminescence experiments to determine the effect of high carbon concentration on the band gap emission. The photoluminescence spectra were analyzed with a simple model assuming indirect transitions between thermalized band-edge conductionband electrons and the deep distribution of valenceband holes in these highly p-type materials. The fitting results yield the bandgap reduction as the carbon-doping concentration increases, and also yield the increasing Fermi-level depth as a function of doping concentration.

The GaAs samples studied in this dissertation were carbon-doped thin films prepared by molecular beam epitaxy (MBE). MBE grown GaAs films are usually deposited on a GaAs substrate kept at 600 C; at this deposition temperature, high-quality single-crystal films are formed. MBE-grown carbon-doped GaAs films grown in this standard way will be referred to in this dissertation as normal GaAs:C or standard GaAs, simply, as GaAs:C. In addition to highly doped GaAs:C, another form of GaAs was

intensively studied in this dissertation. In 1988 it was discovered that if GaAs is grown at a much lower-than-normal substrate temperature (about 250 C), a very different material is formed [2]. It is not a high-quality crystalline semiconductor but is instead filled with defects and is highly insulating. This low-temperature-grown MBE GaAs is now referred to in the literature as LT-GaAs. In spite of its defective character, LT-GaAs has some unusual properties which make it interesting for a special role in certain applications. Infrared, Raman, and photoluminescence investigations of LT-GaAs films are reported in this dissertation. A brief review of the similarities and differences between standard GaAs and LT-GaAs is given in the next section.

1.2 Characteristics of crystalline GaAs

Table 1-1 lists some of the main structural and semiconductor properties of GaAs. The values listed are room-temperature values. Some of the entries provide the reasons that GaAs is used in place of silicon in certain special applications. These include the direct gap (conductionband and valenceband edges at k = 0), the low intrinsic carrier concentration (10^4 times lower than for Si [3]), and the high electron mobility.

GaAs is opaque to visible light, with an optical penetration depth ($d_{opt} = 1/\alpha$ where α is the absorption coefficient) of about 80 nm for light of photon energy 2.54 eV (wavelength 488 nm, corresponding to the blue line of the argon laser). But as wavelength increases, GaAs becomes more and more transparent. At 1.97 eV (630 nm), the optical penetration depth increases to 2500 nm [4]. In the infrared region, GaAs becomes transparent with a refractive index of 3.317. The small penetration depth in the visible region means that Raman scattering with incident light in the visible is an excellent tool to study the near-surface regions of thin films.

Reflection and transmission measurements of infrared light provide another way to study the optical properties of GaAs films. The zone center (k=0) transverse optical (TO) phonon and longitudinal optical (LO) phonon of GaAs are at 268.2 cm^{-1} and 291.5 cm^{-1} respectively [5]. Between these two far-infrared frequencies, the reflectivity is nearly 100%. The TO and LO modes also produce sharp features in the Raman spectrum. In the infrared, the presence of impurity atoms in GaAs can give rise to an absorption band not present in undoped GaAs. Because carbon is lighter than both Ga and As, it gives rise to a localized vibrational mode (LVM) in GaAs:C with a vibrational frequency higher than the LO frequency. The LVM infrared band is discussed further in the next chapter.

1.3 Characteristics of LT-GaAs

LT-GaAs is the widely used abbreviation for GaAs prepared in film form by a variation of molecular beam epitaxy in which the atomic species are deposited on a GaAs substrate kept at a temperature (250 C is typical) much lower than that used (600C) for growing high-quality films. Although LT-GaAs films are of low quality in comparison to standard MBE-grown semiconductor films, the fact that they are rich in defects give them unusual properties which are interesting and also turn out to be technologically valuable.

Table 1-2 compares some of the properties of LT-GaAs with the corresponding properties of standard MBE GaAs. LT-GaAs is crystalline but appreciably off stoichiometry, containing about 1% excess arsenic. The excess arsenic is present in the form of arsenic antisite defects. An arsenic antisite defect (written as As_{Ga})is an arsenic atom located at a host-crystal site at which a gallium atom should be. LT-GaAs is highly resistive, has a higher breakdown field than normal GaAs, and (because of its high trap

density) has an extremely short lifetime for photogenerated charge carriers. The short photo carrier lifetime (as low as 150 femtoseconds [6]) makes LT-GaAs attractive for ultrafast photodetection. It is also useful as a buffer layer for eliminating backgating in GaAs-based metal semiconductor field effect transistors.

In this dissertation, I have carried out extensive optical studies of carbon-doped LT-GaAs, written as LT-GaAs:C. Table 1-3 presents a comparison of some properties of LT-GaAs:C with the corresponding properties of carbon-doped standard-MBE GaAs (GaAs:C). Many of the entries in this table are based on the experimental results reported in this dissertation. These will be discussed in detail in later chapter, but the last row of the table can be briefly mentioned here. Optical studies carried out for a series of films deposited at different substrate temperatures have revealed a narrow T_{growth} range over which the film properties change from LT-GaAs:C properties to those of normal GaAs:C.

1.4 Outline of this Dissertation

Following this overview chapter, this dissertation is divided in to nine additational chapters. Chapter 2 contains a discussion of the optical techniques used in the experimental work reported here. These are infrared transmission measurements on thin-film-on-substrate samples, and Raman-scattering measurements and photoluminescence measurements. This chapter also provides some background about the localized-vibrational–mode (LVM) infrared absorption of carbon in GaAs. Chapter 3 contains a description of the GaAs:C and LT-GaAs:C samples, which are provided by W. K.(Amy) Liu of IQE incorporated. Chapter 4, presents the results of the infrared studies on the carbon-impurity LVM band in GaAs:C, while chapter 5 presents the corresponding results for LT-GaAs:C. Raman-scattering studies of the undoped LT-GaAs and their

interpretation to yield an estimate of arsenic-antisite concentration are described in chapter 6. Raman studies of LT-GaAs:C, carried out as a function of both carbon concentration and growth temperature, are reported in chapter 7.The photoluminescence investigations of both GaAs:C and LT-GaAs:C are described in chapter 8, which contains the result for the growth-temperature cross over from LT-to normal-GaAs:C behavior. Optical studies of annealed LT-GaAs:C are described in chapter 9. Suggestions for further studies are given in chapter 10.

A simplified view of the organization of the main parts of the dissertation, given in terms of optical techniques used and materials investigated, is shown in Table 1-4.

References

1. M.W. Holtz, Ph.D. Dissertation, Physics Department, Virginia Tech ,1987.
2. F. W. Smith, A. R. Calawa, C. L. Chen, M. J. Manfra, L. J. Mahoney, IEEE Electron Dev. Lett. **9**, 77 (1988).
3. Ghandhi, S.K., *VLSI Fabrication Principles Silicon and Gallium Arsenide* (Wiley, New York, 1994), p.59.
4. D. E. Aspnes and A.A. Studna, Phys. Rev. B **27**, 985 (1983).
5. P. Y. Yu and M. Cardona, *Fundamentals of Semiconductors* (Springer-Verleg, Berlin Heidelberg, 1996), p.290.
6. Frank W. Smith, Mater. Res. Soc. Symp. Proc. **241**, 3 (1992)
7. J. S. Blakemore, J. Appl. Phys. **53**, R123 (1982).
8. W. K. Liu, D. I. Lubyshev, P. Specht, R. Zhao, E. R. Weber, J. Gebauer, A. J. Springthorpe, R. W. Streater, S. Vijarnwannaluk, W. Songprakob, and R. Zallen, J. Vac. Sci. Technol. B **18**, 1594 (2000).
9. W. Songprakob, R. Zallen, W. K. Liu, K. L. Bacher, Phys. Rev. B **62**, 4501 (2000); W. Songprakob, R. Zallen, D. V. Tsu, and W. K. Liu, J. Appl. Phys. **91**, 171 (2002).

Table 1-1. Properties of crystalline GaAs at 300°K (adapted from [3], [5] and [7])

Property	
Crystal Structure	Zincblende
Lattice constant	4.653 A
Bond length	2.448 A
Molecules per cm^3	2.21×10^{22} cm^{-3}
Molecular weight	144.7
Density	5.32 g/cm^3
Melting point	1238°C
Static dielectric constant	12.9
Infrared refractive index (λ = 2 μm)	3.317
Energy gap	1.423 eV
Conductionband minimum	k=0
Valenceband maximum	k=0
Electron effective mass	0.063 m_e
Heavy-hole effective mass	0.50 m_e
Light-hole effective mass	0.088 m_e
Split-off valenceband effective mass	0.155 m_e
Intrinsic carrier concentration	2.25×10^6 cm^{-3}
Valenceband effective density of states	9.6×10^{18} cm^{-3}
Conductionband effective density of states	4.2×10^{17} cm^{-3}
Electron mobility	8500 cm^2/Vs
Hole mobility	400 cm^2/Vs
Transverse-optical k=0 phonon frequency	268.2 cm^{-1}
Longitudinal-optical k=0 phonon frequency	291.5 cm^{-1}

Table 1-2. Characteristics of MBE-grown LT-GaAs [6,8] versus those of GaAs grown by MBE in the standard way. In the standard method, the GaAs substrate is kept at 600 C; for LT-GaAs, it is kept at about 300 C.

	Standard MBE	LT –GaAs
Structure	Crystalline	Crystalline
Composition	Stoichiometric	1% excess As
Trap density	under10^{15} cm^{-3}	10^{19} cm^{-3}
Lifetime	1 nanosecond	under 1 picosecond
Breakdown field	3×10^{4} $V.cm^{-1}$	5×10^{5} $V.cm^{-1}$
Resistivity	1-10 Ω-cm.	(10^{2}-10^{7}) Ω-cm

Table 1-3. Characteristics of LT-GaAs:C versus those of GaAs:C, where GaAs:C is MBE grown carbon-doped GaAs deposited at standard substrate temperature (T_{growth} = 600 C) while LT-GaAs:C is MBE-grown carbon-doped GaAs deposited at low substrate temperature (about 300 C). Entries marked with an asterisk * are based on experimental work reported in this dissertation (the chapter containing the discussion of that work is given in parenthesis).

	GaAs:C	LT-GaAs:C
Crystal quality	high	many arsenic-antisite (As_{Ga}) defects
Semiconductor type	p-type	nonconducting
Carbon incorporation	C_{As} [9]	C_{As} and $C_{interstitial}$
Mid-infrared reflectivity	plasmon dip [9]	*flat in the mid-IR (chapter 9)
LVM IR absorption	*sharp	*broad (chapter 5)
Raman signature	*L- plasmon-phonon	*LO phonon (chapter 7)
Photoluminescence	*bandgap PL	*no PL (chapter 8)
T_{growth} range	*400 C and higher	*below 400 C (chapter 7)

Table 1-4. Organization of the main parts in terms of optical techniques used and materials investigated

Experiments	GaAs:C	LT-GaAs:C	LT-GaAs
Infrared (LVM)	Chapter 4	Chapter 5	-
Raman	-	Chapter 7	Chapter 6
Photoluminescence	Chapter 8	Chapter 8	

Chapter 2. Optical techniques

2.1 Introduction

This chapter deals primarily with the several types of optical experiments carried out in the work reported in this dissertation. Since both the general techniques used, and their specific implementation in this work, are relatively standard, backgrounds and details available elsewhere will not be repeated here. Instead, sources will be given for these aspects in the form of published work and (for the details) previous dissertations from this group. However, a few special optical aspects specific to this dissertation will be discussed in this chapter.

The following section briefly describes the optical techniques and their instrumentation. Section 2.3 describes special aspects of the spectral resolution in the infrared and Raman measurements. Section 2.4 contains a Raman study addressing the issue of sample heating. Section 2.5 provides a discussion of the localized vibrational mode of carbon in GaAs, which is the main subject in the infrared work included in this dissertation.

2.2 Optical techniques and instrumentation.

The three main optical techniques used here (as indicated on the left side of Table 1-4) are infrared transmission, Raman scattering, and photoluminescence. Infrared transmission measurements provide a straightforward measure of the optical absorption. In the work reported here, the infrared focus is on atomic vibrations and the frequency region of interest is about 200 to 800 cm^{-1}. Wavenumber units ($\bar{\nu}$ given in cm^{-1}) are standard for vibrational studies; $\bar{\nu}$ is the reciprocal of the wavelength (in vacuum) of the light. In Raman scattering, monochromatic high-frequency laser light (usually in the

visible) is incident on the sample, and inelastically scattered redshifted light from the sample is spectrally analyzed by a high-discrimination spectrometer. In effect, Raman scattering is a photon-energy-loss experiment. The redshift is small, corresponding to the energy of the crystal excitation (typically a phonon) created in the scattering event. (This is for a Stokes process; in the less-usually-studied anti-Stokes process, an existing phonon disappears and the scattered light is blueshifted.) Since Raman lines are weak and are spectrally close to the incident laser line, very high discrimination (by a factor of 10^8 or more) against the laser line is needed; this is usually achieved by using two or three monochromators in series. Photoluminescence experiments are operationally similar to Raman experiments, with a laser beam as input to the solid and redshifted emitted light as output. In photoluminescence (PL), the emitted light corresponds to a characteristic electronic transition energy of the solid (such as the bandgap E_g). A PL emission band occurs at a position fixed by the transition energy; it does not shift with laser photon energy $h\nu_L$. This is in contrast to a Raman emission line, which tracks with $h\nu_L$ because it is the small redshift that corresponds to a crystal excitation energy. In PL experiments, the emitted band is usually broad and well separated from $h\nu_L$, so that a single, moderate-resolution, monochromator is usually adequate for the measurements.

Good discussions of the uses of infrared, Raman, and photoluminescence experiments in semiconductor physics can be found in the books by Yu and Cardona [1] and by Perkowitz [2]. Raman-scattering examples are treated in depth in compilations edited by Cardona and Guntherodt [3] and by Weber and Merlin [4]. Infrared studies of localized vibrational modes have been discussed by Barker and Sievers [5] and by Newman [6].

The instrument used for the infrared measurements reported in this dissertation was a Bomem DA3 Fourier-transform spectrometer. It is a vacuum high-resolution version of a Michelson interferometer which features dynamic alignment and electrically-switched selection mirrors for changing between different light source and detectors. It is described in detail in the dissertations by Gonzalez [7] and Songprakob [8], and briefer descriptions are available in papers published by Gonzalez et al. [9], Moret et al. [10], and Songprakob et al. [11].

The main instrument used for the Raman-scattering measurements was a Spex 1403 scanning double monochromator equipped with holographic gratings and internal spatial filtering via a fourth slit. The light detector was a cooled GaAs-photocathode photomultiplier used with photon-counting electronics. The blue (488 nm, 2.54 eV) and green (514 nm, 2.41 eV) lines of an argon ion laser were used for excitation. A quasi-backscattering geometry was used, with the laser beam about 9 degrees from the normal inside the sample. Details of this system are described in the dissertations by Holtz [12] and Doss [13], and briefer descriptions are available in papers published by Holtz et al. [14] and by Doss and Zallen [15].

Both of the instruments described above, the Bomem infrared spectrometer and the Spex Raman spectrometer, are housed in the Physics Department at Virginia Tech. Other instruments, housed elsewhere, were also used in the work reported here. A few Raman measurements were carried out, under the guidance of Dr Jing Ling, with the Dilor XY Raman Microprobe housed in the Department of Geological Sciences at Virginia Tech. This is a micro-Raman system employing a microscope for selecting a small spot on the sample and a charge-coupled-device (CCD) array detector for rapid

data acquisition. An interesting comparison of the Spex and Dilor Raman systems is given in the dissertation by Moret [16]. Other Raman measurements, and all of the photoluminescence measurements, were carried out on two Renishaw RM1000 Raman systems located in England.

It is possible to carry out photoluminescence experiments using the Physics Department's Spex 1403, but with difficulty and over a limited spectral range [17]. (Raman spectrometers generally have narrow spectral windows.) Thanks to research connections established by Prof. Zallen with the group of Prof. Tony Stradling at Imperial College (IC) London and Dr. David Pitt at Renishaw Corporation, photoluminescence measurements were carried out on our GaAs:C and LT-GaAs:C samples using RM1000 micro-Raman spectrometers. The Renishaw RM1000 is an optically fast system using special "notch" interference filters to provide effective rejection of the laser line from the scattered beam, a very sensitive CCD array detector, and a high-quality microscope that is mechanically and optically integrated with a compact single monochromator. The high detector sensitivity and the very high light-collection efficiency allow the instrument to operate with low-power air cooled ion lasers and diode lasers (in contrast to the high-power water-cooled ion lasers needed with the Spex1403). Relative to a conventional system like the Spex, the only drawbacks are a small loss of resolution (limited by array-detector pixel size) and some difficulty in working very close to (within 100 cm^{-1} of) the laser line. The great advantages are ease of use and speed of data acquisition. In a Spex/Renishaw comparison carried out on a weak Raman scatterer [18], a clean spectrum requiring 50 hours of repetitive scanning with the Spex 1403 required about a minute with the RM1000.

Measurements on our samples were carried out at IC by Ming-Liang Hsieh and at Renishaw (Wotton-under-Edge, UK) by Chris Froud. A description of the IC RM1000 spectrometer is given in Hsieh's dissertation [19], and a discussion of recent developments in such systems is given in Ref. 20. Though designed as a Raman spectrometer, the Renishaw has a wide spectral window and is very effective for photoluminescence experiments. In some of the PL spectra reported in chapter 8 and 9, both PL emission and Raman emission are simultaneously present.

2.3 Spectral Resolution.

This section collects some information specific to measurements made with the Bomem and Spex instruments.

The Bomem is an interferometer, so that its spectral resolution depends on the range of motion chosen for the moving mirror, L_{mirror}. The instrumental spectral width Γ_{inst} is set by the range used and is approximately given by the simple relation $\Gamma_{inst}=(1/L_{mirror})$. Increasing L_{mirror} increases resolution but also increases data-acquisition time. In order to study the effect of instrumental resolution on the observed spectra, measurements with the Bomem were carried out on the infrared absorption band at 620 cm^{-1} of a polystyrene sheet. With increasing instrumental spectral width Γ_{inst}, the observed transmission dip broadens and becomes shallower, with the integrated transmission drop holding constant. The experimental width $\Gamma_{observed}$ (full width at half maximum) is shown plotted against Γ_{inst} in Fig. 3-1. Over the range covered, the results are reasonably well described by the empirical relation

$$\Gamma_{observed} = \Gamma_0 + a\Gamma_{inst}^2 \qquad (2\text{-}1)$$

Here Γ_0 is the actual linewidth (4.3 cm^{-1}) of the polystyrene band and the parameter a (0.08 cm) is a characteristic of the Bomem spectrometer, as shown on Fig. 2-1. In the measurements reported here on the absorption band of the localized vibrational mode of carbon in GaAs:C, the Bomem was set up with Γ_{inst} = 4.0 cm^{-1}, so that $\Gamma_{observed}$ is 1.3 cm^{-1} larger than the actual linewidth. The LVM linewidth observed in our experiments ranged from 4 cm^{-1} (for GaAs:C at low doping) to 18 cm^{-1} (for LT-GaAs:C at high doping), so that this instrumental resolution was quite adequate.

The Spex 1403 consists of two synchronized rotating-grating dispersive spectrometers in series. The instrumental spectral slit width is set by the mechanical slit width of the entrance and exit slits, which are set to be equal. Figure 2-2 shows a calibration of the relation between the mechanical slit width x and the spectral slit width Γ_{spex} obtained by measurements on the longitudinal optical (LO) Raman line of undoped GaAs. A typical slitwidth used in our measurements was 300 microns; the range of x covered in Fig. 2-2 is from 100 to 500 microns. We assume that Γ_{spex} is proportional to x, Γ_{spex}=Ax, where A is a spectrometer characteristic determined by the grating dispersion and the double-monochromator geometry. Figure 2-2 shows $\Gamma^2_{observed}$ plotted against x^2, where $\Gamma_{observed}$ is the measured FWHM linewidth of the observed Raman line. The results are well described by

$$\Gamma^2_{observed} = \Gamma^2_0 + A^2 x^2 \qquad (2\text{-}2)$$

Γ_0 is the actual room-temperature linewidth (2.0 cm^{-1}) of the GaAs LO Raman line. The result for A shows that each 100 microns of mechanical slit width corresponds to 1.13 cm^{-1} of spectral slit width.

The wavenumber calibration of the Spex was corrected daily using a sharp mercury emission line present (with the room lights on) in the light emitted by the lab's overhead fluorescent lamps. This line is at 18312.5 cm^{-1}, corresponding to a Raman shift relative to the argon 488 nm blue line (20491.8 cm^{-1}) of 2179.3 cm^{-1} This was done to correct for slow temperature-induced shifts which, if corrected, could amount to a 1 or 2 cm^{-1} drift in the absolute-wavenumber calibration of the spectrometer.

2.4 Sample heating during Raman measurements

The question of possible sample heating during Raman measurements with the Spex, because of light absorbed from the incident laser beam, was addressed by measuring the ratio between the intensities of the Stokes and the anti-Stokes Raman lines corresponding, respectively, to LO-phonon emission and LO-phonon absorption in GaAs. The ratio of the Stokes and the anti-Stokes components, adapted from [21], is

$$\frac{I(h\nu_L - \Delta_{phonon})}{I(h\nu_L + \Delta_{phonon})} = S = \left(\frac{h\nu_L - \Delta_{phonon}}{h\nu_L + \Delta_{phonon}}\right)^4 e^{\frac{\Delta_{phonon}}{kT}} \qquad (2\text{-}3)$$

Here $I(h\nu_L - \Delta_{phonon})$ is the intensity of the Stokes line, $I(h\nu_L + \Delta_{phonon})$ is the intensity of the anti-Stokes line, Δ_{phonon} is the energy of the phonon, and T is the temperature of the sample. As shown in (2-3), we use S to denote the intrinsic Stokes/anti-Stokes ratio. S is temperature-dependent via the exponential in (2-3). It is large at low temperature and about 1 at very high temperature.

Raman scattering occurs within the solid, and since $h\nu_L$ is above the bandgap of GaAs, the effects of optical absorption must be considered. Suppose that the scattering event occurs in a layer of thickness dx at depth x below the surface. The laser intensity incident on that layer is

$$I_{incident} = I_0 e^{-\alpha(h\nu_L)x} \tag{2-4}$$

where $\alpha(h\nu_L)$ is the GaAs absorption coefficient at the laser photon energy and I_0 is the intensity of the laser light at the surface. The relative intensities of the Stokes and anti-Stokes light coming from the sample are given by the expressions in (2-5)

$$\begin{aligned} I_{stokes} &= \int_0^\infty dx I_0 S e^{-[\alpha(h\nu_L)+\alpha(h\nu_L-\Delta_{phonon})]x} \\ I_{antistokes} &= \int_0^\infty dx I_0 e^{-[\alpha(h\nu_L)+\alpha(h\nu_L+\Delta_{phonon})]x} \end{aligned} \tag{2-5}$$

S is not a function of x, and the integral can be calculated to give

$$\frac{I_{stokes}}{I_{antistokes}} = \frac{[\alpha(h\nu_L)+\alpha(h\nu_L+\Delta_{phonon})]}{[\alpha(h\nu_L)+\alpha(h\nu_L-\Delta_{phonon})]} S \tag{2-6}$$

From this equation and equation (2-3) for S(T), we can determine the temperature T from measurements of the intensity ratio $I_{Stokes}/I_{anti\text{-}Stokes}$. $\alpha(h\nu)$ is known for GaAs [22]; at 2.54 eV, α is 1.24×10^5 cm^{-1} and $\frac{d\alpha}{d\bar{\nu}}$ is 38.

Three samples were used; all were carbon-doped GaAs having a carbon concentration of 6×10^{19} cm^{-3}. Two were LT-GaAs:C samples grown at 225 C and 240 C. Since free carriers are compensated by defects in LT-GaAs, these two samples exhibit the undoped-GaAs LO line, at 290 cm^{-1}. The third sample was normal GaAs:C grown at 600C. This sample is p-type conducting with a plasma of holes. The LO Raman line is replaced by an L- plasmon-phonon line at 265 cm^{-1}. The 488nm blue line was used for excitation at $h\nu_L$ = 2.54 eV. Relatively high power (500 mw at the laser head) was used, since the purpose was to test for appreciable laser-induced sample heating. The Stokes/anti-Stokes intensity ratio was determined from our measured Raman spectra, and

the factor multiplying S in equation (2-6) was determined from the GaAs absorption coefficient data (given at the end of the preceding paragraph) of Aspnes and Studna [22]. S was then determined and, from the known $h\nu_L$ and Δ_{phonon} (or $\Delta_{plasmon\text{-}phonon}$), the temperature T was then determined from the S(T) expression in (2-3). The results are shown in Table 2-1.

The Spex Raman lab is kept at about 295 K (22 C). Table 3 shows that there is no appreciable sample heating from the laser. The fact that the largest deviation from room temperature is actually on the low-temperature side is probably attributable to the experimental error involved in measuring Raman intensities. It has been reported that LT-GaAs has a thermal conductivity about 4 times smaller than that of GaAs [23], but Table 2-1 shows that this presented no problem in terms of sample heating during the Raman experiments.

2.5 Localized Vibrational Modes in GaAs

When doped with a substitutional impurity atom that is lighter than the Ga and As host-crystal atoms, a new vibrational mode appears with frequency higher than the GaAs LO frequency. This mode of vibration does not propagate through the crystal. The vibration is restricted to the impurity atom and its nearest neighbors. This is called a localized vibrational mode (LVM). Table 2-2 shows the frequency of LVM modes for several light impurities in GaAs [5].

If we assume that the impurity atom of mass m vibrates at frequency ω_{LVM} and has a damping constant Γ_{LVM}, and that the LVM absorption has an oscillator strength characterized by effective charge q, then the equation of motion in the presence of the electromagnetic field of the incident light is [24].

$$m[\ddot{x} + \Gamma_{LVM}\dot{x} + \omega_{LVM}^2 x] = qE(x, \omega, t) \tag{2-7}$$

The resulting oscillating dipole moment is

$$p = qx = \frac{q^2 E}{m(\omega_{LVM}^2 - \omega^2 - i\omega\Gamma_{LVM})} \tag{2-8}$$

If N is the concentration of the impurity atoms, the total polarization per cubic centimeter is Np. The total dielectric constant of the material can be written as a linear combination of four parts:

$$\begin{aligned}
\varepsilon &= \varepsilon_\infty + \varepsilon_{phonon} + \varepsilon_{plasmon} + \varepsilon_{LVM} \\
\varepsilon_{phonon} &= \frac{\varepsilon_\infty(\omega_{LO}^2 - \omega_{TO}^2)}{\omega_{TO}^2 - \omega^2 - i\omega\Gamma_{phonon}} \\
\varepsilon_{plasmon} &= -\frac{\varepsilon_\infty \omega_p^2}{\omega(\omega + i\Gamma_{plasmon})} \\
\varepsilon_{LVM} &= \frac{4\pi N q^2}{m(\omega_{LVM}^2 - \omega^2 - i\omega\Gamma_{LVM})} \\
\omega_p^2 &= \frac{4\pi p e^2}{\varepsilon_\infty m_h^*}
\end{aligned} \tag{2-9}$$

In (2-9), ε_∞ is the high-frequency dielectric constant, ε_{phonon} is the phonon contribution to the dielectric constant, $\varepsilon_{plasmon}$ is the free-carrier contribution, and ε_{LVM} is the LVM contribution. In ε_{phonon}, ω_{TO} and ω_{LO} are the transverse-optical and longitudinal-optical phonon frequencies respectively. Γ_{phonon} and $\Gamma_{plasmon}$ are the phonon and plasmon damping constants, p is the carrier concentration (assumed to be holes and equal to the impurity concentration N), e is the electron charge, and m_h^* is the density-of-states hole mass. The total absorption coefficient can be written as [24].

$$\alpha = \frac{4\pi\,\mathrm{Im}[\sqrt{\varepsilon(\omega)}]}{\lambda} \tag{2-10}$$

Because the magnitude of the LVM dielectric constant is many orders of magnitude smaller than the other contributions to the dielectric constant, we can use a Taylor's series expansion and separate the total absorption coefficient α into two terms, written here in terms of wavenumber $\bar{\nu}$ instead of angular frequency ω:

$$\begin{aligned}
&\alpha = \alpha_0 + \alpha_{LVM} \\
&\alpha_{LVM} = \frac{2Nq^2}{nc^2m} \frac{\bar{\nu}^2 \gamma_{LVM}}{(\bar{\nu}_{LVM}^2 - \bar{\nu}^2)^2 + \bar{\nu}^2 \gamma_{LVM}^2} \\
&\omega = 2\pi\bar{\nu}c \\
&\Gamma_{LVM} = 2\pi c\gamma_{LVM} \\
&c = \text{speed of light.}
\end{aligned} \tag{2-11}$$

Here α_{LVM} is the localized-vibrational-mode absorption coefficient, and α_0 is the much larger absorption coefficient corresponding to the rest of the dielectric constant. The integrated absorption (IA), which is defined as the integral of the absorption coefficient over the absorption band, is

$$\begin{aligned}
&\int \alpha_{LVM}(\bar{\nu}) d\bar{\nu} = \frac{\pi Nq^2}{nc^2m} \\
&\int \alpha_{LVM}(\bar{\nu}) d\bar{\nu} = \frac{N}{f}
\end{aligned} \tag{2-12}$$

This relation can be used to determine the impurity concentration, since N is proportional to the integrated absorption.. If the proportionality factor f is found from standard samples for which the impurity concentration is known by other measurements, measuring the absorption coefficient and the integrated absorption can determine the impurity concentration in an unknown sample. Our studies of this will be discussed in chapter 4. High-resolution infrared-absorption studies of GaAs at low temperature show that there are five closely spaced LVM lines near 580 cm^{-1} [25]. However, at room temperature these lines are broadened and merge into one band with approximately

Lorentzian line shape [26]. So at room temperature, the LVM absorption of GaAs:C can be treated as one band.

References

1. P. Y. Yu and M. Cardona, *Fundamentals of Semiconductors* (Springer, Berlin, 1996).
2. S. Perkowitz, *Optical Characterization of Semiconductors: Infrared, Raman and Photoluminescence Spectroscopy* (Academic Press, New York, 1993).
3. M. Cardona and G. Guntherodt (editors), *Light Scattering in Solids II: Basic Concepts and Instrumentation,* Topics Appl. Phys. **50** (Springer, Berlin, 1982).
4. W. H Weber and R. Merlin (editors), *Raman Scattering in Materials Science* (Springer, Berlin, 2000).
5. A. S. Barker, Jr. and A. J. Sievers, Rev. Mod. Phys. **47,** Supplement number 2 , 51-180 (1975).
6. R. C. Newman, in *Growth and Characterization of Semiconductors,* edited by R. A. Stradling and P.C. Klipstein (Hilger, Bristol, 1990), p.119.
7. R. J. Gonzalez, PhD dissertation, Dept. of Physics, Virginia Tech, 1996. Pages 26-35.
8. W. Songprakob, PhD dissertation, Dept. of Physics, Virginia Tech, 2001. Pages 60-66.
9. R. J. Gonzalez, R. Zallen, and H. Berger, Phys Rev. B **55**, 7014 (1997).
10. M. P. Moret, R. Zallen, R. E. Newnham, P. C. Joshi, and S. B. Desu, Phys. Rev B **57**, 5715 (1998).
11. W. Songprakob, R. Zallen, W. K. Liu, and K. L. Bacher, Phys. Rev. B **62**, 4501 (2000).
12. M. W. Holtz, PhD dissertation, Dept of Physics, Virginia Tech, 1987. Pages 34-46.
13. C. J. Doss, PhD dissertation, Dept. of Physics, Virginia Tech, 1994. Pages 21-30.
14. M. Holtz, R. Zallen, O. Brafman, and S. Matteson, Phys. Rev. B **37**, 4609 (1988).

15. C. J. Doss and R. Zallen, Phys. Rev. B **48**, 15626 (1993).

16. M. P. Moret, MS dissertation, Dept. of Physics, Virginia Tech, 1996. Pages 11-15.

17. Reference 8, p. 153. The spectral range covered is from 1.6 to 2.7 eV, pushing to the limit the capabilities of the Spex.

18. R. Zallen, W. Songprakob, and M-L Hsieh, unpublished.

19. M-L. Hsieh, PhD thesis, Dept. of Physics, Imperial College, University of London, 2001. Pages 51-53.

20. S. A. Asher and R Bormett, in Ref. 4, p. 35.

21. M. Cardona, in *Light Scattering in Solids,* Topics Appl. Phys. **8** (Springer, Berlin, 1975), p. 10.

22. D. E. Aspnes and A. A. Studna, Phys. Rev. B **27**, 985 (1983).

23. A. W. Jackson, J. P. Ibbetson, A. C. Gossard, and U. K. Mishra, Appl. Phys. Lett. **74**, 2325(1999).

24. J. D. Jackson, *Classical Electrodynamics* (Wiley, New York, 1975).

25. B. V. Shanabrook, W. J. Moore, T. A. Kennedy, and P.P. Ruden. Phys. Rev. B **30**, 3563 (1984).

26. D-S. Jiang, C-Y. Song, J-F. Zheng, and C-C. Hsu, Chinese Phys. **6**, 749 (1986).

Table 2-1. Estimates of sample temperature, during Raman experiments with the Spex, from measurements of the Stokes/anti-Stokes intensity ratio at higher-than-normal laser power (500 mW of 488 nm light at the laser head, corresponding to about 40 mW at the sample).

Samples	T_{growth}	Raman shift	Stokes/anti-Stokes intensity ratio	Estimated Temperature
LT-GaAs:C	225 C	290 cm^{-1}	4.07	290 K
LT-GaAs:C	240 C	290 cm^{-1}	4.28	280 K
GaAs:C	600 C	265 cm^{-1}	3.51	296 K

Table 2-2 Localized-vibrational-mode frequencies of various substitutional light impurities in GaAs [5]. The notation Si_{Ga} denotes a silicon impurity atom substituting for a host-crystal gallium.

Impurity	LVM frequency [cm^{-1}]	Temperature [K]
Al_{Ga}	362	80
Al_{Ga}	371	4.2
P_{As}	353	300
P_{As}	355	80
P_{As}	363	4.2
Si_{Ga}	384	80
Si_{As}	399	80
Mg_{Ga}	326	80
$^{11}B_{Ga}$	517	77
$^{10}B_{Ga}$	540	77
$^{12}C_{As}$	582	77
$^{13}C_{As}$	561	77

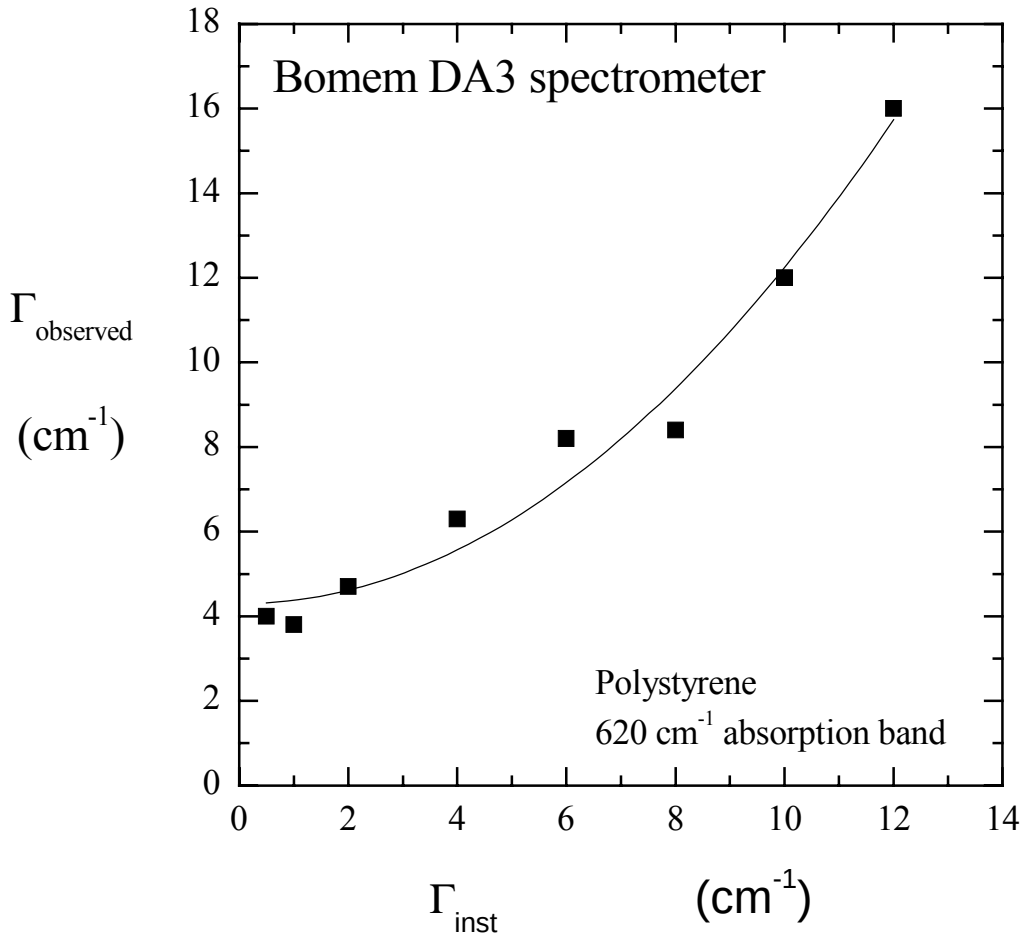

Figure 2-1 The correlation between the observed linewidth and the instrumental resolution for measurements on the 620 cm^{-1} absorption band of polystyrene. $\Gamma_{observed}$ is the experimental linewidth and Γ_{inst} is the instrumental linewidth of the Bomem DA3.

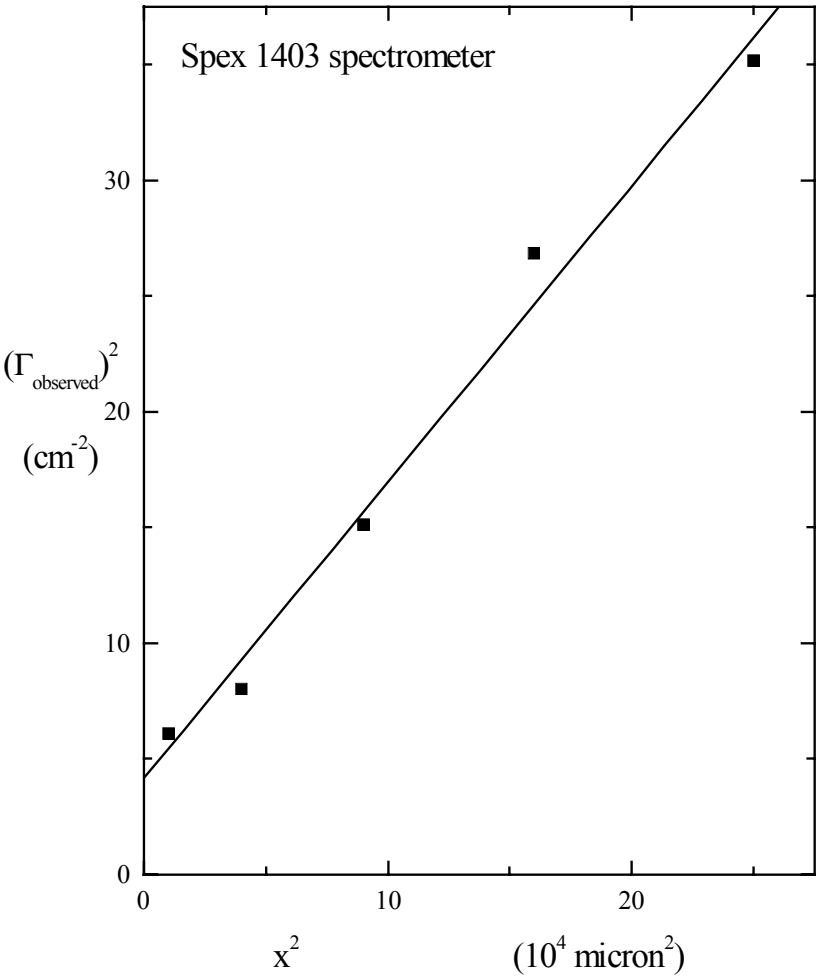

Figure 2-2 The correlation between the observed linewidth and the mechanical slitwidth (x) for measurements made with the Spex 1403 on the LO Raman line (291 cm^{-1}) of undoped GaAs. The slope of the fitted line determines the conversion from entrance/exit slit width to instrumental spectral slit width for the Spex spectrometer. The intercept determines the actual room-temperature linewidth (2 cm^{-1}) of the LO line.

Chapter 3. The semiconductor samples

3.1 MBE growth at IQE

The semiconductor samples studied in this dissertation were GaAs thin films prepared by molecular beam epitaxy (MBE). The samples were prepared at IQE corporation in Bethlehem, Pennsylvania, by Dr. W. K. (Amy) Liu. IQE is the successor to Quantum Epitaxial Designs (QED), and was formed by the merger of QED with EPI corporation in 1999 [1]. IQE supplies high-quality compound-semiconductor multilayer structures to semiconductor device manufacturers, and carries out research and development in compound-semiconductor thin-film growth.

In molecular beam epitaxy [2,3,4], ballistic beams of atoms or molecules, traveling in an ultrahigh-vacuum (UHV) environment, are incident on a temperature-controlled substrate. Because of the UHV environment, electron diffraction can be used to monitor the growing film and film thicknesses are controllable to near atomic scale. MBE is essentially an UHV-based evaporation method capable of high purity and thickness control. In MBE growth of GaAs, two incident beams fall on a GaAs substrate, one made up of Ga atoms and the other of As_4 molecules [3,5]. All Ga atoms stick, and only one As atom per Ga remains on the surface.

The growth system at IQE was an EPI GENII MBE reactor, with special features described by W. K. Liu et al. in Refs. 5 and 6. The MBE films were grown on (100)-oriented Czochralski-grown semi-insulating GaAs wafers of thickness 0.635 mm. Prior to MBE growth a thin (100-250 nm) undoped buffer layer was deposited first. Then the MBE film was deposited at a growth rate controlled at 2.5 Å/sec. The growth rate was established from both high-resolution x-ray diffraction and reflection high-energy

electron diffraction measurements carried out on calibration AlGaAs/GaAs superlattice structures. Substrate temperature was controlled and determined as described in Refs. 5 and 6. Normal GaAs was grown at a substrate temperature close to 600 C, LT-GaAs at temperatures as low as 240 C. Carbon doping was achieved by means of a CBr_4 source kept at 0 C [5].

3.2 The GaAs:C and LT-GaAs:C Films.

Tables 3-1 and 3-2 list the samples studied. These tables include information about the films obtained in characterization studies carried out at IQE.

The GaAs:C films, all deposited at a growth temperature (substrate temperature) close to 600 C, are described in Table 3-1. All of these films are p-type semiconductors; the values of the hole concentration p, determined by Hall-effect measurements, are given in the fourth column. In addition to the information given in the table, infrared measurements of hole-plasmon excitations in these films [7], whose interpretation requires detailed consideration of intervalenceband processes [8], have also been carried out. The Hall-determined hole-mobility values for the films are listed in Ref. 7; μ_{Hall} decreases with increasing doping, going from about 140 cm^2/Vs for sample (a) to about 60 cm^2/Vs for sample (l). An important conclusion from that infrared work is that the Hall-determined p is a very good measure of the carrier concentration in these films.

The three carbon-concentration values in the fifth column of Table 3-1 are from SIMS measurements (secondary ion mass spectrometry). SIMS measures the total carbon concentration [C]. Since p=[C] (within experimental error) for these films, it follows that essentially all of the carbons in the GaAs:C films are present as C_{As} acceptors, in agreement with earlier work on GaAs:C [9]. The last column in Table 3-1 gives results of

HRXRD (high-resolution x-ray diffraction) measurements on four of the films, and shows the lattice contraction perpendicular to the growth direction that occurs in GaAs:C because the C atoms are significantly smaller than the As atoms they replace.

The LT-GaAs:C films, deposited at various growth temperatures, are described in Table 3-2. Most of these films have resistivity too high for Hall-effect measurements, the three p values listed are for films which (as explained in chapter 7 and 8) turn out to be close to normal GaAs:C. The carbon concentrations lists in Table 3-2 are the intended values corresponding to the chosen growth conditions. Three lattice-distortion values measured by HRXRD are given, shown in the last column, and show a crossover from expansion to contraction with increasing carbon concentration. LT-GaAs is expanded (relative to GaAs) because of the As_{Ga} antisite defects [10]; the As-As bond is longer than the Ga-As bond. Since, as seen in Table 3-1, GaAs:C is contracted (relative to GaAs), doping LT-GaAs with carbon can compensate for the expansion intrinsic to LT-GaAs. This "strain compensation" is one of the reasons for the interest in LT-GaAs:C [6].

In addition to the samples listed in Table 3-1 and 3-2, an air-annealed LT-GaAs:C sample was also studied by optical experiments. This sample, covered on both sides by GaAs wafers, was placed in a furnace at room temperature, ramped up to 600 C in 20 minutes, held at 600 C for 20 minutes, and then removed from the furnace and allowed to cool down to room temperature. It is described in more detail in chapter 9.

3.3 Sample Geometry.

Figure 3-1 shows a not-to-scale schematic of the multilayer sample geometry. In this diagram, the growth direction is vertical. Before deposition of the carbon-doped MBE film, an undoped normal-GaAs (T_{growth} = 600 C) MBE film was first deposited on

the substrate wafer. For GaAs:C, the presence of this MBE-grown buffer layer is important for the crystalline quality of the later-deposited top film. The MBE buffer layer is also important for suppressing the introduction of chemical contaminants from the substrate, which, while pure by ordinary standards, is not as pure as the MBE-deposited films. SIMS work at IQE, on LT-GaAs:C films grown directly on the substrate, revealed contamination from unwanted impurities in the absence of the buffer layer.

A complete analysis of the infrared transmittance of the multilayer structure of Fig. 3-1 involves (assuming the sample is in vacuum, as it is when measured in the Bomem DA3 interferometer) light passing through five media: vacuum/film/buffer/substrate/vacuum. Optically the buffer layer and the substrate can be safely treated as one layer, but even so the full analysis is complicated [7]. This analysis is not required in our treatment of the LVM absorption band, since that band is very narrow and all the other absorption processes present in the film and substrate are spectrally broad by comparison. The LVM absorption can be isolated by removing the slowly varying background, as discussed in chapter 4

References

1. IQE Inc., 119 Technology Drive, Bethlehem, PA 18015, USA. Website, http://www.iqep.com
2. P. Y. Yu and M. Cardona, *Fundamentals of Semiconductors* (Springer, Berlin, 1996), p. 8.
3. M. Shur, *GaAs Devices and Circuits* (Plenum, New York, 1987), p. 116.
4. R. F. C. Farrow (editor), *Molecular Beam Epitaxy: Applications to Key Materials* (Noyes, Park Ridge, 1995).
5. W. K. Liu, D. I. Lubyshev, R. Specht, R. Zhao, E. R. Weber, J. Gebauer, A. J. Springthorpe, R. W. Streater, S. Vijarnwannaluk, W. Songprakob, and R. Zallen, J. Vac. Sci. Technol, B **18**, 1594 (2000).
6. W. K. Liu, K. Bacher, F. J. Towner, T. R. Stewart, C. Reed. P. Specht, R. C. Lutz, R. Zhao, and E. R. Weber, J. Crystal Growth. **201/202**, 217 (1999).
7. W. Songprakob, R. Zallen, W. K. Liu, and K. L. Bacher, Phys. Rev. B **62**, 4501 (2000).
8. W. Songprakob, R. Zallen, D. V. Tsu, and W. K. Liu, J. Appl. Phys. **91**, 171 (2002).
9. See references 1,3,8,13,47 of Ref. 7.
10. X. Liu, A. Prasad, J. Nishio, E. R. Weber, Z. Liliental-Weber, and W. Walukiewicz, Appl. Phys. Lett. **67**, 279 (1995).

Table 3-1. Characterization of the GaAs:C samples. All of these films were grown at a substrate temperature close to 600 C. The hole concentration p was measured by means of Hall-effect experiments carried out at IQE. The carbon concentration [C] was measured by secondary ion mass spectrometry at Evans East, Inc., under contract from IQE. The perpendicular lattice contraction Δa/a was measured at IQE by high-resolution x-ray diffraction.

Sample number		Thickness	p	[C]	Δa/a
IQE no.	Refs. 7,8	(Å)	(10^{19}cm^{-3})	(10^{19} cm^{-3})	
10981.02	-	7500	0.014	-	
10982.02	(a)	7500	0.34	-	
10983.02	(b)	7500	0.39	-	
10514.02	(c)	5000	0.52	-	-0.0000
10980.02	(d)	7500	0.68	-	
10979.02	(e)	7500	2.0	-	
10525.02	(f)	5000	2.7	2.6	-0.0004
10985.02	(g)	5000	3.3	-	
10977.02	(h)	5000	6.6	-	
10355.02	(i)	5000	8.2	-	
10986.02	(j)	3500	9.1	-	
10511.02	(k)	5000	10.5	9.9	-0.0017
10512.02	(l)	5000	13.6	13.0	-0.0023

Table 3-3. Characterization of the LT-GaAs:C samples. All of these films are 10,000 Å (one micron) thick. Carbon concentrations are the intended values corresponding to the chosen growth conditions. Hole concentration p and mobility μ_{Hall} were measured by Hall-effect experiments carried out at IQE. Lattice distortion $\Delta a/a$ was measured at IQE by high-resolution x-ray diffraction.

Sample	T_{growth} (C)	[C] ($10^{19}cm^{-3}$)	p ($10^{19}cm^{-3}$)	μ_{Hall} (cm^2/Vs)	$\Delta a/a$
11772.02	240	undoped	-	-	+0.0007
11776.02	240	2	-	-	-
11775.02	240	4	-	-	0.0000
11774.02	240	6	-	-	-0.0002
11777.02	240	8	-	-	-
11858.02	225	6	-	-	-
11856.02	240	6	-	-	-
11855.02	260	6	-	-	-
11857.02	330	6	-	-	-
213049	400	5.5	7.0	69	-
213048	480	5.5	6.2	67	-
213047	600	5.5	5.4	74	-
11854.02	600	6	-	-	-

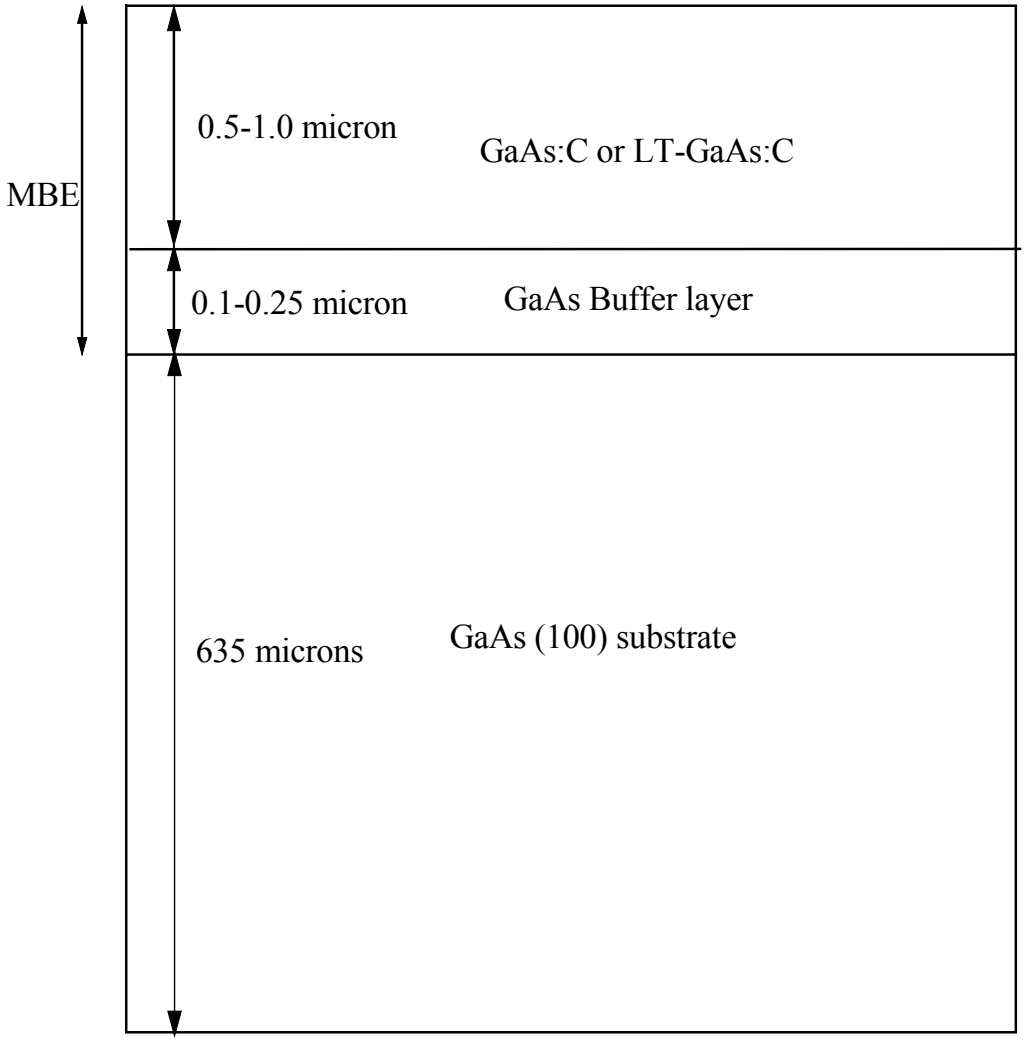

Figure 3-1. Schematic of the multilayer sample geometry.

Chapter 4. The localized vibrational mode of carbon in heavily-doped MBE-grown GaAs:C

4.1 Introduction

Carbon (C^{12}) impurities in GaAs give rise to an infrared absorption band around 580 cm^{-1}. This band is identified as the absorption due to the localized vibrational mode (LVM) of carbon atom substitutionally located at an arsenic site [1]. This absorption band provides a nondestructive way to measure the concentration of the electrically active C_{As} impurities, which act as acceptors because carbon (relative to arsenic) is one valence electron short. This concentration (N) can be estimated using the relation [2].

$$N = \frac{mnc^2}{\pi q^2} \int \alpha_{LVM}(\bar{\nu}) d\bar{\nu} \tag{4-1}$$

Here $\alpha_{LVM}(\bar{\nu})$ is the LVM absorption coefficient at wavenumber $\bar{\nu}$ cm^{-1}, N is the impurity concentration, q is the dynamic charge of the LVM mode, m is the carbon-atom mass, *n* is the refractive index, and c is the speed of light. The integral, taken over the absorption band, is called the LVM integrated absorption and will be denoted as IA. The pre-factor preceding the integral in Eq. (4-1) is a proportionality or conversion factor customarily denoted as f;

$$N = f \int \alpha_{LVM}(\bar{\nu}) d\bar{\nu} = f \times (IA) \tag{4-2}$$

Once the conversion factor f is known, the impurity concentration can be found from infrared measurements of the LVM absorption. The conversion factor, both at room temperature and at low temperature, has been investigated in several studies [3,4,5,6].

Homma et al. [3] studied the relation of the integrated absorption and the carbon concentration [C]. For the integrated absorption, they used the product of the linewidth

(the full width at half maximum, FWHM) and the peak value of the LVM absorption coefficient. They proposed a value for the conversion factor of $(9.5\pm2.9)\times10^{15}cm^{-1}$. They also suggested that, to determine the carbon concentration, the LVM measurements are best done at room temperature. The reason for this is that at low temperature, the LVM band develops a fine structure, which complicates the determination of the integrated absorption. Brozel et al. [5] suggested that a reasonable range for the conversion factor should be between $8\times10^{15}cm^{-1}$ and $11\times10^{15}cm^{-1}$. L.Sargent et al. [6] recommended $(13\pm3)\times10^{15}cm^{-1}$ for the conversion factor. Later [7], they estimated the lower limit of carbon concentration detection with infrared measurements at room temperature to be 1.5×10^{14} cm^{-3}. Those earlier studies, carried out on thick bulk GaAs samples, were confined to carbon doping levels below 10^{17} cm^{-3}.

In this work, we report the results of studies of the carbon induced localized vibrational mode in heavily-doped MBE-grown GaAs:C films. The samples used in our studies have been doped to carbon concentrations in the 10^{18}-10^{20} cm^{-3} range, far exceeding those of previous LVM studies. Infrared absorption was our spectroscopic tool. While we find that the conversion factor reported in previous studies extends to higher concentrations not studied before, at our highest concentrations we observed saturation of the LVM infrared integrated absorption.

4.2 Experiment

The preparation of the GaAs:C films by molecular beam epitaxy has been described elsewhere ([8],chapter 3). Carrier concentrations of the samples were measured by Hall-effect experiments (measured at IQE). Secondary ion mass spectrometry (SIMS) measurements were performed on these samples to determine the carbon concentrations.

The carbon concentrations obtain from SIMS agree well with the Hall concentration within experimental errors (5% for Hall measurements and 20% for SIMS measurements). Thus, the Hall concentration (p) is essentially equal to the carbon concentration ([C]). The detailed numbers on these measurements are given in chapter 3.

Infrared transmission spectroscopy was measured with the Bomem DA3.02 Fourier-transform interferometer. The spectral range was set at 550-600 cm^{-1}, the resolution was 4.0 cm^{-1}, and the moving-mirror scan speed was 0.1 cm/sec. The sample was at normal-incidence configuration in a sample holder having a beam aperture 5 mm in diameter. To improve the signal-to-noise ratio, ten spectra were collected and averaged to obtain the measured transmittance spectrum.

4.3 Results

Figure 4-1 shows a typical transmittance spectrum, obtained for the GaAs:C film with $[C]=2.7\times10^{19}cm^{-3}$. The LVM absorption coefficient spectrum is calculated from the transmittance spectrum using the relation.

$$\alpha_{LVM} + \alpha_0 = \alpha_{total} = -\frac{1}{d}\ln(T) \qquad (4\text{-}3)$$

Here d is the thickness of the MBE layer, T is the transmittance, and α_0 is the slowly-varying background absorption coefficient accounting for the substrate absorption and the reflection losses. Included in α_0 is a small contribution (measured separately) from the 2LO band in the substrate, which overlaps the LVM band. The drop in transmittance at the left side of Fig. 4-1 is caused by two-phonon processes within the thick substrate. In addition, the GaAs:C film contains free holes which give rise to free carrier absorption in the infrared; this free carrier absorption is essentially flat over the narrow range containing the LVM band. After the LVM absorption band $\alpha_{LVM}(\bar{\nu})$ is obtained, the

integrated absorption, the full width at half maximum (FWHM), are determined. The results are given in Table 4-1.

4.4 Discussion

Figure 4-2 presents the results for the LVM integrated absorption (IA) as a function of the Hall-determined carrier concentration (p). When p is lower than $5\times10^{19}cm^{-3}$, the integrated absorption shows a linear correlation with the Hall concentration, as found earlier for much lower doping levels. When the Hall concentration is higher than $5x10^{19}$ cm^{-3}, the integrated absorption levels off. This saturation of the LVM integrated absorption has not been reported before.

The correlation between the Hall concentration and the integrated absorption, when the Hall concentration is less than 5×10^{19} cm^{-3}, gives a value for the conversion factor (f) of $(12.4\pm2.5)\times10^{15}$ cm^{-1}. This value is in agreement with the value $(13\pm3)\times10^{15}cm^{-1}$ reported by Sargent et al. [6]. Figure 4-3 shows the results from this study along with the results of Alt et al. [9] obtained at much lower concentrations. This figure demonstrates the wide doping range (which has been substantially extended by our measurements) over which the strength (IA) of the LVM band is a good measure of the carbon concentration in GaAs:C.

We find (Fig.4-2) that at very high doping, the proportionality between *p* and the LVM IA no longer holds. One previous study of heavily-doped GaAs:C reported that *p* dropped below [C] by as much as 40% for doping larger than 10^{19} cm^{-3}[10]. Also, after annealing at temperatures higher than 600°C, the carrier concentration and the mobility have been found to decrease in heavily-doped GaAs:C (1.3×10^{20} cm^{-3}) but to remain the same at somewhat lower doping (3.5×10^{19} cm^{-3})[11]. These results might be caused by

the formation at high doping of di-carbon defects, in which pairs of carbon atoms bond to each other [12]. Di-carbon defects acts as donors instead of acceptors since they effectively have six valence electrons, so that their presence is expected to reduce the hole concentration in GaAs:C.

Our results do not support the presence of a significant concentration of di-carbon defects in our samples, since *p* remains essentially equal to [C] at our highest dopings (Table 4-1). Since nearly all of the carbons are acting as acceptors, they are evidently present as C_{As}. Using the LVM-absorption conversion factor f of 1.24×10^{16} cm^{-1} (Fig. 4-2 and 4-3), we show in Fig. 4-4 the infrared-derived concentration $[C_{As}]_{LVM}$ plotted against p on a log-log scale. The saturation of $[C_{As}]_{LVM}$ at high p was noted earlier in connection with the IA-versus-p plot of Fig. 4-2, where it is clearly seen on a linear plot. The log scale of Fig. 4-4 allows us to include results estimated from the work of Wagner et al. [13], Shirakashi et al. [14], and Woodhouse et al. [15]. Their results also show the saturation in $[C_{As}]_{LVM}$ at very high doping, although those authors took little note of this effect.

A cluster that could form at high [C] without reducing p/[C] is the (C_{As}-C_{As}) cluster discussed in the work of Goss et al. [16]. The carbons in this cluster (both of which act as acceptors) are at nearby arsenic sites, substituting for arsenics that share an intervening nearest-neighbor gallium. Schematically, C_{As}-C_{As} is the replacement of Ga-As-Ga-As-Ga-As-Ga-As- by –Ga-As-Ga-C-Ga-C-Ga-As-. The vibrational modes of the C_{As}-C_{As} complex have not been investigated. The oscillator strength of the C_{As}-C_{As} LVM infrared band may be partly shifted to frequencies outside of the C_{As} LVM band near 580 cm^{-1}. Also the oscillator strength of the C_{As}-C_{As} band may be smaller than twice

the oscillator strength of the C_{As} band. Either of these conditions (neither of which is implausible) would account for the saturation of the infrared-determined $[C_{As}]_{LVM}$ at very high doping. In any case, from the practical viewpoint, the saturation limits the use of the LVM technique as a measure of $[C_{As}]$ of doping below about 6×10^{19} cm^{-3} (Fig.4-2).

Figure 4-5 shows the increase of the LVM-band linewidth with increasing carbon concentration. Possible interpretations include the increased disorder or the lattice contraction caused by carbon doping. Note that as the linewidth increases for *p* above 5×10^{19} cm^{-3}, the integrated absorption (as discussed above) levels off, as the increase in FWHM is compensated by the decrease in peak height.

4.5 Summary

The localized vibrational mode of C_{As} in MBE-grown GaAs:C films was studied by infrared transmittance, to very high carbon doping levels. The strength (infrared absorption) of the LVM infrared absorption band has been used as a measure of the hole concentration in GaAs:C at lower doping, and our work shows that the linear relation between the LVM-band integrated absorption (IA) and the carrier concentration (p) extends to higher doping ($\approx5\times10^{19}$ cm^{-3}) than previously known. Over this range, $p=[C_{As}]=f\times(IA)$, with the conversion factor $f = (12.4\pm2.5)\times10^{15}$ cm^{-1}, in good agreement with the value found at low doping. Above $p = 5\times10^{19}$ cm^{-3}, the LVM-band IA saturates and levels off as p increases. This may be caused by a decrease in infrared oscillator strength per C_{As} as C_{As}-C_{As} clusters form at very high doping.

References

1 A. S. Barker Jr.and A. J. Sievers, Rev. Mod. Phys. 47, S40 (1975).

2 R. C. Newman, in *Infra-Red Studies of Crystal Defects* (Taylor & Francis Ltd, London, 1973), p.13.

3 Y. Homma, Y. Ishii, T. Kobayashi, J. Osaka, J. Appl. Phys. **57**, 2931 (1985).

4 Jiang Dasheng, Song Chungying, Zheng Jiefei, and Hsu Chenchia, Chin. Phys., **6**, 749 (1986).

5 M. R. Brozel, E. J. Foulkes, R. W. Series, and D. T. J. Hurle, Appl. Phys. Lett. **49**, 337 (1986).

6 L. Sargent and J. S. Blakemore, Appl. Phys. Lett. **54**, 1013 (1989).

7 S. B. Saban, J. S. Blakemore, P. E. R. Nordquist, R. L. Henry, and R. J. Gorman, J. Appl. Phys. **72**, 2505 (1992).

8 W. K. Liu, K. Bacher, F. J. Towner, T. R. Stewart, C. Reed, P. Specht, R. C Lutz, R. Zhao, E. R. Weber, J. Vac. Sci. Technol. B **17**, 1200 (1999).

9 H. Ch. Alt, B. Wiedemann, J.D. Meyer, R. W. Bethge, in *Proceeding of the 10th conference on semiconducting and insulating materials (SIMC-X), Berkeley, 1998.* edited by Z. Liliental-Weber and C. Miner (IEEE, Inc.,1999), p. 53.

10 T. J. de Lyon, J. M. Woodall, M. S. Goorsky, and P. D. Kirchner, Appl. Phys. Lett. **56**, 1040 (1990).

11 K. Watanabe and H. Yamazaki, Appl. Phys. Lett. **59**, 434 (1991).

12 B. R. Davidson, R. C. Newman, C. D. Latham, R. Jones, J. Wagner, C. C. Button, and P. R. Briddon, Phys. Rev. B **60**, 5447 (1999).

13 J. Wagner, K. H. Bachem, B. R. Davidson, R. C. Newman, T. J. Bullough, and T. B. Joyce, Phys. Rev. B **51**, 4150 (1995) .

14 Jun-ichi Shirakashi, Thshiaki Azuma, Fumihiko Fukushi, Makoto Konagai, and Kiyoshi Takahashi, J. Cryst. Growth **150**, 585 (1995).

15 K. Woodhouse, R. C. Newman, T. J. de Lyon, J. M. Woodall, G. J. Scilla, and F. Cardone, Semicond. Sci. Technol. **6**, 330 (1991).

16 J. P. Goss, R. Jones, S. Öberg, and P. R. Briddon, Phys. Rev. B **55**, 15576 (1997).

Table 4-1. Integrated absorption (IA) and FWHM of each GaAs:C sample

Sample	p (10^{19} cm^{-3})	[C] (10^{19} cm^{-3})	IA (10^{3} cm^{-2})	FWHM (cm^{-1})
10981.02	0.014	-	-	-
10983.02	0.39	-	0.50	3.4
10514.02	0.52	-	0.77	3.9
10980.02	0.67	-	0.94	3.7
10979.02	2.0	-	2.3	4.5
10525.02	2.7	2.6	2.3	3.6
10985.02	3.3	-	3.0	4.2
10977.02	6.6	-	5.3	5.5
10355.02	8.2	-	6.0	5.5
10986.02	9.1	-	5.5	5.2
10511.02	10.5	9.9	4.8	5.5
10512.02	13.6	13.0	6.6	8.2

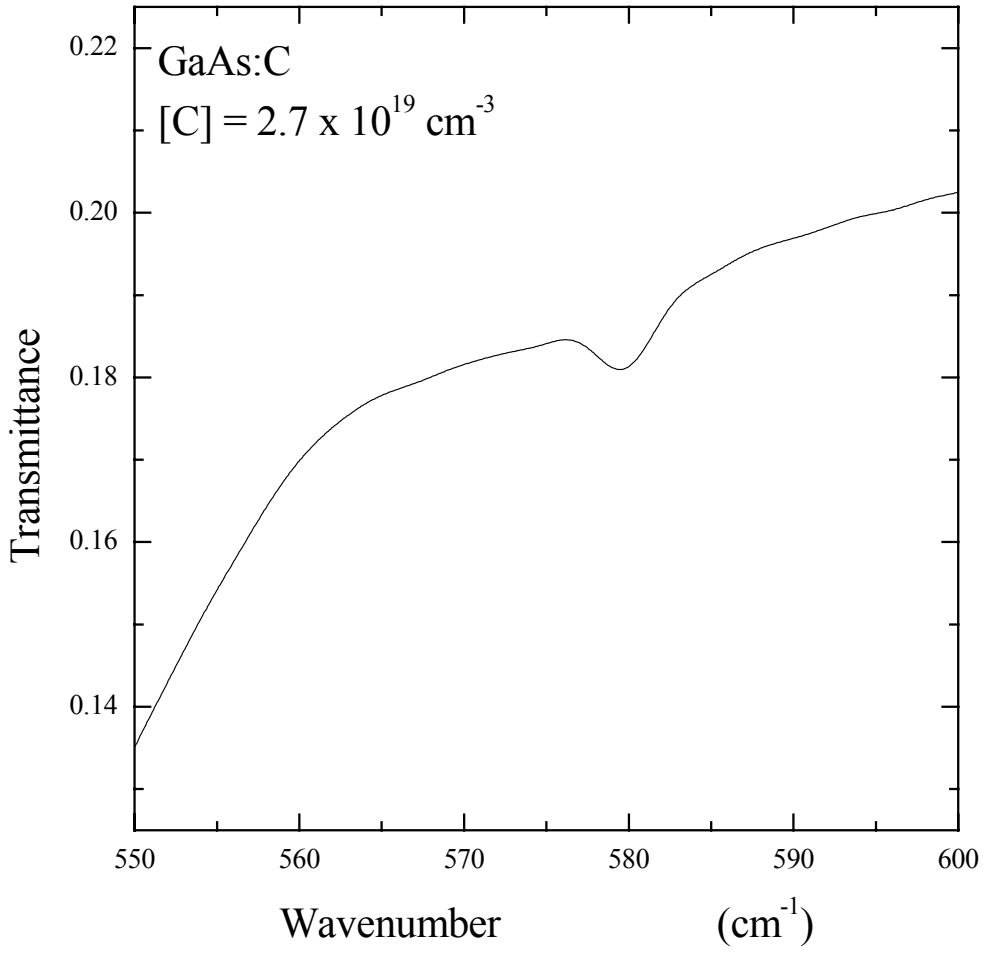

Figure 4-1. Infrared transmittance spectrum of the GaAs:C sample with carbon concentration $2.7 \times 10^{19} cm^{-3}$ showing the transmittance dip associated with the LVM band.

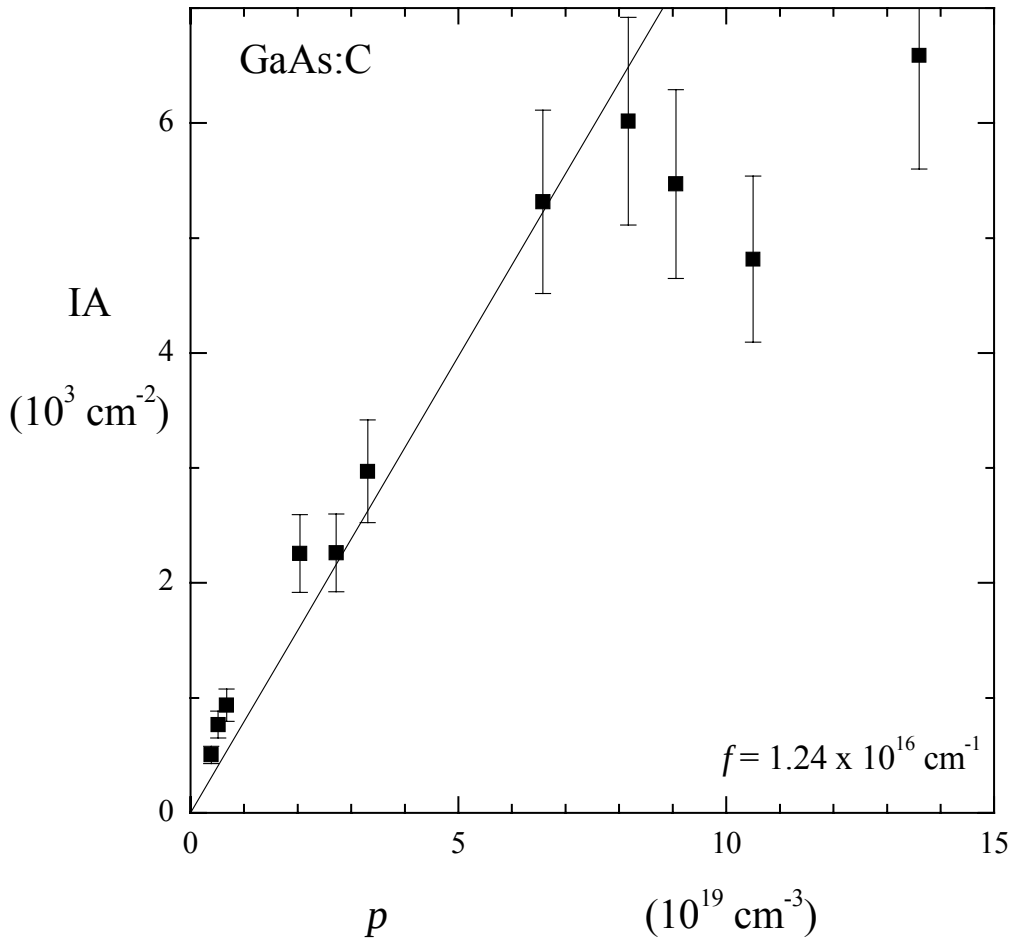

Figure 4-2. The integrated absorption of the carbon-induced localized-vibrational-mode, infrared band as a function of the Hall-determined carrier concentration in the MBE-grown p-type GaAs:C films. The straight line has a slope of (1/f), where f is $1.24\times10^{16}\text{cm}^{-1}$.

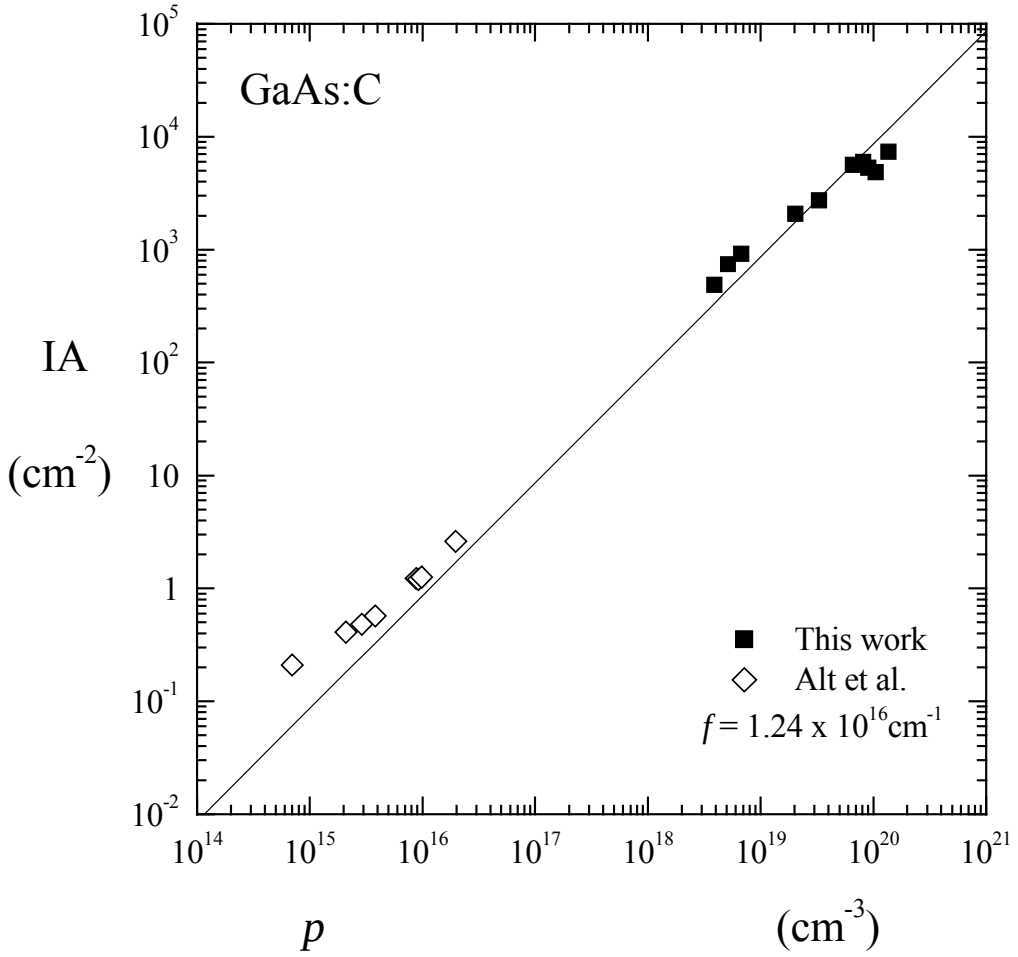

Figure 4-3. The LVM integrated absorption plotted against the hole concentration over a very wide doping range, comparing our results on the MBE GaAs:C thin films to the results obtained by Alt et al. [9] on a set of thick crystals grown from the melt. The line corresponds to a value of $1.24\times10^{16}\text{cm}^{-1}$ for the conversion factor *f*.

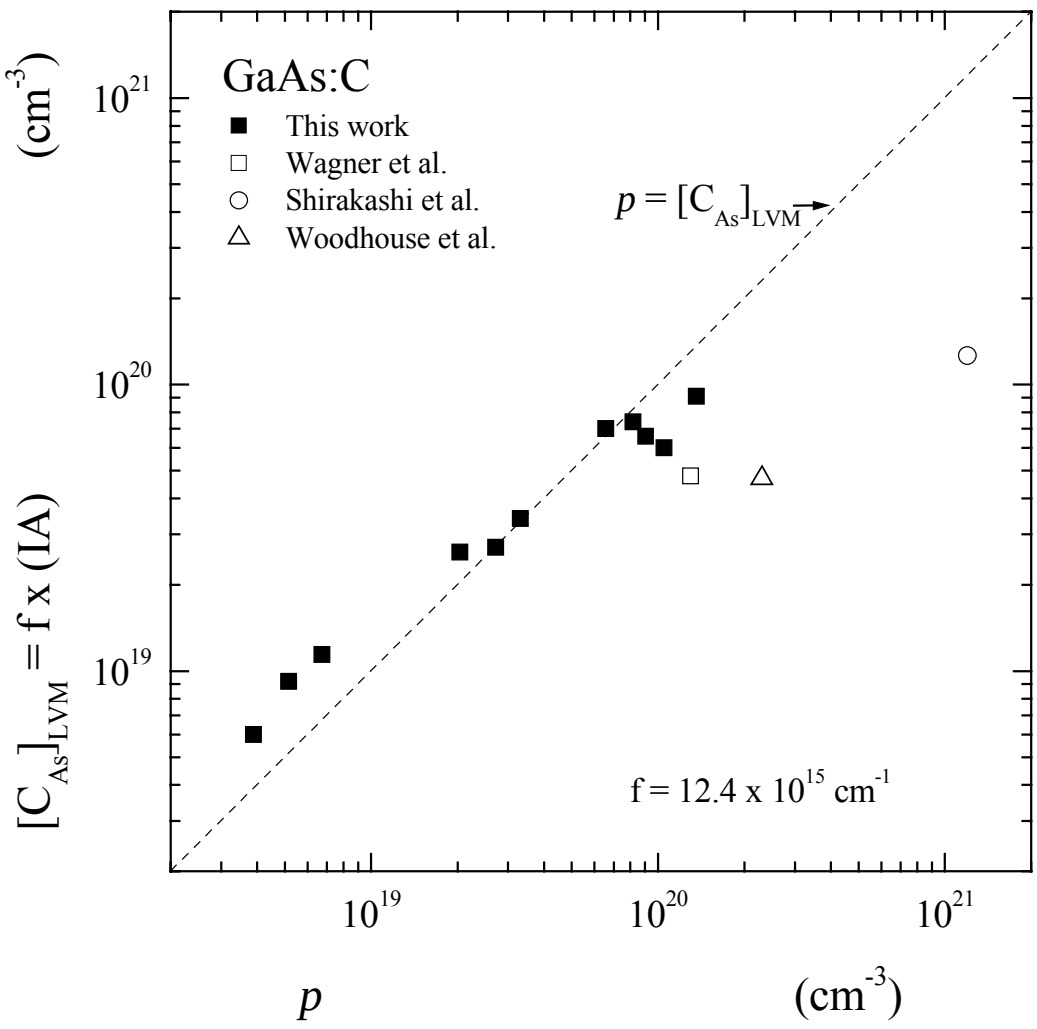

Figure 4-4. The infrared-estimated carbon concentration, $[C_{As}]_{LVM}$, as a function of the Hall-determined hole concentration in GaAs:C. The closed squares are our results, the open symbols are results reported by Wagner et al.[13], Shirakashi et al.[14], and Woodhouse et al. [15].

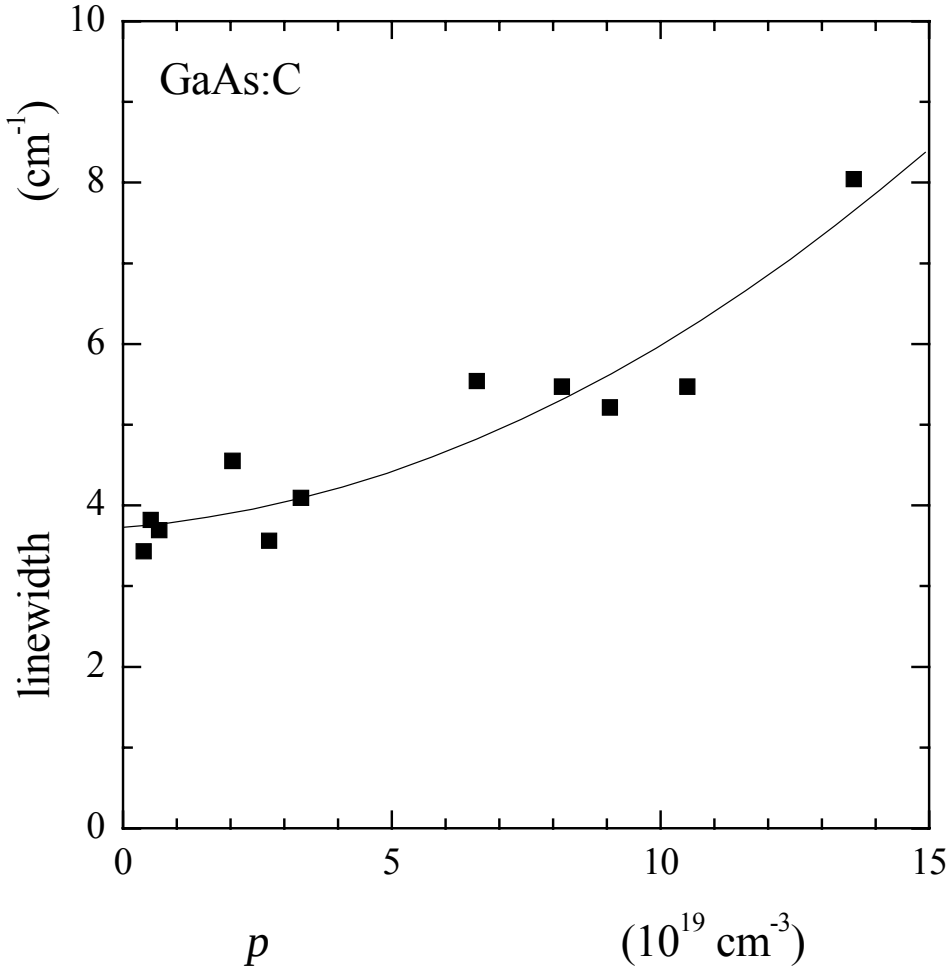

Figure 4-5. The linewidth (full width at half maximum) of the LVM infrared band, as a function of carrier concentration.

Chapter 5. The localized vibrational mode of carbon in LT-GaAs:C.

5.1 Introduction

Recently, LT-GaAs (GaAs grown by molecular beam epitaxy with the substrate at low temperature, i.e. significantly lower than the standard growth temperature of 600 C) has become an interesting material because of its properties. Studies on LT-GaAs have found that it has excess As (1%-1.5%) in the form of arsenic antisite (As_{Ga}, an arsenic atom occupying a site normally occupied by gallium), high resistivity (10^2 Ω-cm), and very short photoexcited carrier lifetime (150 fs).

These characteristics make LT-GaAs very useful as a buffer layer in GaAs-based-metal-semiconductor field effect transistors. It has been shown that a buffer layer of LT-GaAs can eliminate sidegating and backgating in integrated circuits [1]
Most studies on LT-GaAs have been done on undoped samples, but several studies of doped material have recently appeared [2-5]. Undoped LT–GaAs has a slightly larger lattice constant than that of bulk GaAs, and doping it with the correct concentration of suitable impurity can reduce the lattice distortion. For a growth temperature of 250 °C, the lattice distortion is removed if the LT-GaAs is grown as doped LT-GaAs:Be with a Be concentration of 2×10^{19} cm^{-3} [3]. Also, Be doped LT-GaAs can maintain short carrier trapping times after annealing at temperatures as high as 700 °C, while undoped LT-GaAs shows an increasing in trapping time with annealing [3]. However, after annealing at a temperature of 600 C or higher, free holes are activated into the valence band, reducing the resistivity by as much as 5 orders of magnitudes. The material is changed from semi-insulating to p-type semiconducting [3,4]. In other words, LT-GaAs:Be is thermally unstable at high temperature. For LT-GaAs:C, the situation appears to be

different. A recent study reports a fair degree of stability (of the insulating properties of LT-GaAs:C) with respect to annealing: resistivity higher than 10^4 Ω-cm after 700 C anneal[2]. Annealing experiments on LT-GaAs:C form part of this dissertation; they are described in chapter 9.

One way to determine the spectroscopic fraction of dopants occupying electrically active substitutional sites is through localized-vibrational-mode (LVM) study. Studies in Be-doped and Si-doped LT-GaAs reveal that only a fraction of the dopant are at active sites [4,5] and this fraction decreases with decreasing temperature. Since LT-GaAs has a much higher defect density than standard GaAs (grown at about 600 C), we expect that the LVM absorption spectra of LT-GaAs should be significantly different. Thus the accepted conversion factor used in infrared absorptivity studies of standard GaAs is inapplicable. The objective of the study reported here is to estimate the fraction of carbon atoms occupying arsenic sites (acceptor sites) at various growth temperatures and to study the behavior of the LVM infrared absorption band with changing growth temperature and doping concentration.

5.2 Samples and Experiment

The samples used in this study are MBE-grown GaAs:C on SI GaAs substrate with orientation 2° off (100). All samples were grown at Quantum Epitaxial Designs (QED, now IQE) using EPI GEN II MBE reactor with a custom-designed CBr_4 source at an As to Ga beam equivalent pressure (BEP) ratio of 20. The substrate temperature was controlled by a thermocouple close to the substrate. The one-micron thick film of MBE-grown LT-GaAs:C was deposited on a 2500-angstrom MBE GaAs buffer layer that was first grown on the substrate. Secondary Ion Mass Spectroscopy (SIMS) measurements

were used to estimate the carbon concentrations of the samples. The main controlling factors determining the properties of these samples are the substrate temperature during growth and the doping concentration. A first set of samples was grown at a fixed substrate temperature of approximately 240 C, with different carbon concentration ranging from $2x10^{19}$ cm^{-3} to $8x10^{19}$ cm^{-3}. A second set of samples was prepared that maintained a carbon concentration of about 6×10^{19} cm^{-3}, with different growth temperatures ranging from 225°C to 480°C.

Far infrared transmission spectra of the samples were measured using Bomem DA3.01 Fourier transform spectrometer. The region of interest, containing the localized vibrational modes of the light carbon impurity atoms, is from 550 cm^{-1} to 600 cm^{-1}. The sample was held at normal incidence to the incident beam, which filled an aperture of 5 mm diameter. The system was operated at a resolution 4.0 cm^{-1} with scan speed of 0.1 cm/sec. To reduce noise, ten transmittance spectra were obtained for each sample, and the results averaged. Figures 5-1 and 5-2 show the transmittance spectra in the LVM region of LT-GaAs:C films grown at different growth temperatures and grown with different doping concentrations, respectively. Figure 5-1 shows the results for the growth-temperature series at constant doping; Figure 5-2 shows the results for the doping series at constant growth temperature.

The LVM absorption coefficient is determined from the transmittance using the relation

$$\alpha_{LVM} + \alpha_0 = -\frac{1}{d}\ln(T) \qquad (5\text{-}1)$$

Here T is the transmittance, d is the thickness of the MBE layer, and α_0 is the slowly – varying background absorption coefficient accounting for the substrate absorption and the

reflection losses. α_0 is estimated from the transmittance of the undoped sample. The integrated absorption and the FWHM line width of the LVM band is determined for each samples. The results are given in Table 5-1.

5.3 Discussion

Figure 5-3 compares the transmittance of undoped bulk GaAs, undoped LT-GaAs grown at 240 C, LT-GaAs:C grown at 240 C, and normal GaAs:C grown at 600 C. The two GaAs:C samples have a carbon concentration at about 6 x10^{19} cm^{-3}.The last three samples have the same film thickness of one micron. In this spectral region, the overall transmittance level of LT-GaAs is close to that of bulk GaAs, except for the LVM feature. The overall transmittance level of normal GaAs:C is much lower, because of free-carrier (hole) absorption. This demonstrates the lack of free carriers in LT-GaAs:C. Electrons from native defects in the disordered LT material, such as arsenic antisites, compensate the free holes induced by carbons at arsenic sites. The concentration of arsenic antisites in undoped LT-GaAs grown at 240 C, estimated by Raman scattering, is 2.1×10^{20} cm^{-3}[chapter 6]. This arsenic-antisites (As_{Ga}) concentration is enough to compensate the free holes activated by carbon doping (C_{As} acceptors).

Figure 5-4 shows a plot of the integrated absorption (IA) against the growth temperature, obtained from the transmittance spectra of Fig.5-1. The integrated absorption of the carbon-impurity LVM absorption band increases with increasing growth temperature. Extrapolation of the linear fit indicates that the LVM band disappears at about 145 C. These results show that only a small fraction of the carbons occupy arsenic sites in LT-GaAs, and this fraction increases as the growth temperature increases. At a growth temperature lower than 145 C, none of the carbon atoms appear to

be at arsenic sites. At the other side of Fig. 5-4, for 400 C growth temperature, the LVM band is not observable because it is masked by strong free carrier absorption. Our Raman-scattering study of LT-GaAs [chapter 7] shows that when the growth temperature reaches 400 C, the sample changes from LT-GaAs:C to normal GaAs:C; i.e., free holes are activated. At growth temperatures higher than this, the hole concentration (determined from Hall-effect measurements) is comparable to the doping concentration (estimated from SIMS measurements), indicating that all of the carbons are at arsenic sites. Therefore, we conclude that essentially 100% of the carbons are at arsenic site once the growth temperature reaches 400 C. As shown in Fig. 5-4, as a crude but reasonable, approximate, working assumption, we assume the linear relation between active fraction ($[C_{As}]/[C]$) and the growth temperature that is shown in Fig. 5-4. Using this as a guide, we estimate that the activation fraction is about 45% for a growth temperature of 260 C.

As in normal GaAs, the strength of the carbon impurity LVM absorption band increases with increasing carbon concentration. Figure 5-5 shows the results for the increase in LVM integrated absorption with doping concentration (for a growth temperature of 240 C), obtained from the transmittance spectra of Fig. 5-2. Since $IA \sim [C_{As}]$, the roughly linear dependence of IA and [C] indicates that the active fraction $[C_{As}]/[C]$ does not change significantly over the doping range of Fig. 5-5. From Fig. 5-4, $[C_{As}]/[C]$ is estimated to be about 37% for T_{growth}=240 C.

The FWHM linewidth of the LVM band decreases with increasing growth temperature. This is seen in Fig. 5-1 and the linewidth results are displayed in Fig. 5-6. As the growth temperature increases, the native concentration of defects decreases. The crystal becomes less disordered, closer to normal GaAs:C.

In the concentration series (Fig. 5-2) the linewidth of the LVM band increases as the doping concentration increases. Figure 5-7 shows the increase in linewidth with doping concentration. This increase in LVM damping, as [C] increases, may be connected with the contraction of GaAs:C lattice that is produced by carbon doping, as well as with the increased disorder that accompanies a larger impurity concentration.

5.4 Summary

The infrared absorption of the localized vibrational mode that is a signature of substitutional carbon (C_{As}) in LT-GaAs:C has been studied as a function of growth temperature (T_{growth}) and doping level ([C]). The results show that only a modest fraction (typically30-40%) of the carbon impurity atoms occupies electrically active (acceptor) arsenic sites. Extrapolation of the integrated-absorption results indicates that the active fraction, $[C_{As}]/[C]$, is negligible in LT-GaAs grown below 145 C. At growth temperatures higher than 400 C, the samples are essentially similar to normal GaAs:C, with $[C_{As}] \approx [C]$. (This follows from Hall and SIMS measurements, as well as from Raman measurements presented in Ch. 7.) For LT-GaAs:C grown at 260 C, we estimate the fraction of carbons at arsenic sites to be about 45%. The linewidth of the LVM band decreases with increasing growth temperature. We attribute this to the reduction of native defects. With increasing doping concentration (for fixed growth temperature), the LVM linewidth increases. This may be connected with the contraction of the lattice that is produced by carbon doping, as well as by the doping-induced disorder.

References

1. F. W. Smith, Mat. Res. Symp. Proc. **241**, 3 (1992).
2. W.K. Liu, K. Bacher, F.J. Towner, T.R. Stewart, C. Reed, P. Specht, R.C. Lutz, R. Zhao, E.R. Weber, J.Cryst. Growth **201/202**, 217, 1999.
3. P. Specht, R.C. Lutz, R. Zhao, E.R. Weber, W.K. Liu, K. Bacher, F.J. Towner, T.R. Stewart, M. Luysburg, J. Vac. Sci. Technol. B **17**, (1999).
4. D.E. Bliss, W. Walukiewicz, J.W. Ager, III, E.E. Haller, K.T. Chan, S. Tanigawa; J. Appl. Phys. **71**, 1699 (1992).
5. M. O. Manasreh, K. R. Evans, C. E. Stutz, D. C. Look, J. Hemsky, Appl. Phys. Lett. **60**, 2377 (1992).

Table 5-1. Results of the infrared measurements on the LVM absorption band in the LT-GaAs:C samples.

Sample number	T_{growth} (C)	[C] ($10^{19}cm^{-3}$)	α_{max} (10^{2} cm^{-1})	Linewidth (cm^{-1})	IA (10^{3} cm^{-2})
11858.02	225	6	4.4	14	7.0
11856.02	240	6	5.8	14	8.2
11855.02	260	6	6.5	12	8.6
11857.02	330	6	13.5	10	15.6
11854.02	600	6	8.5	5.9	5.1
11772.02	240	undoped	-	-	-
11776.02	240	2	2.0	9.3	2.0
11775.02	240	4	3.5	13	5.1
11774.02	240	6	5.1	14	7.5
11777.02	240	8	7.3	18	14.7

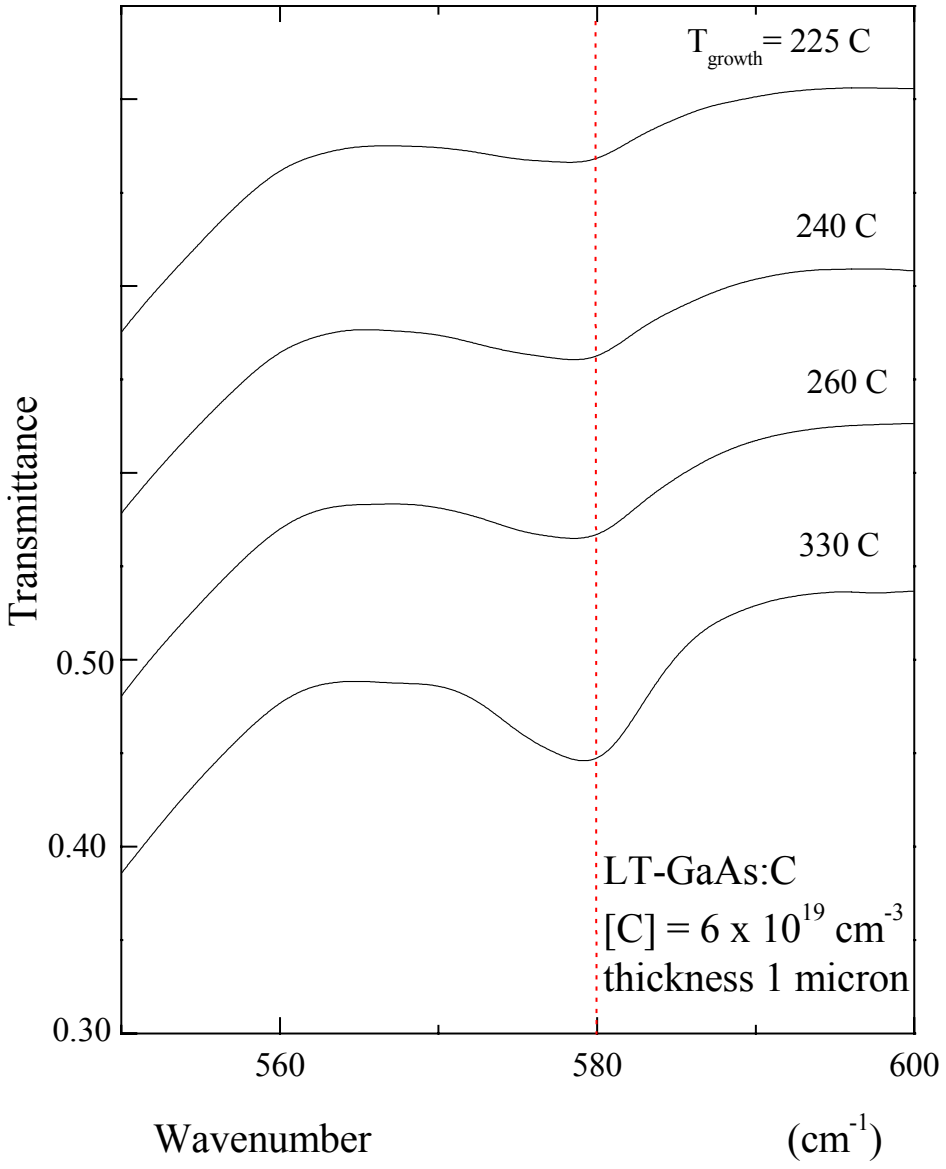

Figure 5-1. Transmittance spectra of LT-GaAs:C for different growth temperatures, for a series of films of thickness 1.0 micron and carbon concentration 6×10^{19} cm^{-3}. The transmittance scale is shown for the 330 C sample; the other spectra are successively shifted upward by 0.10, for clarity.

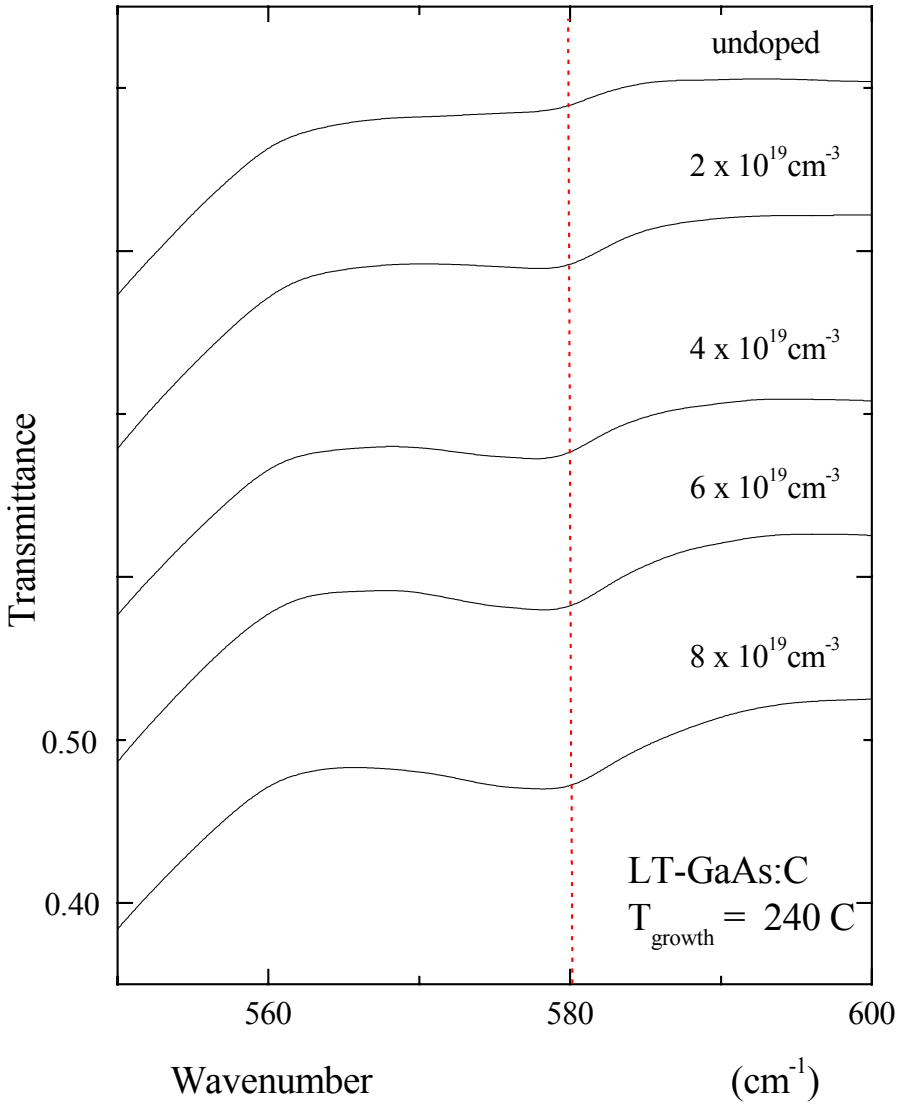

Figure 5-2. The transmittance spectra of LT-GaAs:C at different doping concentrations, for a series 1.0-micron films grown at about 240 C. The transmittance scale is shown for the 8×10^{19} cm^{-3} sample; the other spectra are successively shifted upward by 0.10, for clarity.

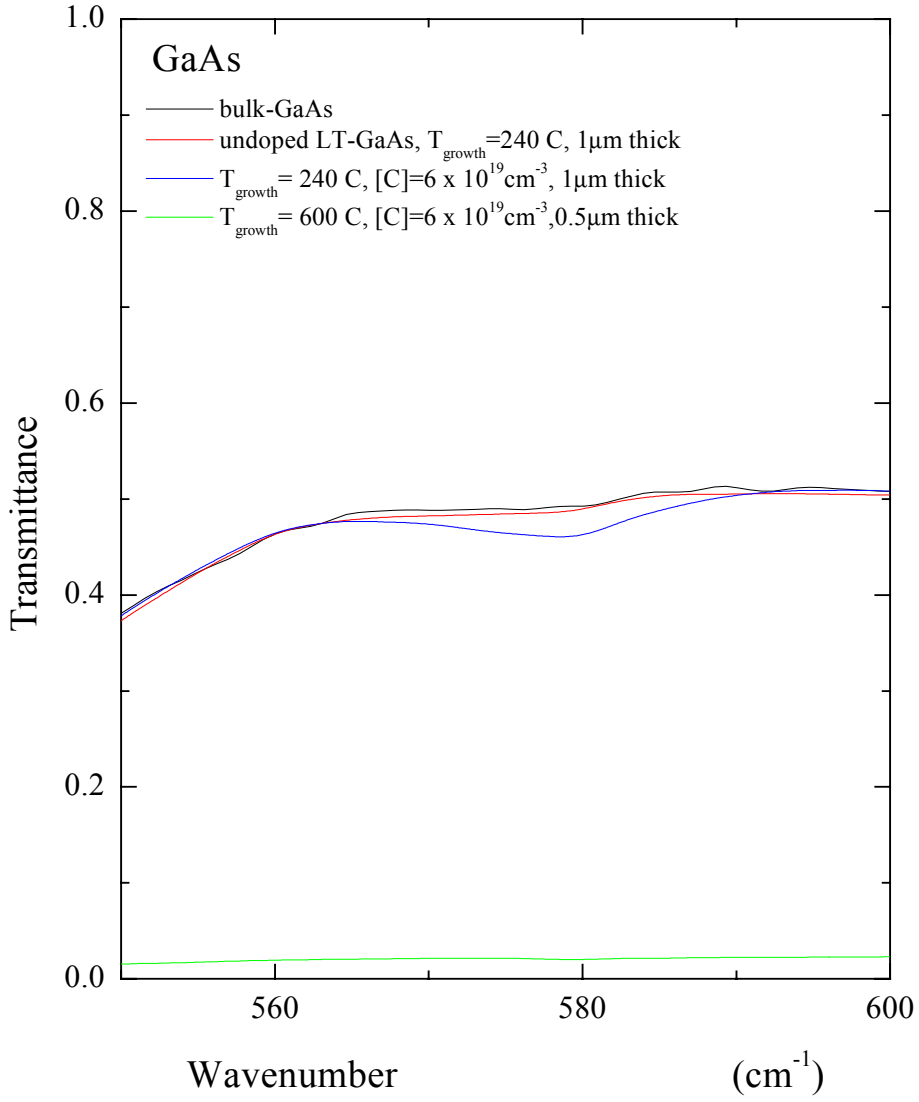

Figure 5-3. Transmittance of carbon-doped and undoped LT-GaAs compared to bulk GaAs and normal GaAs:C over the LVM band. The transmittances of LT-GaAs are the same as the transmittance of the bulk GaAs except for the absorption band of the LVM. The transmittance of normal GaAs:C is much lower because of the absorption by free holes.

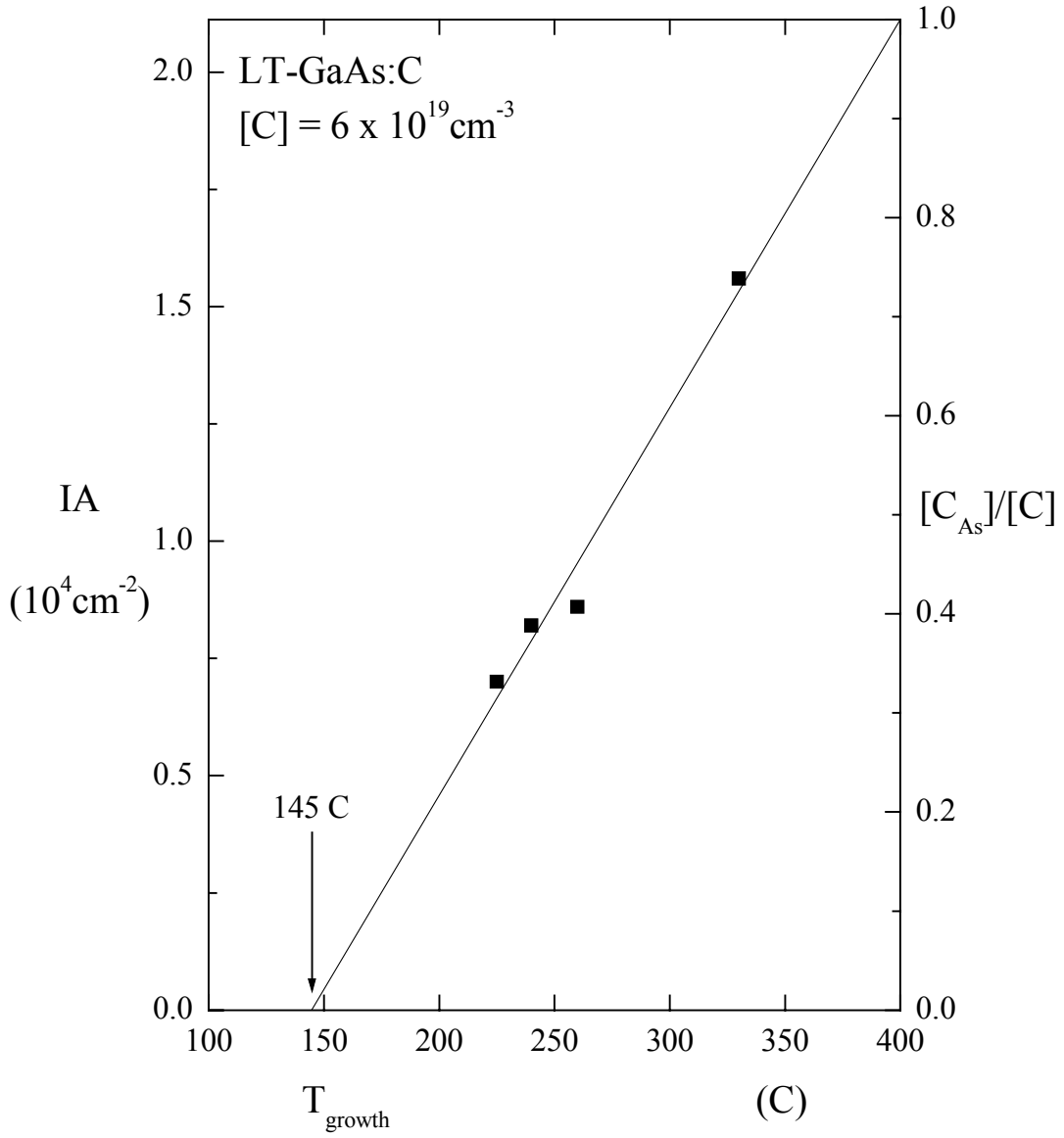

Figure 5-4. The integrated absorption of the LVM band in LT-GaAs:C samples grown at different temperatures, for films having a carbon concentration of 6×10^{19}cm^{-3}. These results correspond to the transmittance spectra of Fig. 5-1

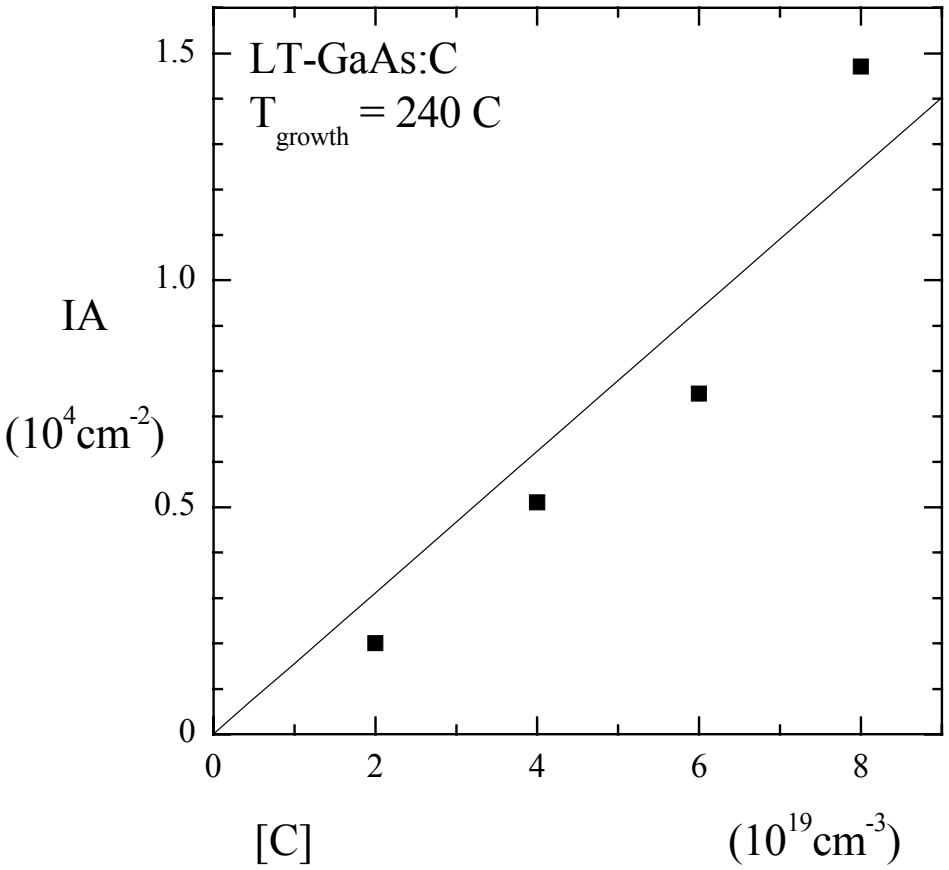

Figure 5-5. The integrated absorption of the LVM band in LT-GaAs:C samples prepared with different doping concentrations, for films grown at 240 C. These results correspond to the transmittance spectra of Fig. 5-2.

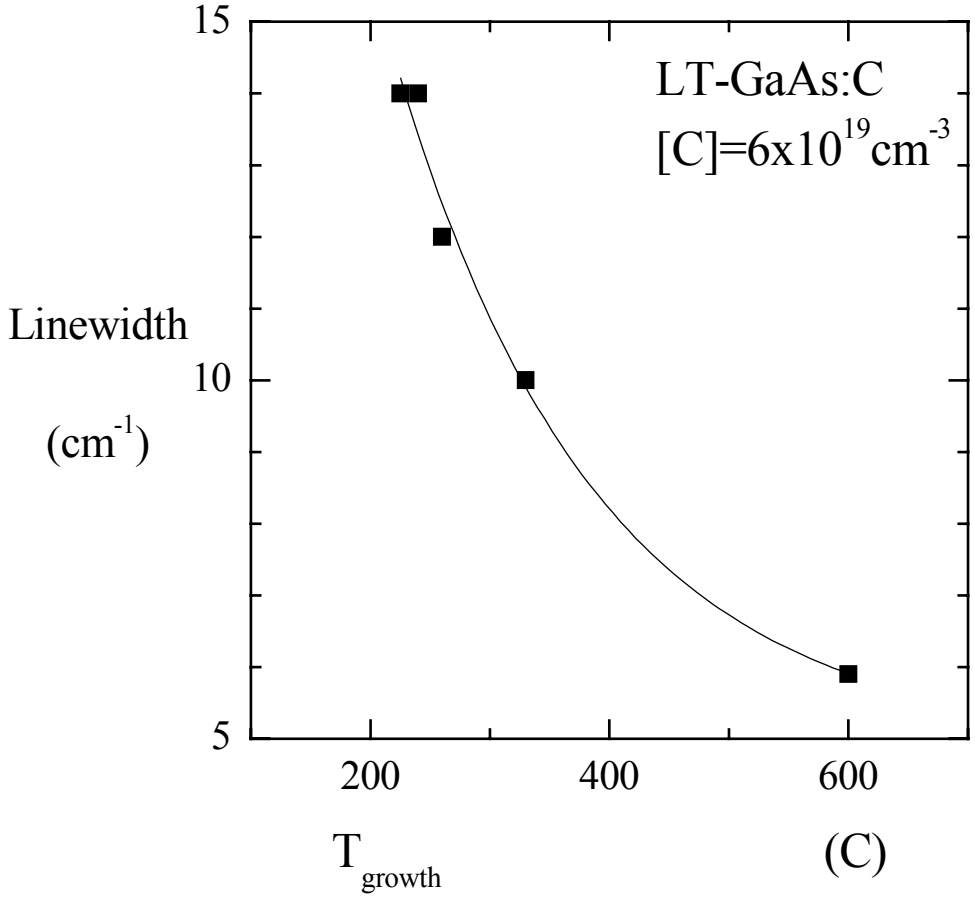

Figure 5-6. The linewidth of the LVM band in LT-GaAs:C samples grown at different temperatures, for one-micron films having a carbon concentration of $6\times10^{19}cm^{-3}$. These results correspond to the transmittance spectra of Fig. 5-1. There are no data in the region from 330 C to 600 C because of the absorption by free carriers (holes). The result for the sample grown at 600 C comes from a 0.5-micron thick film.

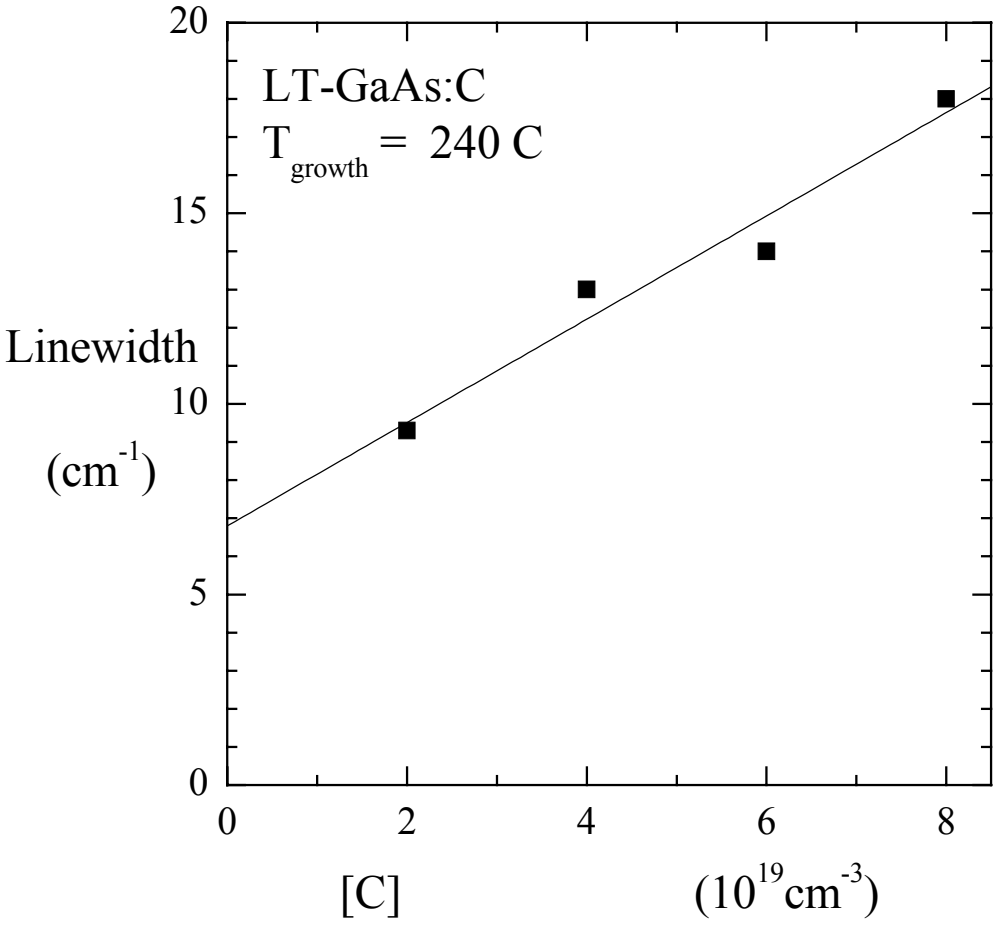

Figure 5-7. The linewidth of the LVM band in LT-GaAs:C samples prepared with different doping concentrations, for films grown at 240 C. These results correspond to the transmittance spectra of Fig. 5-2.

Chapter 6. Raman study of undoped LT-GaAs

6.1 Introduction

Previous studies of low-temperature-grown GaAs (LT-GaAs in short) indicated numerous point defects in the material. It has been estimated that LT-GaAs contains as much as 1-2% of arsenic-antisite defects (As_{Ga}, an arsenic atom occupying a site where a gallium atom should be). T.A. Gant et al [1] studied the Raman spectra of LT-GaAs and reported that the longitudinal optical (LO) phonon line of LT-GaAs is downshifted from that of bulk GaAs while the transverse optical (TO) phonon line remains the same. They interpreted the LO downshifted as arising from a reduced TO-LO splitting caused by a reduction of the macroscopic electric field associated with LO phonon. A competing interpretation, in which the effect is ascribed to the lattice expansion of LT-GaAs, is not indicated because lattice expansion would be expected to shift the TO and LO line equally. In their model, they considered LT-GaAs as an alloy, $Ga_{1-x}As_{1+x}$, where x is the As_{Ga} fraction, the fraction of gallium sites occupied by arsenics. Considering the material in a dielectric continuum model, the TO-LO splitting can be written as [2]

$$\omega_{LO}^2 - \omega_{TO}^2 = \omega_p^2$$
$$\omega_p^2 = \frac{4\pi q^2}{\mu \nu \varepsilon_\infty} \qquad (6\text{-}1)$$

Here ω_{TO} and ω_{LO} are the TO-phonon and LO-phonon frequencies, q is the effective ionic charge, ν is the volume of a unit cell, μ is the vibrational reduced mass, and ε_∞ is the high-frequency dielectric constant.

Since x is small, ε_∞ is taken to be the same as that of bulk GaAs. The effect of x on the optical-mode reduced mass is straightforwardly determined from the atomic masses, $\mu(x)=(1+0.037x)\mu_{GaAs}$; the coefficient of x is small because the gallium and arsenic masses are so similar. The effect of x on effective charge is to reduce it as the presence of arsenics at gallium sites substitutes homopolar As-As bonds for heteropolar GaAs bonds. The form is assumed to be $q(x)=(1-x)q_{GaAs}$.

LT-GaAs is known to have an expanded lattice relative to bulk GaAs. The lattice constant of LT-GaAs, at growth temperature 240 C is reported to be 0.03% larger than that of bulk GaAs[3], so that the unit-cell volume is about 0.1% larger than that of bulk GaAs. Using the known pressure dependence of LO and TO frequencies, Toufella et al. [5] show that the shift in both the TO and LO line, due to the lattice strain ε, is given by

$$\Delta\omega_x = -40\varepsilon$$
$$\varepsilon = \frac{a_{LT-GaAs} - a_{GaAs}}{a_{GaAs}} \qquad (6\text{-}2)$$

Here ε is the strain, $a_{LT\text{-}GaAs}$ is the lattice constant of LT-GaAs and a_{GaAs} is the lattice constant of bulk GaAs. For LT-GaAs grown at 240 C, ε is 0.0003 [3], so that the corresponding $\Delta\omega$ (from equation (6-2)) is 0.01 cm^{-1}. This is negligible in the current context, so the strain effect can be safely ignored.

In differential form, the frequency shifts of the LO and TO modes are related by

$$2\omega_{LO}\Delta\omega_{LO} - 2\omega_{TO}\Delta\omega_{TO} = \omega_p^2\left(\frac{2\Delta q}{q} - \frac{\Delta\mu}{\mu}\right) \qquad (6\text{-}3)$$

The shift in the TO line comes from two contributions, the mass disorder and the strain effect [4]. The mass effect on the TO line can be estimated as follows [4]. Assume the TO frequency can be written as

$$\omega_{TO}^2 = \frac{K_{TO}}{\mu} \tag{6-4}$$

where K_{TO} is the effective force constant describing the short-range interactions. The shift in the TO frequency due to the change in the reduced mass μ is

$$\Delta\omega_{TO} = -\frac{\omega_{TO}}{2}\left(\frac{\Delta\mu}{\mu}\right) \tag{6-5}$$

Substituting (6-5) into (6-3) yields

$$\Delta\omega_{LO} = \left(\frac{\omega_{LO}^2 - \omega_{TO}^2}{\omega_{LO}}\right)\frac{\Delta q}{q} - \left(\frac{\omega_{LO}}{2}\right)\frac{\Delta\mu}{\mu} \tag{6-6}$$

For $Ga_{1-x}As_{1+x}$, $\Delta q/q = -x$ and $\Delta\mu/\mu = 0.037x$. Providing the TO and LO frequencies as inputs into (6-6) and expressing $\Delta q/q$ and $\Delta\mu/\mu$ in terms of x yields the relation between the LO shift and the fraction of arsenic atoms at gallium sites. This relation (using the room-temperature TO and LO frequencies given in Table 6-1) is.

$$\Delta\omega_{LO} = (-51\text{cm}^{-1})x \tag{6-7}$$

In (6-7), 90% of the effect comes from Δq, the rest from $\Delta\mu$.

6.2 Experiments and results

In this experiment, an undoped, MBE-grown, LT-GaAs film was studied. The sample was grown at IQE Inc. using an EPI GEN II MBE reactor. The substrate was a standard semi-insulating GaAs wafer with surface orientation 2° off (100). The substrate temperature was controlled by a thermocouple adjacent to the substrate. The MBE growth started with a thin (250nm) buffer layer of GaAs grown at 600 C, then the temperature was reduced to 240 C and the LT-GaAs layer was grown to the thickness of 1 micron. This is a large thickness for MBE growth, and was chosen to simplify the spectroscopic measurements.

Raman spectra were measured at Virginia Tech using a SPEX 1403 scanning double monochromator with photomultiplier detection in photon-counting mode. The sample was set in nearly-back-scattering geometry. The slit width of the monochromator was 300 microns, corresponding to a resolution of 3.4 cm^{-1}. The laser line used for excitation was is the Ar^{+} blue line at 488 nm, operated at a power of 500 milliwatts at the laser head (about 30-40 milliwatts at the sample). The Raman spectra of both the front side (LT-GaAs) and the backside (SI-GaAs) were taken, the latter to provide a convenient comparison with standard bulk GaAs observed under the same experimental conditions. The measured positions of the TO and LO lines are given in table 6-1.

6.3 Discussion

From table 6-1, the LO and TO frequencies observed for LT-GaAs are 290.6 and 267 cm^{-1} respectively, compared to 291.05 and 267 cm^{-1} for bulk GaAs. No shift is observed for the weak TO line, which is consistent with the results obtained by Gant et al

[1]. As discussed earlier, the shift in the TO line comes from two contributions, mass disorder and strain effect [4]. The strain effect is too small to be observed. For the mass effect, substituting $\Delta\mu/\mu = 0.037x$ into (6-5) yields $\Delta\omega_{TO}$=-5.4x. With the fraction of arsenic atoms at gallium site under 2% (x≈0.02), the shift in the TO line is under 0.1cm^{-1}. Considering the weakness of the TO line, this shift cannot be observed.

The LO spectral line, on the other hand, is very strong and sharp and clearly shows a reproducible shift which we estimate to be –(0.45±0.1) cm^{-1}. From equation (6-7), this downshift translates into an As_{Ga} fraction x given by (-0.45 cm^{-1})/(-51 cm^{-1})=0.009. The molecular density (number of GaAs units per unit volume) in GaAs is 2.2×10^{22} cm^{-3} [6], so that $Ga_{1-x}As_{1+x}$=$Ga_{0.991}As_{1.009}$ corresponds to an arsenic-at-gallium site concentration [As_{Ga}] of 2×10^{20} cm^{-3}. Figure 6-1 compares this result with [As_{Ga}] estimates reported in previous studies of LT-GaAs by Liliental-Weber et al. [3,7] and Lee et al. [8]. Our result is in agreement with the work of Lee et al. [8].

Our infrared-transmission studies (chapter 5) and Raman-scattering studies (chapter 7) of carbon-doped MBE-grown LT-GaAs films shows that at growth temperatures up to about 400 C, the LT-GaAs:C films remain insulating. For LT-GaAs:C films grown at 240 C with a carbon doping concentration of 8×10^{19} cm^{-3}, the infrared studies show that about 37% of the carbon atoms occupy arsenic sites and act as acceptors, introducing about 3×10^{19} cm^{-3} holes in the valence band. For these films to remain semi-insulating, there must be at least 1.5×10^{19} cm^{-3} As_{Ga} donor defects (As_{Ga} is a double donor) compensating the holes introduced by the C_{As} acceptors. This confirms that in LT-GaAs, there are plenty of As_{Ga} defects present to compensate the free holes

induced by carbon doping. If [As_{Ga}] decreases with growth temperature at the rate indicated (Fig. 6-1) by the results of Lee et al.[8], at T_{growth}=330 C , [As_{Ga}] should be approximately 5×10^{19} cm^{-3}, Still large enough to compensate the C_{As} acceptors in LT-GaAs:C films doped in the 10^{19} cm^{-3} range, such as those discussed in chapter 5 and 7. However, when T_{growth} reaches 400 C, Lee et Al. estimate that the antisite-defect concentration [As_{Ga}] drops to about 2×10^{19} cm^{-3}. This is not enough to compensate the holes introduced by doping with carbon to 6×10^{19} cm^{-3}. In fact, Hall measurements performed on LT-GaAs:C doped to this level and grown at 400 C shows that this material is conducting and has a Hall concentration which is roughly the same as the doping concentration, showing that there is little compensation. This indicates that at a growth temperatures of 400 C, [As_{Ga}] is reduced to a level at least an order of magnitude smaller than 6×10^{19} cm^{-3}. If we take this level to be roughly $5\times10^{18}cm^{-3}$, this is a factor of 4 lower than the estimate of Lee et al. Thus our Hall-effect results on LT-GaAs:C generally support the [As_{Ga}]-versus-T_{growth} estimates of Lee et al. (in preference to the much steeper drop off of Liliental-Weber et al.), but suggest a somewhat greater reduction in [As_{Ga}] at T_{growth}= 400 C.

6.4 Summary

Raman-scattering measurements were carried out on an MBE-grown undoped LT-GaAs film (T_{growth} = 240 C) and, using the same experimental conditions, compared to Raman measurements made on the bulk-GaAs (semi-insulating) substrate. There is a small but definite downshift in the frequency of the longitudinal-optical (LO) phonon in LT-GaAs. The transverse-optical (TO) phonon frequency shows no discernible shift. Treating LT-GaAs, with its many As_{Ga} antisite defects, as $Ga_{1-x}As_{1+x}$, we consider several

mechanisms by which the excess-arsenic fraction (*x*) could influence the TO-LO splitting and find (like Gant et al.[1]) that the main contribution comes from the reduction in vibrational effective charge caused by the substitution of homopolar As-As bonds for heteropolar Ga-As ones. From equation (6-7), which includes the small contribution arising from the reduced-mass change as well as the main contribution arising from effective-charge reduction, we use the LO downshift to estimate the fraction of gallium sites occupied by excess arsenic atoms to be 0.009. This estimate supports recent results reported by Lee et. al.[8], as shown at the upper left of Fig 6-1. This figure indicates the decrease of [As_{Ga}] with T_{growth} for LT-GaAs. In addition to our Raman-derived result for undoped LT-GaAs at T_{growth}= 240 C, results obtain for carbon-doped LT-GaAs (chapter 5 and 7) show that this material is no longer insulating but is instead p-type when T_{growth} is raised to 400 C. From this observation and the known acceptor (C_{As}) concentration in the LT-GaAs:C films, a crude estimate of [As_{Ga}] at $T_{growth=}$=400 C is obtained and included in Fig 6-1

References

1. T.A. Gant, H. Shen, J.R. Flemish, L. Fotiadis, and M.Dutta, Appl. Phys. Lett. **60**, 1453 (1992)
2. Yu. P and Cardona, M., *Fundamentals of Semiconductors* (Springer-Verleg, Berlin,1995) p.284.
3. Zuzanna Liliental-Weber, J. Ager, D. Look, X. W. Lin, J. Nishio, K. Nichols, W. Schaff, W. Swider, K. Wang, J. Wasburn, E. R. Weber and J. Whitaker, in *Proceeding of the 8th conference on semi-insulating III-V materials, Warsaw, Poland, 1994*, edited by M. Godlewski (World Scientific,1994), p.305.
4. J. Grocnen, R. Carles, G. Linda, C. Guerret-Pi'ecourt, C. Fontaine, M. Gendry, Phys. Rev. B **58**, 10452 (1998).
5. M. Toufella, P. Puech, R. Carles, E. Bedel, C. Fontaine, A. Claverie, and G. Benassayag, J. Appl. Phys. **85**, 2929 (1999).
6. S. Adachi, *GaAs and related materials* (World Scientific, Singapore, 1994),p.15
7. X. Liu, A. Prasad, W.M. Chen, A. Kurpiewski, A. Stoschek, Z. Liliantal-Waber and E.R. Weber, Appl. Phys. Lett. **65**, 3002 (1994)
8. W. C. Lee, T. M. Hsu, J.-I. Chyi, G. S. Lee, W.-H. Li, K. C. Lee, Appl. Surf. Sci. **92**, 66 (1996).

Table 6-1. Raman peak positions observed, under the same experimental conditions, for bulk GaAs and the undoped MBE LT–GaAs film. Frequency is given in cm^{-1}.

Spectral lines	GaAs	LT-GaAs	Shift
TO	267	267	0
LO	291.05	290.6	-0.45

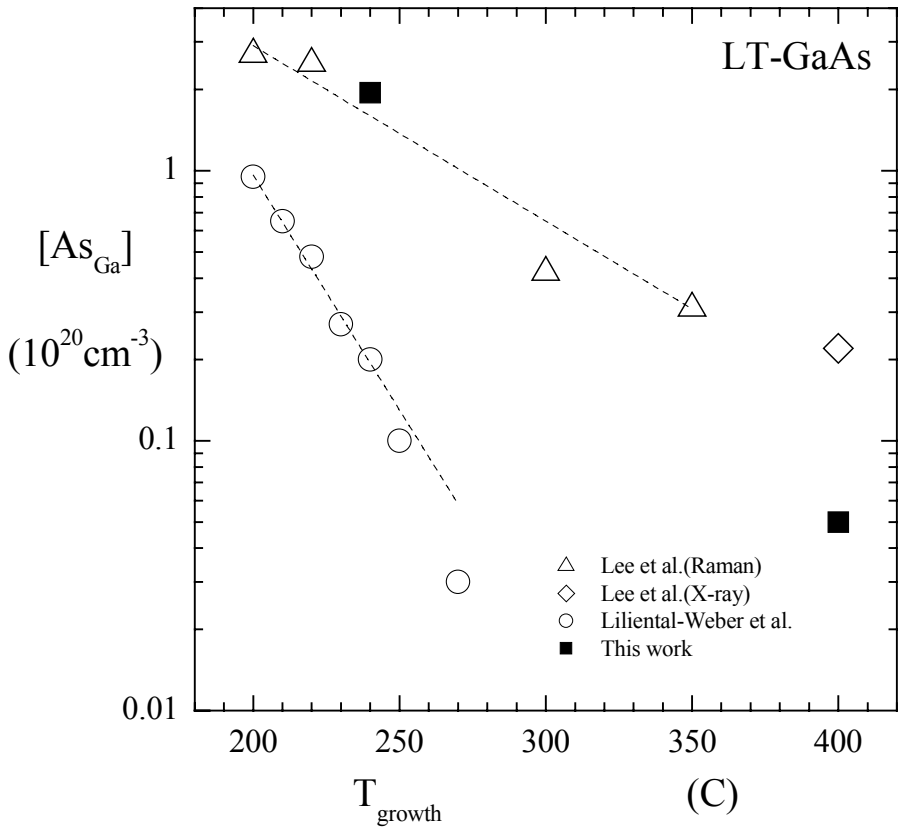

Figure 6-1. A plot of the concentration of arsenic atoms at gallium sites, [As_{Ga}], against growth temperature. The solid squares (■) are the result of this work. The [As_{Ga}] value at at T_{growth}=240 C is estimated by Raman scattering and the value at T_{growth}=400 C is estimated from the Hall measurements and infrared transmission studies of LT-GaAs:C. The open triangles (△) and the open diamonds (◊) are the results reported by Lee et al.[8] using Raman scattering and x-ray crystallography respectively. The open circles (○) are the results reported by Liliental-Weber et al. [3,7] using near-infrared absorption.

Chapter 7. Raman-scattering study of LT-GaAs:C

7.1 Introduction

Earlier Raman-scattering studies on LT-GaAs have been done mostly on undoped samples. Abe et al. [1] and Lee et al. [2] reported a downshift in the longitudinal optical (LO) phonon line. Abe et al**.** also reported a broadening and the appearance of an asymmetric tail on the low frequency side [1]. They conclude that the broadening is mainly defect-induced. Broadening and lineshape asymmetry are also effects known to accompany the finite-size-induced relaxation of the Raman-scattering q-selection rule [3,4]. Gant et al**.** [5] successfully accounted for the downshift of the LO line in undoped LT-GaAs in terms of the reduction of effective charge when arsenic atoms replace gallium atoms.

Unlike the case for undoped LT-GaAs, Raman-scattering studies on doped LT-GaAs are rare. Bliss et al. [6] used Raman spectra to determine the beryllium concentration in LT-GaAs:Be, but did not report anything about the TO and LO line of LT-GaAs:Be. Specht et al. [7] reported that the lattice expansion in LT-GaAs grown at 250 C can be compensated by $2\times10^{19}cm^{-3}$ doping of Be. Carbon doping has been shown to have a similar effect on LT-GaAs [7]. By replacing arsenic atoms with lighter carbon atoms should also affect the Raman spectrum of LT-GaAs. Substituting carbons for some of the arsenics results in a smaller vibrational reduced mass. Additionally, replacing Ga-As bonds by Ga-C bonds alter the vibrational effective charges of the optical phonons. Let N_{As} be the host-crystal concentration of arsenic sites ($N_{As}=2.21\times10^{22}cm^{-3}$) and let $[C_{As}]$ be the concentration of carbons that occupy arsenic sites. Then the fraction of arsenic sites occupied by carbons is $x = \frac{[C_{As}]}{N_{As}}$. The optical-phonon reduced mass,

$\mu(x)$, and the vibrational effective charge, $q(x)$, of $GaAs_{1-x}C_x$ are given by equations (7-1) and (7-2) where reduced mass μ is given in atomic mass units (amu):

$$\mu(x) = (1-x)\mu_{GaAs} + x\mu_{GaC} = (1-0.72x)\mu_{GaAs}$$
$$\mu_{GaAs} = \left(\frac{1}{M_{Ga}} + \frac{1}{M_{As}}\right)^{-1} = 36 \quad \text{(amu)} \tag{7-1}$$
$$\mu_{GaC} = \left(\frac{1}{M_{Ga}} + \frac{1}{M_{C}}\right)^{-1} = 10.2 \quad \text{(amu)}$$

$$q(x) = (1-x)q_{GaAS} + xq_{GaC}$$
$$q(x) = [1-Ax]q_{GaAs} \tag{7-2}$$
$$A = \frac{q_{GaAs} - q_{GaC}}{q_{GaAs}}$$

We use these expressions to roughly estimate the size of the reduced-mass and effective-charge contributions to the phonon frequency shifts. In the absence of better information, we use 0.5 for the ratio given by A in equation (7-2), base on the locations of Ga and C and As in columns 3 and 4 and 5 of the periodic table. The expression for the LO-TO splitting in terms of μ and q is [8] given by

$$\omega_{LO}^2 - \omega_{TO}^2 = \frac{4\pi N q^2}{\mu\varepsilon_\infty} \tag{7-3}$$

Using the differential form of (7-3), as given in (6-3) of the preceding chapter, we find that

$$(\Delta\omega_{LO})_{mass} \approx (0.36\omega_{LO})x \approx 105x \quad (cm^{-1})$$
$$\tag{7-4}$$
$$(\Delta\omega_{LO})_{charge} \approx -45Ax \approx -23x \quad (cm^{-1})$$

The expected total shift, from the effects on reduced mass and effective charge of replacing a fraction *x* of the arsenics by carbons, is +82*x* (cm^{-1}), indicating that the LO line should shift to higher frequency with increasing doping concentration.

$$(\Delta\omega_{LO})_{mass-and-charge} \approx +82x \quad (cm^{-1}) \tag{7-5}$$

7.2 Experiments

The Raman measurements were done at room temperature. The blue line (488nm) of an Ar^+ laser was used as the excitation source. The laser power was set at 300 milliwatts at the laser head, corresponding to about 20 milliwatts at the sample. The sample was set up in a near-back scattering geometry. The laser beam was incident at about 40 degrees from the normal (less than 9 degree from the normal inside the sample). The orientation of the sample to the polarization of the incident light provided a scattering configuration of $x(y,z)\bar{x}$, where x, y, and z correspond to the (100), (010) and (001) crystal directions respectively. The scattered light was collected by a paraboloidal mirror and focused on the entrance slit of the SPEX-1403 double monochromator. The entrance and exit slits were set at 300 microns, providing an instrumental spectral resolution of 3.4 cm^{-1}. The detector was a cooled GaAs-photocathode photomultiplier tube operated in photon-counting mode. The signal was collected and stored by a SPEX DATAMATE computer for future use. Some of the main results are given in table 7-1.

7.3 Results and discussions

Figure 7-1 shows a set of Raman-scattering results for LT-GaAs:C films prepared at different growth temperatures. Raman scattering intensity is plotted against the frequency downshifted defined as $\Delta\bar{\nu} = \bar{\nu}_L - \bar{\nu}$, where $\bar{\nu}_L$ is the frequency (in wavenumber units) of the laser line. The results reveal a pronounced change in the

growth-temperature range 340-390 C. Below this range, at low growth temperature, the Raman spectra show a strong zone-center longitudinal-optical (LO) phonon line near 290 cm^{-1} and a very weak zone-center transverse-optical (TO) phonon line near 267 cm^{-1}. For the scattering configuration used in our experiments, back scattering along the (100) direction, the TO line is symmetry forbidden. But because the samples used are deliberately grown 2° off (100), and because the incident beam geometry deviates from exact back scattering, a weak TO line is seen. These Raman spectra, containing the LO and TO phonon lines characteristic of undoped GaAs, appear even though the acceptor doping concentrations in these LT-GaAs:C samples are as high as 6×10^{19} cm^{-3}. This shows that the acceptors are not activated, there is no hole plasmon, and the samples are not conducting in the low-T_{growth} range. At very low T_{growth} values, the shape of the LO-phonon line become asymmetric, an effect which will be discussed below in terms of disorder.

As seen in Fig. 7-1, when the growth temperature is above 400 C, the LO line becomes very weak and a strong line appears at 264 cm^{-1}. This line is the coupled plasmon-phonon line L_-. L_- corresponds to the lower frequency coupled mode formed by the LO phonon and the hole plasmon. In heavily-doped 3-5 semiconductors, the L_- LO phonon/plasmon coupled mode occurs at a frequency below the LO frequency while the higher-frequency L_+ coupled mole occurs close to the plasmon frequency of the free carriers [9]. In p-type GaAs, the L_+ mode is not observed in Raman scattering because of the presence of strong intervalenceband Raman processes [10]. The disappearance of the LO line and the appearance of the L_- line shows that a free-carrier plasma is present and that the samples are now conducting. This conclusion is supported by the Hall-effect

measurements, which gives hole concentrations between 5×10^{19} cm^{-3} and 7×10^{19} cm^{-3} (Table 3-3 in chapter 3) and by photoluminescence measurements (chapter 8). The Raman spectra of Fig. 7-1 show that the samples are essentially normal GaAs:C when T_{growth} is 400 C or higher.

Figure 7-2 shows series of Raman-scattering spectra of LT-GaAs:C at different doping concentrations. All of these samples were grown at about 240 C, well within the T_{growth} range for the preparation of LT-GaAs. As the doping concentration increases, the LO line gets weaker and become asymmetric, developing a broad low-frequency tail. Also the position of the LO line shifts to higher frequency. We will discuss the frequency shift first, then the broadening and asymmetry effects and their dependences on T_{growth} and [C].

Figure 7-3 shows a plot of the LO line shift against the chemical composition *x*, the fraction of arsenic sites occupied by carbon atoms: $x = ([C_{As}]/N_{As})$, where $N_{As}=2.21\times10^{22}$ cm^{-3}. Our infrared transmission experiments on LT-GaAs:C (chapter 5) show that at T_{growth} = 240 C, 37% of the dopant carbon atoms are at arsenic sites: $[C_{As}]=0.37[C]$, where [C] is the total concentration of carbon atoms introduced during the MBE film growth. The LO line shift starts out initially as a small negative shift (about -0.5 cm^{-1}) for undoped LT-GaAs, and then becomes a positive shift as *x* increases. The linear fit to the data shows that the point of zero shift is at about $x = 2.7\times10^{-4}$, corresponding to $[C_{As}] = 6.0\times10^{18}$ cm^{-3}. Since our infrared results (chapter 5) show that $[C_{As}]/[C]$ is 0.37 for LT-GaAs:C grown at 240 C, it follows that the doping concentration [C] at this point is 1.6×10^{19} cm^{-3}. This number agrees with the concentration reported by Specht et al. [7] for LT-GaAs:Be, for the doping level of [Be] needed to introduce a

concentration (because of the small size of Be) that compensates for the lattice expansion characteristic of undoped LT-GaAs. The tetrahedral-coordination covalent radii of Be, C, Ga and As are 1.06,0.77,1.26 and 1.18 Angstrom, respectively [11]. In GaAs:C, the C_{As} size deficit (in terms of radius) is 0.41 Å, In GaAs:Be the acceptor site is Be_{Ga} and the size deficit is 0.20 Å, so that it is somewhat surprising that the Be dopant seems to be about as effective as carbon is in introducing contraction to compensate the lattice expansion of LT-GaAs.

From the results of Fig. 7-3, the observed shift of the LO line as a function of the fraction of arsenic sites occupied by carbons, as given by the line fit to the experimental points, is approximately (1700±300)x, in cm^{-1}. Despite the scatter, the positive shift with increasing x is evident. The shift of about +1700x (from here on, we suppress the cm^{-1} units when express this way) is much larger than the +82x estimated earlier for the reduced-mass and effective-charge effects. Toufella et al. [12] estimated the shift from the effect of strain to be -40ε, where ε is the lattice strain. Specht et al [7] reported a lattice strain of -0.01% for LT-GaAs:C grown at 250 C and doped to $4.5\times10^{19}cm^{-3}$. For ε = -0.0001, -40ε is +0.004 cm^{-1}, which also is much smaller than the observed shifts. Another possibility that we can consider is the effect of the carbon atoms that are not at arsenic sites but at interstitial sites. For LT-GaAs:C grown at 240 C, about 37% of the carbons are at arsenic sites so that about 63% are at interstitial sites and (x_i/x) is about 1.7, where x_i is the number of interstitial carbons per GaAs unit. If interstitial carbon were in fact mainly responsible for the observed shift, its contribution would be about +900x_i.

Standard GaAs:C (T_{growth} = 600 C), in addition to showing the L_- phonon-plasmon line, also shows (weakly) the LO line as well. This unscreened LO line arises from a thin

near-surface depletion layer in which free carriers are absent. This depletion layer LO line shifts downward in frequency with increasing [C_{As}]. At [C_{As}] = 3×10^{19} cm^{-3} (corresponding to the top of the range in Fig. 7-3), the shift is –2 cm^{-1} [13]. This doping-induced shift is opposite in sign to the one shown for LT-GaAs:C in Fig. 7-3. But the two effects have this in common: neither one has, thus far, a definitive explanation.

Figure 7-4 shows the effect of growth temperature on the position of the LO line, For LT-GaAs:C films having a carbon concentration close to [C] = 6×10^{19} cm^{-3}. Also shown in this figure (lower panel) is the effect of growth temperature on the LO position in undoped LT-GaAs. The T_{growth} range in Fig. 7-4 is confined to the region below 400 C, since at and above that growth temperature the material is conducting (Fig. 7-1), not insulating "LT" material. For undoped LT-GaAs, the LO line is shifted to lower frequency. For carbon-doped LT-GaAs:C, the LO line is shifted to the higher frequency. Both effects are largest at low growth temperature.

At low growth temperatures, the native defects (including vacancies and As_{Ga} antisites) and disorder and lattice expansion characteristic of LT-GaAs produce a downshift in ω_{LO}. In LT-GaAs:C, the additional effect caused by carbon doping produces a net upshift of ω_{LO}. Although the total carbon concentration [C] is the same for the five LT-GaAs:C samples of Fig. 7-4, [C_{As}] is not the same because the [C_{As}]/[C] fraction decreases with decreasing T_{growth}. This means that [C_{As}] decreases, and ([C]-[C_{As}]) increases, with decreasing T_{growth}. Let us assume that ([C]-[C_{As}]) is equal to [$C_{interstitial}$], the concentration of carbon atoms occupying interstitial sites (mainly because any LVM spectrum corresponding to C_{Ga} has not yet been detected [14]). [$C_{interstitial}$] increases with decreasing T_{growth}. Interstitial carbon is thus a carbon-associate defect whose

concentration increases with decreasing T_{growth} for the LT-GaAs:C samples plotted in Fig. 7-4, and it is not implausible to consider interstitial carbon as a possible explanation for LT-GaAs:C—LT-GaAs different in behavior that is seen in that figure.

Figure 7-5 plots corrected $\Delta\omega_{LO}$ shifts against $[C_{interstitial}]$ for the five $[C] = 6\times10^{19}$ cm^{-3} LT-GaAs samples of the top panel of Fig. 7-4, grown at various temperatures. For each T_{growth}, $[C_{As}]$ was determined from the infrared measurements of chapter 5, and $[C_{interstitial}]$ from $[C]$-$[C_{As}]$. From the observed $\Delta\omega_{LO}$, we have subtracted the (negative) $\Delta\omega_{LO}$ attributed to the native-defect concentration of undoped LT-GaAs at the same T_{growth}, estimated from the work of Lee et al. [2] via the dash curve in the lower panel of Fig. 7-4. Also subtracted off is the much smaller correction (equation 7-5) corresponding to the reduced-mass and effective-charge changes accompanying $[C_{As}]$. The resulting $(\Delta\omega_{LO})_{corrected}$ values represent an attempt to remove the effect of native defects, reduced mass, and effective charge from the experimentally observed values. What remains is $(\Delta\omega_{LO})_{corrected}$. From Fig. 7-5, we see that there is, in fact, a rough correlation between $(\Delta\omega_{LO})_{corrected}$ and $[C_{interstitial}]$, supporting the idea that interstitial carbon is responsible for the positive $\Delta\omega_{LO}$ in carbon-doped LT-GaAs.

Figure 7-6 shows a plot of the LO linewidth against growth temperature over the limited T_{growth} range in which carbon-doped LT-GaAs is insulating, for LT-GaAs:C with $[C] = 6\times10^{19}$ cm^{-3}. The linewidth decreases as growth temperatures increases. The horizontal line shows the room temperature linewidth of bulk GaAs. The increase in linewidth at low growth temperatures reflects the increase in defect concentration at low T_{growth}, both the native defects characteristics of low-temperature GaAs and the interstitial carbons (as discuss above) present in the doped material.

Figure 7-7 shows the relation between the LO linewidth and the doping concentration in LT-GaAs:C samples grown at 240 C. The quantity plotted in Fig. 7-7 is $\Delta\Gamma = \Gamma - \Gamma_0$, the increase in linewidth relative to the linewidth Γ_0 in undoped LT-GaAs grown at 240 C. Γ_0 is 3.9 cm^{-1} (Table 7-1). Figure 7-7 is plotted on a log-log scale and indicates (the dash line) that the doping-induced broadening $\Delta\Gamma$ is proportional to $[C]^{\frac{1}{2}}$. We attribute this doping-induced broadening in LT-GaAs:C to interstitial carbon.

The low-T_{growth} Raman lines of Fig. 7-1 are asymmetric, having a low-frequency half-width (at half maximum) that is larger than the half-width on the high frequency side. We shall refer to the ratio of the half-width on the low-frequency side (Γ_{low}) to the half-width on the high-frequency side (Γ_{high}) as the lineshape ratio. For a symmetric line, this ratio is 1.0; this is the case for the LO line in bulk GaAs. We define the lineshape asymmetry to be the deviation of the lineshape ratio from one:

$$\text{Asymmetry} = \left(\frac{\Gamma_{low}}{\Gamma_{high}}\right) - 1 \qquad (7\text{-}6)$$

Figures 7-8 shows the dependence of the lineshape ratio in LT-GaAs on growth temperatures and Fig. 7-9 shows the dependence of the asymmetry on doping concentration. Low growth temperature and high doping concentration increases the asymmetry. Figure 7-9 shows that the asymmetry, at constant growth temperature, is strongly correlated with doping concentration; undoped LT-GaAs has little LO-lineshape asymmetry.

The effect on LO-line asymmetry produced by carbon doping is very different for LT-GaAs and ordinary GaAs. [C] produces pronounced asymmetry for LT-GaAs but not for high-quality crystalline GaAs. For normal GaAs:C, The LO Raman line (from the

depletion layer) remains very symmetric even when the carbon concentration reaches a level as high as 1×10^{20} cm^{-3} [10, 15]. Thus the asymmetry is not produced by carbons at arsenic sites, instead, it is produced by the interstitial carbons present in the doped LT-material.

Figures 7-10 and 7-11 show plots of Raman peak position versus asymmetry for LT-GaAs:C samples having the same doping but grown at different temperatures (Fig.7-10) and for samples grown at the same temperature but having different dopings (Fig. 7-11). The strong correlation between asymmetry and $\Delta\omega_{LO}$, over a wide range of LT-GaAs:C materials, shows that the two effects arise from the same underlying mechanism. This mechanism is assumed to be the disorder introduced into LT-GaAs by the presence of doping-induced interstitial carbon. Also Fig. 7-12 shows the plot of a change in LO Raman linewidth versus asymmetry for both LT-GaAs:C sample with the same growth temperatures and the same doping concentration. The plot shows a strong correlation between broadening and asymmetry. This correlation shows that the broadening also arises from the same mechanism related to the presence of doping-induced interstitial carbon.

7.4 Summary

In this chapter, we report the results of Raman measurements performed at room temperature on LT-GaAs:C films grown at different growth temperatures (T_{growth}) and carbon concentrations ([C]). As the growth temperature decreases or the doping concentration increases, the LO line broadens, become weaker and asymmetric, and its peak shifts upward relative to the LO line of bulk GaAs. The shift in peak position, the broadening, and the asymmetry are all correlated, suggesting that all of these effects arise

from the same underlying mechanism. We suggest that these effects are caused by interstitial carbon in the LT-GaAs:C films.

References

1. Hajime Abe, Hirishi Harima, Shin-ichi Nakashima, Masahiko Tani, Kiyoni Sakai, Yasumori Takuda, Kyozo Kanamoto, Yuji Abe, Jap. J. Appl. Phys. **35**, 5955 (1996).
2. W. C. Lee, T. M. Hsu, J-I Chyi, G. S. Lee, W. – H. Li, K. C. Lee, Appl. Surf. Sci. **92**, 66 (1996).
3. M. Holtz, R. Zallen, O. Brafman, and S. Matteson, Phys. Rev. B **37**, 4609 (1988)
4. K. K. Tiong, P. M. Amirtharaj, F. H. Pollak, and D. E. Aspnes, Appl. Phys. Lett. **44**, 122 (1983)
5. T. A. Gant, H. Shen, J. R. Flemish, L. Fotiadis, and M. Dutta, Appl. Phys. Lett. **60**, 1453 (1992).
6. D. E. Bliss, W. Walukiewicz, J. W. Ager,III, E. E. Haller, K. T. Chan, and S. Tanigawa, J. Appl. Phys. **71**, 1699 (1992).
7. P. Specth, R. C. Lutz, R. Zhao,E. R. Weber, W. K. Liu, K. Bacher, F. J. Towner, T. R. Stewart, and M. Luysberg, J. Vac. Sci. Technol. B. **17**, 1200 (1999).
8. Yu. P and Cardona, M., *Fundamentals of Semiconductors* (Springer-Verleg, Berlin,1995) p.284.
9. Y. B. Li, I. T. Ferguson, R. A. Stradling, and R. Zallen, Semicond. Sci. Technol. **7**, 1149 (1992).
10. M. Seon, M. Holtz, W. M. Duncan, and T. S. Kim, J. Appl. Phys. **85**, 7224 (1999); R. Zallen, W. Songprakob, S. Vijarnwannaluk, M. L. Hsieh, R. A. Stradling, W. K. Liu, and K. L. Bacher, Bull. Am. Phys. Soc. **44**, 1679 (1999)
11. G. Burns, *Solid state physics* (Academic press,1985), p. 163.

12. M. Toufella, P. Puech, R. Carles, E. Bedel, C. Fontaine, A. Claverie, and G. Benassayag, J. Appl. Phys. **85**, 2929 (1999).

13. W. Songprakob, doctoral dissertation, Virginia Tech, August 2001: Fig. 5.3 on p. 133. This thesis is available electronically at http://scholar.lib.vt.edu/theses/available/etd-09102001-091811/.

14. J. Wagner, K. H. Bachem, B. R. Davidson, R. C. Newman, T. J. Bullough, and T. B. Joyce, Phys. Rev. B **51**, 4150 (1995).

15. Measurement by Ming-Liang Hsieh at Imperial College, London, shown in Fig. 5.4 on p.135 of Ref. 13.

Table 7-1. The results of Raman-scattering experiment on LT-GaAs:C. Γ is the linewidth, $\Delta\omega_{LO}$ is the shift of the LO line, and the lineshape ratio is the ratio of the low-frequency and high-frequency half width ($\Gamma_{low}/\Gamma_{high}$). For the doped samples grown at 400 and 600 C, the (depletion-leyer) LO line was too weak for an estimation of linewidth and asymmetry.

Sample	[C] ($10^{19}cm^{-3}$)	T_{growth} (C)	$\Delta\omega_{LO}$ (cm^{-1})	Γ (cm^{-1})	$\Gamma_{low}/\Gamma_{high}$
Bulk (Back side)	undoped	600	0.0	3.8	1.5
11772.02	undoped	240	-0.45	3.9	1.2
11776.02	2	240	0.4	6.7	1.5
11775.02	4	240	0.0	8.7	1.5
11774.02	6	240	1.0	9.4	2.1
11777.02	8	240	2.3	10.4	2.6
Bulk (Back side)	undoped	600	0.0	3.2	1.0
11858.02	6	225	0.8	8.0	1.8
11856.02	6	240	1.5	9.7	2.8
11855.02	6	260	0.1	9.6	1.4
11857.02	6	330	0.2	6.0	1.2
049	5-6	400	-0.8	-	-
048	5-6	480	-0.3	4.0	1.0
047	5-6	600	-0.8	-	-

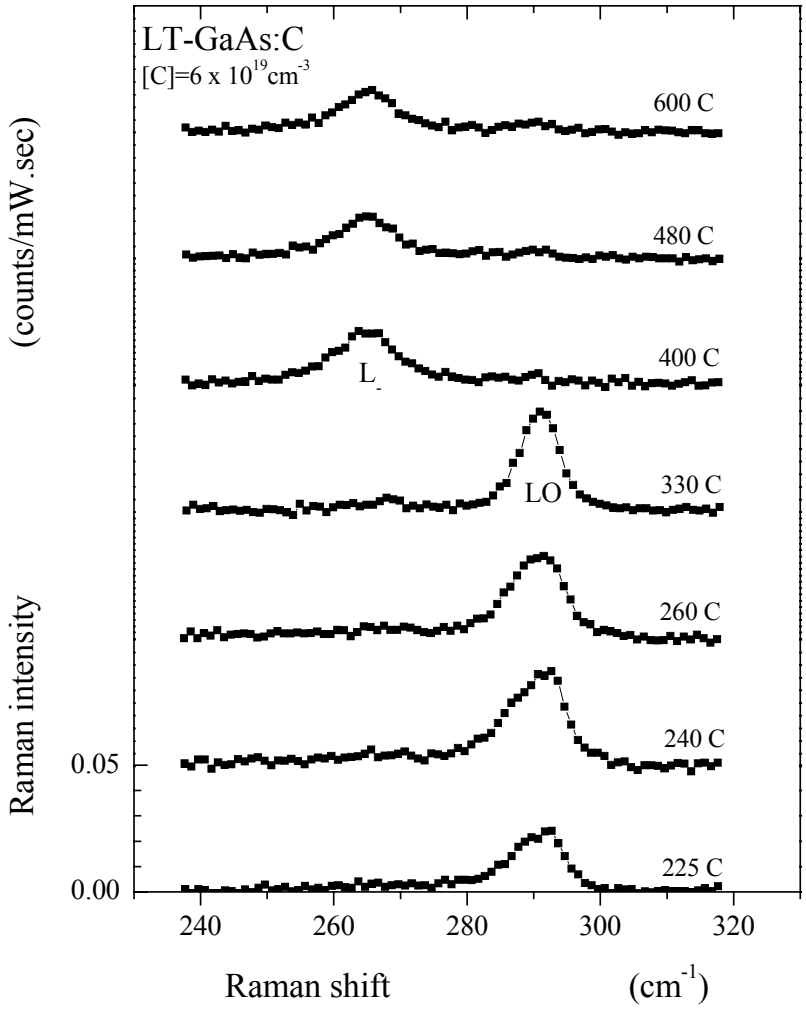

Figure 7- 1. Raman spectra of LT-GaAs:C films prepared at different growth temperatures. The plots are vertically shifted by 0.05 counts/mWsec, and have the same scale. At T_{growth} of 400 C and higher, the films lose their insulating LT-GaAs character and become essentially indistinguishable from normal semiconducting p-type GaAs:C. This is signaled by the appearance of the *L*- phonon-plasmon line. The very weak LO line remaining for T_{growth}>400 C is from the thin near-surface carrier-free depletion layer.

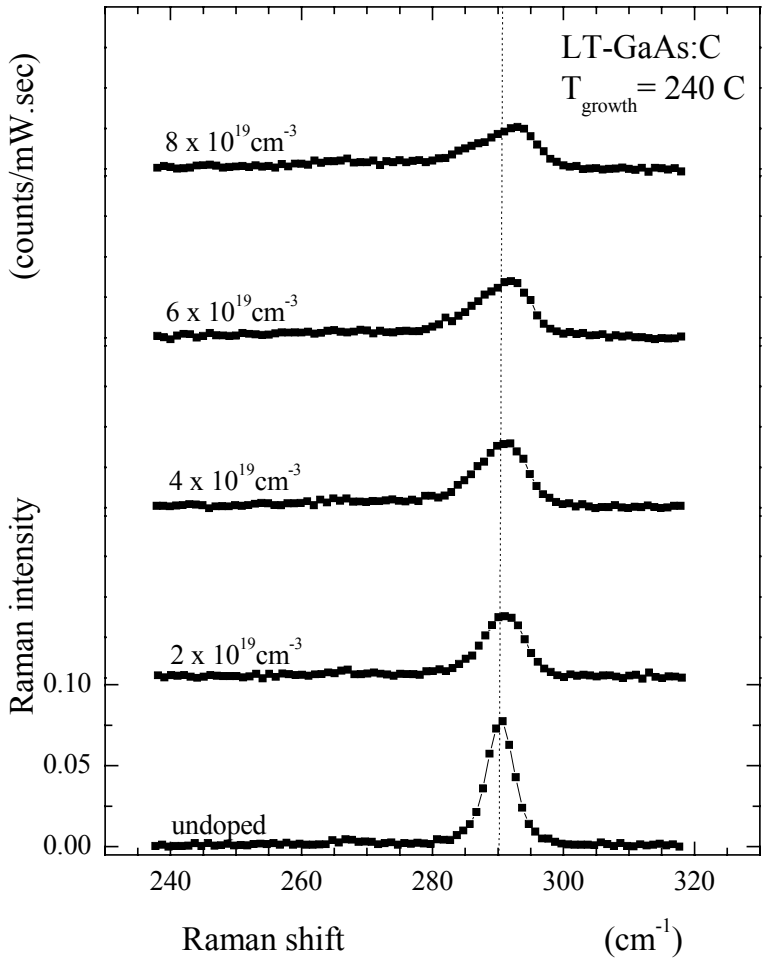

Figure 7-2. The effect of carbon doping on the Raman spectrum of LT-GaAs:C for a growth temperature of 240 C. The plots are vertically shifted for clarity by 0.10 counts/mWsec, and have the same scale.

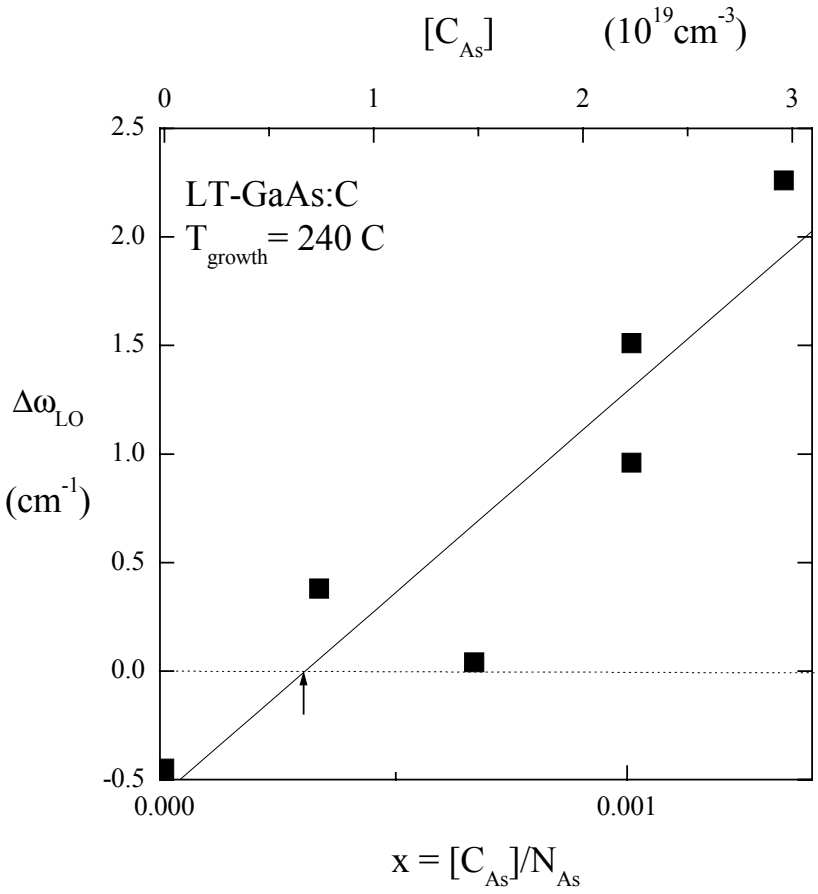

Figure 7-3. The observed LO shift against the fraction *x* of arsenic sites occupied by carbon atoms for LT-GaAs:C films grown close to 240 C. For these films, $[C_{As}]/[C]$ is about 0.37 (chapter 5). The slope of the line is +1700 cm^{-1}. The arrow represents the point at which the doping-induced upshift compensates the small downshift (relative to bulk GaAs) of undoped LT-GaAs.

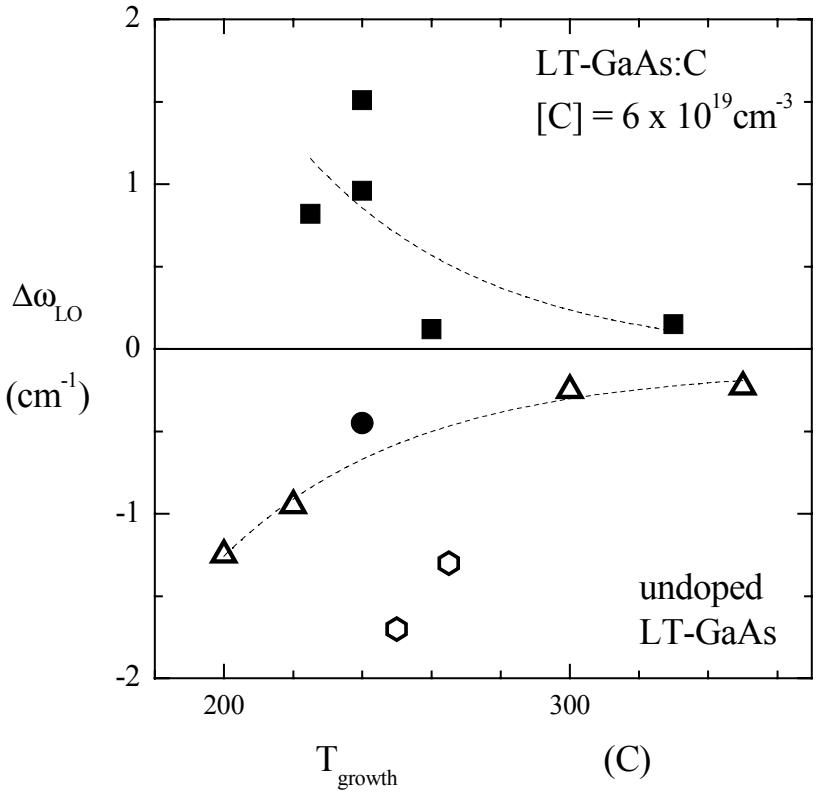

Figure 7-4. The effect of growth temperature on the LO frequency in undoped (lower panel) and carbon-doped (upper panel) LT-GaAs. The solid symbols are our results, the open symbols (for undoped LT-GaAs) are from the work of Lee et al. (triangles, Ref. 2) and Abe et al. (hexagons, Ref. 1).

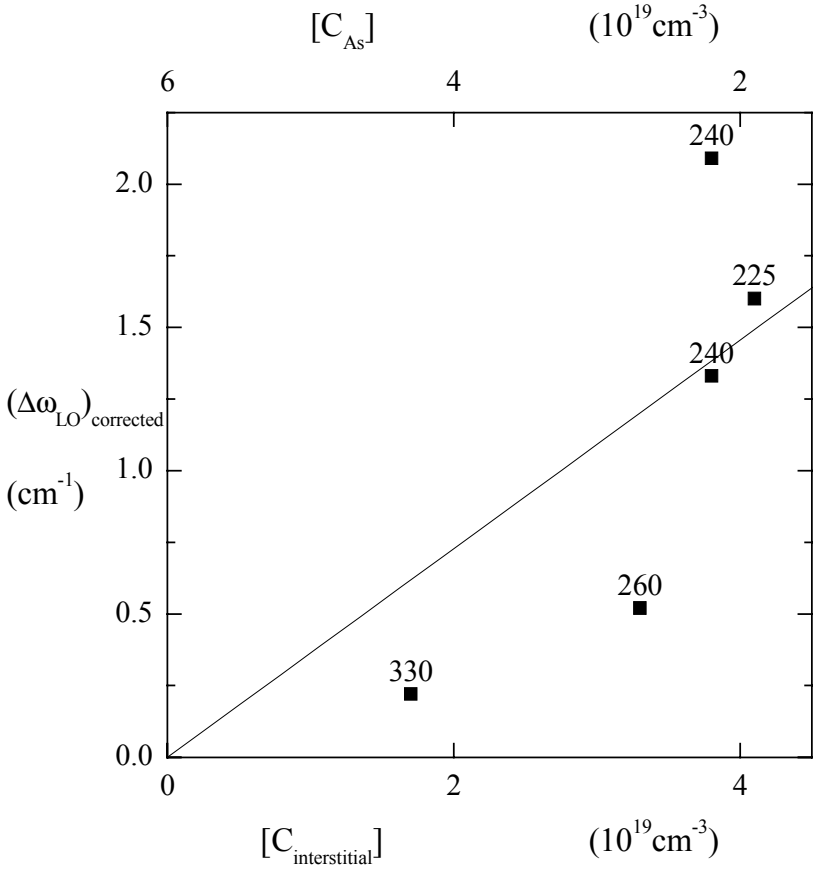

Figure 7-5. Doped LT-GaAs:C samples having the same total carbon concentration [C] have different carbon-for-arsenic [C_{As}] concentrations because [C_{As}] depends on growth temperature (chapter 5). Here $(\Delta\omega_{LO})_{corrected}$ is shown plotted against [$C_{interstitial}$] for samples having [C] = 6×10^{19} cm^{-3} and grown at various temperatures (indicated, in degrees celsius, above each data points). $(\Delta\omega_{LO})_{corrected}$ is the observed shift of the LO line (upper panel of Fig. 7-4) after removing the effect of native defects in LT-GaAs (dashed curve in the lower panel in Fig. 7-4) as well as the effects of the reduced mass and effective charges (equation 7-5) caused by [C_{As}]. [$C_{interstitial}$] is taken to be equal to [C]-[C_{As}].

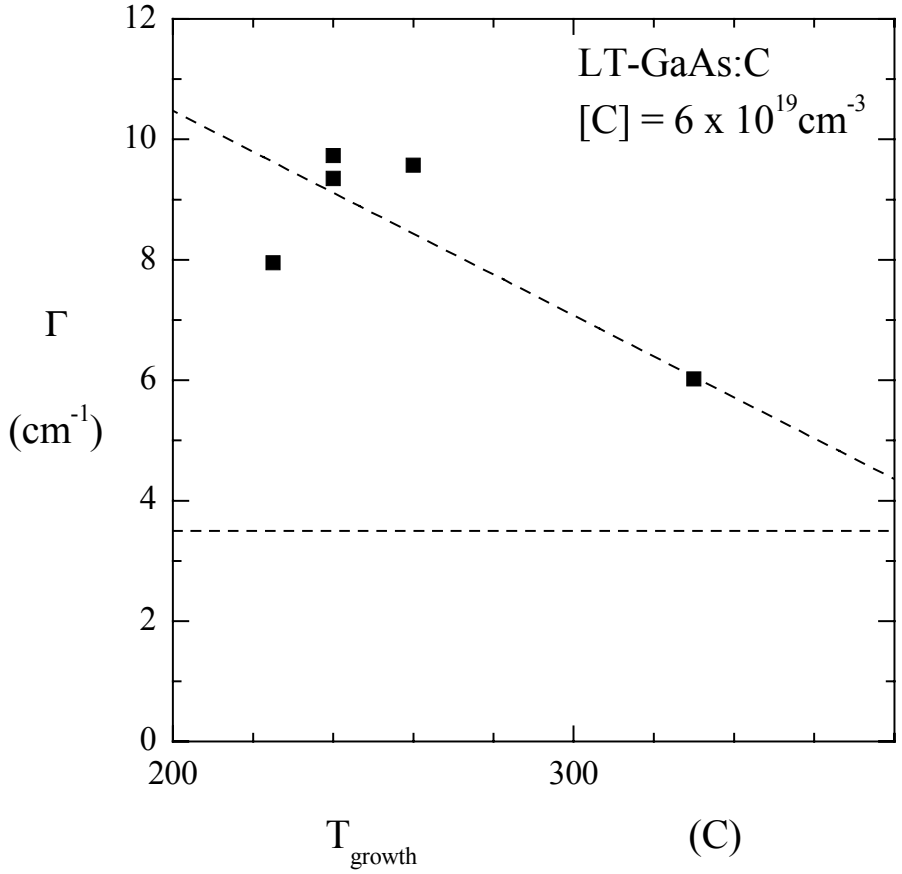

Figure 7-6. The LO linewidth of LT-GaAs:C plotted against growth temperature, for samples doped with a carbon concentration of 6×10^{19} cm^{-3}. The horizontal line shows the LO linewidth of bulk GaAs.

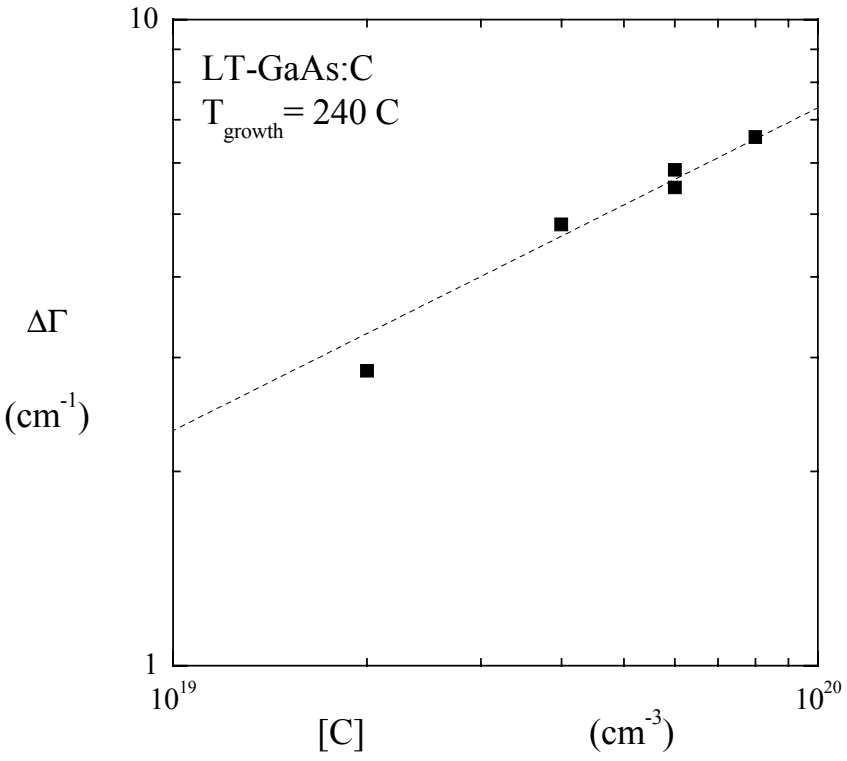

Figure 7-7. Log-log plot of the concentration dependence of the doping-induced broadening of the LO Raman line in LT-GaAs:C grown at 240 C. $\Delta\Gamma$ is Γ-Γ_0, where Γ is the linewidth in the doped material and Γ_0 is the linewidth in undoped LT-GaAs. The dash line indicates that $\Delta\Gamma$ goes as $[C]^{\frac{1}{2}}$ with a proportionality constant of about $7\times10^{10}cm^{1/2}$.

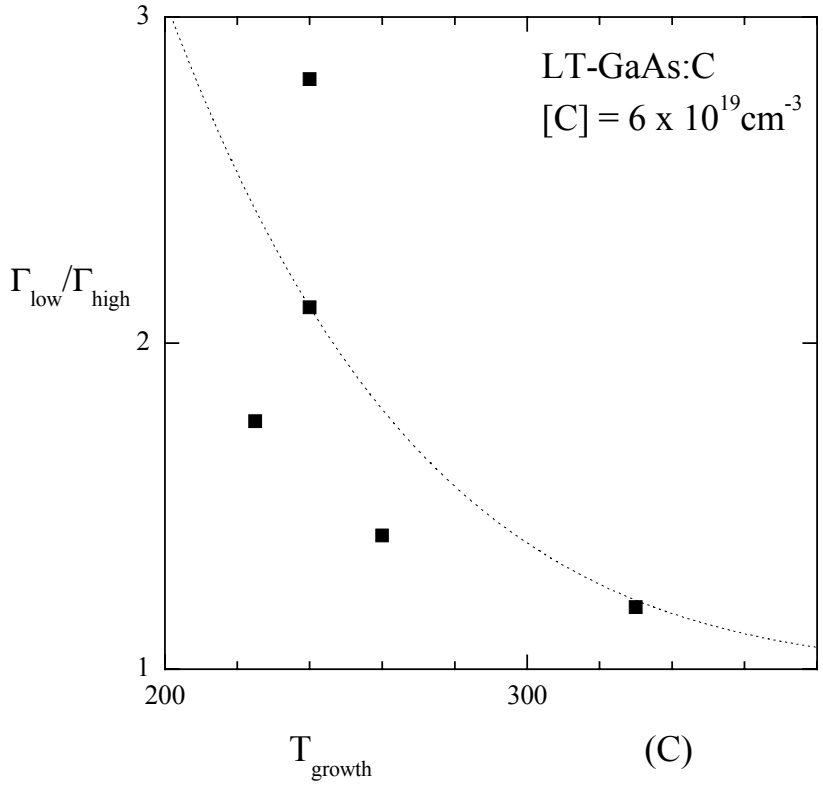

Figure 7-8. The growth-temperature dependence of the LO lineshape ratio $\Gamma_{low}/\Gamma_{high}$ in LT-GaAs:C. Γ_{low} and Γ_{high} are the low-frequency and high-frequency halfwidths at half maximum. The lineshape ratio is 1.0 for a symmetric line.

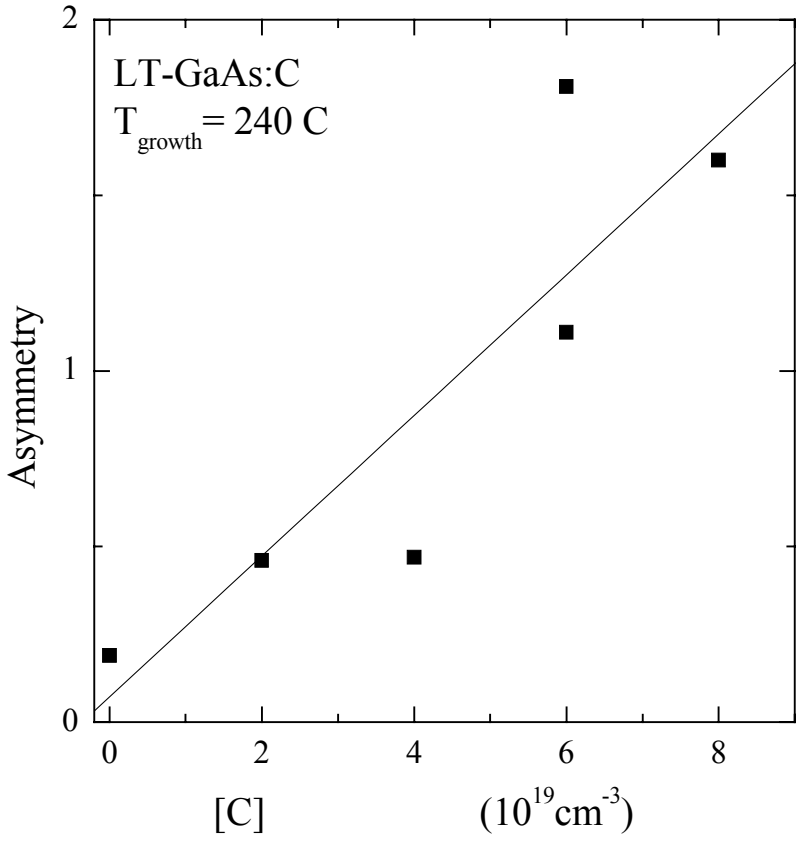

Figure 7-9. Doping dependence of the LO lineshape asymmetry in LT-GaAs:C. The asymmetry is taken to be $(\Gamma_{low}/\Gamma_{high})$-1, where Γ_{low} and Γ_{high} are the halfwidths defined in the caption for Fig. 7-8

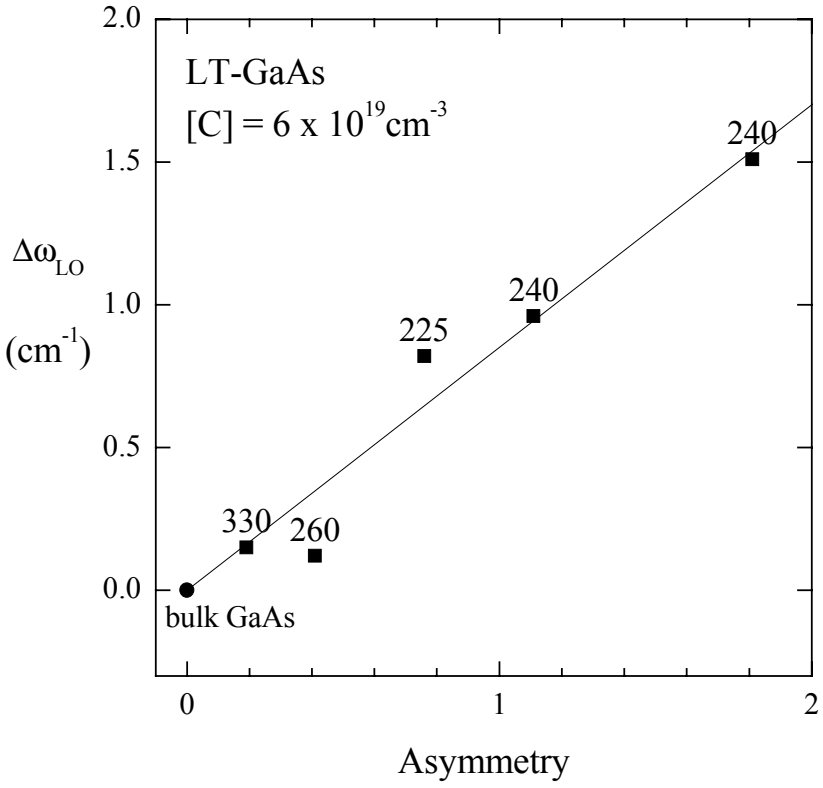

Figure 7-10. The correlation between the shift in the peak position of the LO line ($\Delta\omega_{LO}$) and the LO lineshape asymmetry (equation 7-6) for LT-GaAs:C samples (with [C] = 6×10^{19} cm^{-3}) grown at various temperatures. Growth temperatures are indicated in degrees Celsius. For undoped bulk GaAs, $\Delta\omega_{LO}$ and the LO asymmetry are equal to zero.

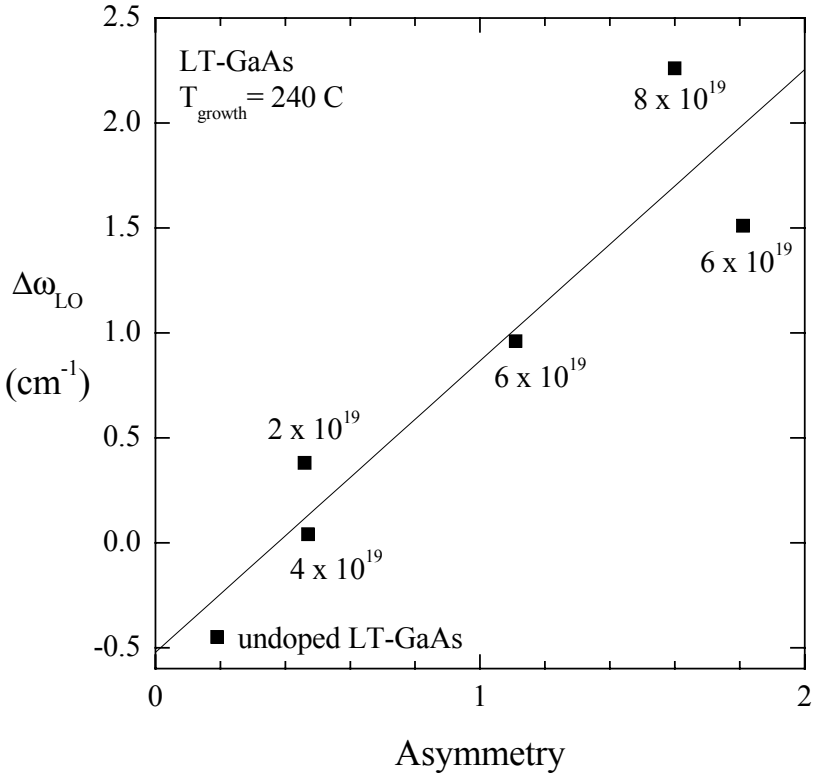

Figure 7-11. The correlation between the shift in the peak position of the LO line ($\Delta\omega_{LO}$) and the LO lineshape asymmetry for the LT-GaAs:C samples (grown at 240 C) doped at various carbon concentrations, Doping levels [C] are indicated in cm^{-3}.

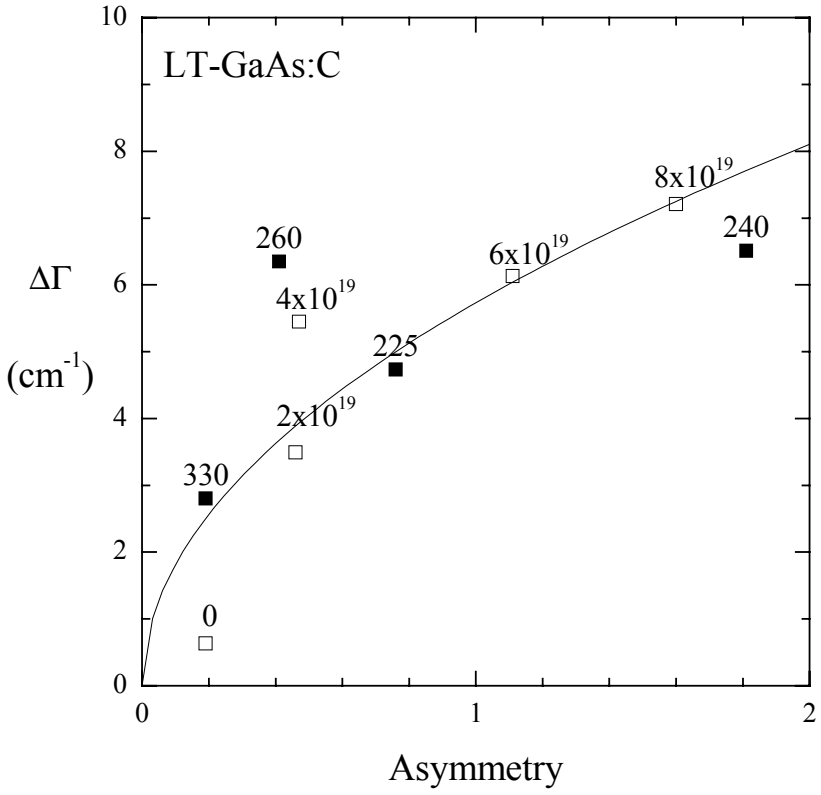

Figure 7-12. The correlation between the change in LO linewidth ($\Delta\Gamma$) and the LO lineshape asymmetry for LT-GaAs:C samples compared to that of bulk GaAs. The open squares represent the results for LT-GaAs:C samples that are grown at 240 C with various carbon concentrations. The carbon concentrations are indicated above the points in units of cm^{-3}. The solid squares represent the results for LT-GaAs:C samples (with [C] = 6×10^{19} cm^{-3}) grown at various temperatures. The growth temperatures are indicated above the points in degree Celsius. The solid line shows that the change in LO linewidth is roughly proportional to $[\text{asymmetry}]^{\frac{1}{2}}$.

Chapter 8. Photoluminescence study of GaAs:C and LT-GaAs:C.

Photoluminescence is a powerful tool for studying electronic states, impurity levels, and defects in semiconductors. In this chapter, photoluminescence results on GaAs:C and LT-GaAs:C are presented and discussed.

8.1 Photoluminescence studies of GaAs:C

Introduction.

In 1976, Casey and Stern [1] presented a model for the calculation of the absorption and photoluminescence (PL) emission spectra for GaAs at carrier concentrations above 1×10^{18}cm^{-3} and compared the calculated absorption and emission spectra with previous experimental spectra obtained at room temperature. They found that increasing the doping concentration decreases the bandgap energy of p-type GaAs as

$$E_g = 1.424 - (1.6\times10^{-8})p^{\frac{1}{3}} \tag{8-1}$$

Here, as well as in the following energy-versus-doping-concentration relations, E_g is in eV and p is in cm^{-3}. Later, Titkov et al. [2] fitted the low-energy side of the GaAs:Zn photoluminescence spectra, obtained at 4.2 K, with the simplest joint (interband) density-of-states function

$$f(E) = \alpha(E - E_g)^{\frac{1}{2}} \tag{8-2}$$

The samples used in their study had doping concentrations (p) ranging from 2×10^{18} cm^{-3} to 5×10^{19} cm^{-3}. They found that the bandgap change, $\Delta E_g = E_g(p) - E_g(0)$, was given by

$$\Delta E_g = -(2.2\times10^{-8})p^{\frac{1}{3}} \tag{8-3}$$

On the high-energy side of the PL spectra, Titkov et al. estimated the Fermi energy from the point where the PL intensity is reduced by a half. The concentration-dependent position of the Fermi level, relative to the top of valence band was fit using the expression.

$$\Delta E_F = -(6\times 10^{-15})p^{\frac{2}{3}} \tag{8-4}$$

For standard GaAs:C (grown at 600 C), all carbons occupy arsenic sites. Because C_{As} is a shallow acceptor (activation energy is small compared to kT), at room temperature all acceptors are activated (ionized) and provide holes to the valence band. This number of holes is much higher than the number of intrinsic thermally-induced holes at room temperature (approximately 10^6 cm^{-3} [3]), so that the hole concentration is approximately the doping concentration. The hole concentration satisfies the relation

$$p = \int_{-\infty}^{E_v} \rho_h(E) f_h(E) dE \tag{8-5}$$

Here $\rho_h(E)$ is the density of states in the valence band and $f_h(E)$ is the Fermi distribution function for holes, $f_h(E) = 1-f(E)$, where f(E) is the Fermi function for electrons. $\rho_h(E)$ and $f_h(E)$ are given by

$$\begin{aligned} \rho_h(E) &= \frac{1}{2\pi^2}\left(\frac{2m_h}{\hbar^2}\right)^{\frac{3}{2}}(E_v - E)^{\frac{1}{2}} \\ f_h(E) &= \frac{1}{1+e^{\frac{E_F - E}{kT}}} \\ m_h &= \left(m_{lh}^{\frac{3}{2}} + m_{hh}^{\frac{3}{2}}\right)^{\frac{2}{3}} \end{aligned} \tag{8-6}$$

E_v is the energy at the top of the valence band, E_F is the Fermi energy, m_{lh} and m_{hh} are the light-hole and heavy-hole masses, and m_h is the valence band density-of-states mass.

Substituting (8-6) into (8-5) and introducing the dimensionless quantities η and x, we obtain [4]

$$
\begin{aligned}
p &= N_v F(\eta) \\
N_v &\equiv 2\left(\frac{2\pi m_h kT}{h^2}\right)^{\frac{3}{2}} \\
F(\eta) &= \frac{2}{\pi^{\frac{1}{2}}} \int_0^{\infty} \frac{x^{\frac{1}{2}}}{1+e^{x-\eta}} dx \\
\eta &\equiv \frac{E_v - E_F}{kT} \\
x &= \frac{E_v - E}{kT}
\end{aligned}
\tag{8-7}
$$

N_v is called the effective density of states of the valence band and η is the degree of degeneracy. The function $F(\eta)$ is the Fermi-Dirac integral, which can be evaluated numerically for each η [5]. The expression shown above for N_v can be expressed in terms of m_h and T as [4]

$$N_v = (2.5\times 10^{19})\left(\frac{m_h}{m_e}\right)^{\frac{3}{2}}\left(\frac{T}{300}\right)^{\frac{3}{2}} \tag{8-8}$$

where N_v is in cm^{-3}, T is in Kelvin and m_e is the electron mass.

We use the relations shown in (8-7) and (8-8) to obtain an experimental estimate for the density-of-states hole mass m_h from the photoluminescence spectra of Fig. 8-1. As described in the next section, the depth of the Fermi level inside the valence band (E_v-E_F) is estimated from the shape of each PL spectrum. This then determines the degree of degeneracy $\eta = (E_v-E_F)/kT$. Evaluating $F(\eta)$ then determines N_v from p, using the first relation listed in (8-7), and m_h is then determined from (8-8). The values of η and $F(\eta)$ obtained for our samples are shown as the points presented on the $F(\eta)$-versus-η plot given in Fig 8-2. $F(\eta)$, for each η, was determined using Microcal Origin 6, by

numerically integrating the integrand stated in (8-7) from 0 to 100 using increments of 0.1. After doing this, a tabulation of $F(\eta)$ was discovered in Ref. 5 which was essentially the same on the scale of Fig. 8-2. The result for m_h is discussed in the following section. It is in reasonable agreement with the known band-structure parameters (m_{hh} and m_{lh}) of GaAs and the m_h expression in equation (8-6). This agreement provides support for the model used here to analyzed the PL spectra.

Experiment and Results

Photoluminescence spectra were measured, at room temperature, on two overlapping sets of GaAs:C samples having a range of doping concentrations. The first set was measured at Imperial College, London by M. L. Hsieh, using a Renishaw Raman-microprobe system. The excitation energy was provided by an Argon ion laser operating at 488 nm (2.541 eV). The other set was measured at the Renishaw Company, Wotton-under-Edge, UK, also with a Renishaw microprobe. Here two different excitation sources were used in different scans, an Argon ion laser operating at 514.5 nm (2.410 eV) and a He-Ne laser operating at 633 nm (1.959 eV). Figure 8-1 shows the PL spectra of the samples measured at Imperial College, London.

For the undoped GaAs sample, the photoluminescence spectrum has a low-energy edge at 1.41 eV, close to the room-temperature bandgap of 1.42 eV [6]. As the doping concentration increases, the low-energy edge downshifts and the peak becomes broader and extends to higher energies as the Fermi level moves down into the valence band. For the highest doping, an extra feature appears at 1.7 eV. This feature corresponds [7,8] to transitions from the conduction band to the spin-orbit split-off valence band which lies 0.3 eV below the highest (heavy-hole) valence band.

The undoped-GaAs photoluminescence spectrum of Fig. 8-1 (bottom spectrum) was taken on the substrate material. The MBE films are relatively thick, but the possibility of luminescence originating from the substrate needs to be considered. Relative to PL emission from the film, PL from the substrate suffers an additional attenuation of at least $e^{-\alpha d}$ where d is the film thickness of 500 nm (for the minimum thick ness) and α is the optical absorption coefficient at the laser-line photon energy. With the argon-laser blue line at 2.54 eV, this attenuation is about 2×10^{-3}, and it can be seen in Fig 8-1 that the sharp band gap peak of the undoped-GaAs spectrum is absent in the spectrum of our highly doped GaAs:C samples. For the green and Red laser line used, The substrate attenuation is less pronounced, but still adequate to prevent appreciable interference from substrate luminescence.

In order to estimate the band gap energy and the Fermi energy from the photoluminescence results, each PL spectrum was fitted using a function of the form shown in equation (8-9).

$$I(E) = \frac{A(E - E_g)^{\frac{1}{2}}}{1 + e^{\frac{(E - E_F')}{kT}}} \qquad (8\text{-}9)$$

Here I(E) is the intensity of light emitted with photon energy E, E_g is the bandgap, and E_F' is $E_g+(E_v-E_F)$, the energy separation between the Fermi energy (within the valence band for these degenerate p-type semiconductor) and the bottom of the conduction band. E_F' determines the high-energy cutoff of I(E). I(E) is the product of a parabolic joint density of states (as in equation 8-2) and the Fermi distribution for holes. The thermal energy kT was set at 0.026 eV, corresponding to T=300 K. The results of using equation (8-9) to fit the spectra inFig.8-1 are shown in Fig.8-3, with the

corresponding E_g, E_F', and (E_v-E_F) values given in Table 8-1. Table 8-1 also includes the E_g, E_F', and (E_v-E_F) values obtained from similar fits to the PL spectra taken using the two longer-wavelength laser lines, and shows that results obtained on a given sample are consistent and do not depend on the (above-bandgap) photon energy of the exciting light.

Figure 8-3 shows that the fits give a reasonable account of the observed spectra except for the highest doping. In the 10^{20} cm^{-3} range of hole concentration, the high-energy peak arising from transitions to the split-off valence band becomes prominent. This process is not included in our simple model (equation 8-9).

Discussion

The physical arguments supporting the simple form given in (8-9), for the spectral shape I(E), will now be discussed. Photoluminescence (PL) studies [9], as well as photoluminescence-excitation (PLE) studies [10], show that indirect transitions play an important role in light-emission processes in heavily doped GaAs. Due to the large concentration of impurity ions and free carriers, the k-conservation selection rule is relaxed. Indirect-transition recombination of electrons at the bottom of conduction band (k=0) and holes at different crystal-momentum values (k different from zero) can occur. Figure (8-4) illustrates three such transitions. The lowest photon-energy transition occurs at the bandgap energy E_g, while the highest-energy transition occurs at E_g+E_F. Here E_F is the dept of the Fermi level within the valence band for our highly doped, degenerate, p-type samples. In other words, as shown in Fig. 8-4, the Fermi energy is –E_F if the zero of energy is taken to be the top of the valence band. If only direct transitions were significant, the photoluminescence spectrum would be very narrow, confined to the photon-energy region close to the bandgap energy. The PL spectra of Fig. 8-1 show that

this is not the case at high doping. Also, Wang et al., using PLE [10], showed that indirect transitions are dominant in heavily doped GaAs:C.

The shape of photoluminescence spectra depends on three factors; the distribution of electrons in the conduction band, the distribution of holes in the valence band, and the matrix element determining the oscillator strength of the transitions. Borghs et al. [11] proposed that, under special conditions, the photoluminescence spectra of p-type heavily doped GaAs can be fitted with a simple expression

$$I(E) = \rho_h(E) f_h(E) \tag{8-10}$$

In (8-10), $\rho_h(E)$ is the valence band density-of-states and $f_h(E)$ is the Fermi distribution for holes. The assumptions are the following. The density of electrons generated by photoexcitation is small compared to the hole concentration and the photogenerated electrons rapidly thermalized to the bottom of the conduction band. As a result, the electrons involved in radiative recombination originate from the bottom of the conduction band, as sketched in Fig. 8-4. The emitted photons come from the recombination of these photogenerated band-edge electrons with the degenerate distribution of holes in the valence band. Indirect transitions dominate, and the matrix element is well approximated by a constant. In equation (8-10), E in I(E) is the energy of the emitted photon (the transition energy), so that the electronic-state energy E in $\rho_h(E)$ and $f_h(E)$ is taken to be measured downward from the bottom of the conduction band.

In our measurements, the laser power at the samples was fairly low. For the measurements with the green and red laser lines at 514 nm (2.41 eV) and at 633 nm (1.95 eV), the laser power at the sample was under 0.03 mW. For the measurements with the blue laser line at 488 nm (2.54 eV), the laser power at the sample was less than 1 mW.

Considering the maximum laser power used, the number of photons entering the sample can be estimated from $\frac{I(1-R)}{h\nu_L}$, here I is the laser intensity at the sample, R is the reflectance of GaAs at the corresponding wavelength, and $h\nu_L$ is the photon energy. For the blue line, $h\nu_L$ = 2.54 eV, I = 1 mW, R = 0.4 [12], and the photon flux entering the sample is 1.5×10^{15} photon/seconds. The smallest spot sized used (on the sample surface) had a diameter of about 30 microns. At 2.54 eV, the optical penetration depth (reciprocal of the optical absorption coefficient) for GaAs is 0.081 micron [12]. The excitation volume is then 3×10^{-11} cm^3. Assuming that every entering photon excites an electron to the conduction band, the electron photogeneration rate is 2.1×10^{25} electrons/cm^3sec. The resulting steady-state number density of electrons in the conduction band is the photogeneration rate times the recombination lifetime. For doped p-type GaAs, the recombination lifetime is inversely proportional to the hole concentration; $\tau = \frac{1}{Bp}$, where p is the hole concentration and where B is the interband recombination constant [14] and is about 2×10^{-10} cm^3s^{-1}. In our experiments, the highly doped samples of main interest have a typical concentration of about 7×10^{19} cm^{-3}, so that the recombination lifetime is estimated to be about 7×10^{-11} s or 70 picoseconds (ps). This estimate agrees well with estimated obtained by Ahrenkiel et al. [15] from the time-resolved PL measurements on AlGaAs/GaAs:C/AlGaAs multilayers.

This lifetime, combined with the photogeneration rate of 2.1×10^{25} electrons/(cm^3sec), corresponds to a steady-state photo-induced conductionband concentration of 1.5×10^{15} cm^{-3}. An equal steady-state concentration of photo-induced

excess holes is added to the valence band, but this is negligible compared to the hole concentration (p) already present in our carbon-doped samples. From mobility and infrared measurements on our samples [16,17], the intraband scattering time for holes is found to be about 0.06 ps. For conduction band electrons, the intraband scattering time (estimated from the minority-carrier mobility in p-type GaAs[18]), is also in the sub-picosecond range. Since this is much shorter than the 70 ps recombination lifetime of the photo-induced conductionband electrons, these electrons reach thermal equilibrium at the bottom of the conduction band before recombination take place. Since the concentration of the photogenerated electrons is small, the band filling is small (less than 10^{-5} eV) and it is a good approximation to assume that the thermalized conductionband electrons taking part in the photoluminescence transitions are at the bottom of the conduction band. This supports the model presented in Fig. 8-4, as well as equation 8-9.

For our samples, the doping concentrations are comparable to those in previous studies, even larger in some cases [9,10,11]. At this level, the photoluminescence spectrum is dominated by indirect transitions [10,13] and a constant matrix-element model works very well for fitting the photoluminescence spectra [11]. Therefore, an expression in Equation (8-10) should yield acceptable results for our samples.

From the fitting results, two energies are determined (at each concentration): the bandfap E_g, and the Fermi-level depth E_F within the valence band. E_g decreases with increasing doping concentration. Eg(p) was compared to a form originally proposed by Casey and Stern [1], in which the bandgap reduction is proportional to $p^{\frac{1}{3}}$. Figure 8-5 shows our results for the concentration dependence of bandgap reduction ΔE_g, presented on a log-log plot. A fit to the Casey-Stern form yields:

$$E_g = E_g(0) - A[p]^{\frac{1}{3}}$$
$$E_g(0) = 1.415 \pm 0.002\text{eV} \qquad (8\text{-}11)$$
$$A = (1.58 \pm 0.07) \times 10^{-8}\,\text{eV.cm}$$

The proportionality factor A agrees with the value reported earlier [1].

Figure 8-6 shows our results for E_F versus p. E_F, as defined here by means of Fig. 8-4, is the Fermi-level depth E_V-E_F and is positive for our high doping but negative (Fermi level in the gap) at low doping. Since its cross zero, Fig.8-6 is linear in E_F. Our results for $E_F(p)$ agree reasonably well with those of Silberman et al. [19] and Wang et al. [10] which are included in Fig. 8-6. Assuming a simple parabolic form

$[\rho(E) \sim (E_V - E)^{\frac{1}{2}}]$ for the valence band density of states and assuming band filling up to E_F (a good approximation when E_F is larger than kT) gives $E_F \sim p^{\frac{2}{3}}$. Using this power law to fit the results of Fig. 8-6 yields

$$E_F = B[p]^{\frac{2}{3}}$$
$$B = (7.7 \pm 0.3) \times 10^{-15}\,\text{eV.cm}^2 \qquad (8\text{-}12)$$

Our value for B agrees well with that reported by Titkov et al. [2].

From the E_F results, the degeneracy level $\eta=(E_V\text{-}E_F)/kT$ and the Fermi-Dirac integral $F(\eta)$ was determined at each p. Figure 8-7 shows the linear correlation between the hole concentration and the Fermi-Dirac integral. The slope gives a room temperature effective density of states (N_V) equal to 8.0×10^{18} cm^{-3}. This N_V value translate into a density of states mass of $0.47m_e$. This value is not far from $0.52m_e$, the value obtained from the heavy hole ($0.50m_e$) and light hole ($0.088m_e$) masses of Blakemore's compilation [6] and the expression $[m_{hh}^{\frac{3}{2}} + m_{lh}^{\frac{3}{2}}]^{\frac{2}{3}}$ for the density of state mass. This

reasonable result, along with those discussed above, shows that the simple two-parameter spectral form of Equation (8-10), which is much simpler than expressions typically used to analyze PL spectra [9,11] is effective for analyzing the room temperature photoluminescence.

Photoluminescence measurements were taken with three different laser lines (photon energy 2.54, 2.41, and 1.96 eV). The observed PL spectra were not very sensitive to excitation photon energy, and we have not made a systematic investigation of the photon-energy dependence. Figure 8-8 shows three spectra obtained with the different laser lines, two for the GaAs:C film doped to 1.05×10^{20} cm^{-3} and one for the film doped to 1.4×10^{20} cm^{-3}, our highest doping. For the 1.05×10^{20} cm^{-3} sample, the shape of the bandgap emission band (which we have analyzed to obtain E_g and E_F) is the same with green (2.41 eV) and red (1.96 eV) excitation. (We do not have measurements with the blue line on this sample.) The weak PL band near 1.7 eV is associated with the split-off valence band (it corresponds to cb→so transitions in Fig. 8-4) and is stronger with green excitation than with red. Our clearest view of this cb→so PL band is shown in the top panel of Fig. 8-8, taken with the blue line for out most highly doped film.

8.2 Photoluminescence study of LT-GaAs:C

Introduction

GaAs grown by molecular-beam epitaxy at low substrate temperatures (LT-GaAs) has been used as a buffer layer in field-effect transistor devices due to its high resistivity [20]. Previous studies reported either weak [21] or absent [20,22] photoluminescence in as-grown and annealed LT-GaAs samples. This PL quenching effect is believed to be associated with excess arsenic in the samples [22]. In the present study, the PL spectra of LT-GaAs:C are measured and the results discussed.

Experiment and Results

The photoluminescence spectra were measured at room temperature. The measurements were done at Imperial College, London, by M. L. Hsieh, using a Renishaw Raman microprobe, and also at Renishaw plc, Wotton-under-edge, UK, by Chris Froud, with Renishaw RM1000 Raman system. The excitation source in both series of experiments was an argon ion laser operating at 514.5 nm (2.41 eV).

Discussion

Figure 8-9 shows the photoluminescence spectra of LT-GaAs:C films grown at different values of the growth temperature T_{growth}, for a series of samples doped to a carbon concentration close to 6×10^{19} cm^{-3}. The spectra show a dramatic change when the growth temperature increases from 330 to 400 C. Once T_{growth} reaches and exceeds 400 C, the PL spectrum shows the strong bandgap emission feature at 1.4 eV. The PL spectra of these samples are the same as that exhibited by normal GaAs:C grown at 600 C. The presence of the strong bandgap PL emission indicates that the $T_{growth} \geq 400$ C material is essentially the same as the GaAs:C discussed in the preceding section, and now contains

(in contrast to the $T_{growth} \leq$ 400 C material) a large concentration of holes. Hall-effect measurements on these samples indeed confirm that p is about $6 \times 10^{19} cm^{-3}$. From these results, we conclude that when the growth temperature is higher than 400 C, the sample is, in fact, normal GaAs:C.

Unlike the strong photoluminescence of normal GaAs:C, the PL of LT-GaAs:C, for the growth temperature under 400 C, is quenched. But under the highest sensitivity of the Renishaw system, very weak broad band features are seen, for $T_{growth} <$ 400 C LT-GaAs:C films, in the region 1.5-2.0 eV. These are shown in Figs.8-10 and 8-11. Figure 8-10 shows a T_{growth} series at constant [C]; Fig. 8-11 shows a [C] series at constant T_{growth}. (The middle –panel spectrum is common to both figures.)

From Fig. 8-9 it can be seen that the magnified weak features of Fig. 8-10 and Fig. 8-11 are roughly a factor of 10^5 down in intensity from the bandgap PL emission peak in normal GaAs:C. It can be risky to interpret such weak and broad PL features because, as shown in a classic study by B. A. Wilson [23], they can easily be caused by traces of organics on the sample surface. The very broad band near 2.0 eV that is seen for the lowest-T_{growth} sample (shown in the bottom panel of Fig. 8-10) has characteristics of a "Wilson-effect" feature, and will not be discussed further.

The other main features appearing in Figs 8-10 and 8-11 are a low energy cutoff near 1.4 eV and broad peaks near 1.6 and 1.8 eV. The cutoff near the GaAs bandgap and the position of the 1.6 eV peak suggest these features correspond to transitions to the deep split-off valence band.

Both broad peaks decrease in intensity with decreasing T_{growth} (Fig. 8-10) and increasing [C], i.e., with increasing disorder. Disorder increases the importance of

nonradiative recombination processes relative to radiative recombination. At the lowest doping (Bottom panel of Fig. 8-11), both peaks shift down and become closer to the results reported by Metha et al. [21]. One of the most interesting aspects of these very weak LT-GaAs:C PL spectra is that the higher-energy emission corresponding to the split-off valence band is equal in intensity to the emission corresponding to the uppermost valence bands.

8.3 Summary

The photoluminescence of GaAs:C films grown by molecular beam epitaxy has been investigated, at room temperature, over a wide range of doping concentration extending from 1.4×10^{17} cm^{-3} to 1.4×10^{20} cm^{-3}. The PL spectra were successfully analyzed with a very simple model assuming indirect transitions involving thermalized band-edge conductionband electrons and the deep distribution of valence band holes in our highly doped p-type films. The analysis yielded estimates of the concentration dependence of the bandgap energy and the depth of the Fermi energy within the valence band. The concentration dependence of the doping-induced bandgap reduction is reasonably well described by a $p^{\frac{1}{3}}$ Casey-Stern power law, while the Fermi-level depth is in reasonable agreement with a band-filling $p^{\frac{2}{3}}$ dependence. In addition to the main near-bandgap emission band near 1.4 eV, a second weaker above-bandgap PL band was observed near 1.7 eV which corresponds to transitions from the conduction band to the split-off (deeper) valence band. This split-off-band PL peak increased with doping and with excitation photon energy.

The room-temperature photoluminescence of LT-GaAs:C was investigated as a function of growth temperature T_{growth}. A pronounced change occurs at a T_{growth} of about 370 C which evidently signals the demarcation between LT-GaAs and normal GaAs. For higher T_{growht}, the PL spectrum shows the strong bandgap emission characteristic of normal (T_{growth} = 600 C) GaAs:C. For lower T_{growth}, the PL intensity is quenched by a factor of about 10^5. The very weak PL exhibited by LT-GaAs:C shows two broad bands, of about equal intensity, at about 1.6 and 1.8 eV. Their intensities decrease with increasing disorder (decreasing T_{growth} or increasing [p]). The 1.6 eV band is interpreted as band gap emission and the 1.8 eV band as emission to the split-off valence band in highly disordered LT-GaAs:C.

References

1. H. C. Casey, Jr. and Frank Stern, J. Appl. Phys. **47**, 631 (1976).
2. A. N. Titkov, E.I. Chaĭkina, E'. M. Komova, and N. G. Ermakova, Sov. Phys. Semicond. **15**, 198 (1981).
3. C. Kittel, *Introduction to Solid State Physics* (Wiley, Singapore, 1991), p.204.
4. G. Burns, *Solid State Physics* (Acadamic, Orlando, 1985), p. 315.
5. J. S. Blakemore, *Semiconductor Statistics* (Pergamon, Oxford, 1962), Table B2 p.351-353.
6. J. S. Blakemore, J. Appl. Phys. **53**, R123 (1982).
7. D. Olego and M. Cardona, Solid State Commun **32**, 1027 (1979).
8. R. Zallen, W. Songprakob, S. Vijarnwannaluk, M. L. Hsieh, R. A. Stradling, W. K. Liu, and K. L. Bacher, Bull. Am. Phys. Soc. Abstract WC15.03 (March 1999) on the web at http://www.aps.org/meet/CENT99/BAPS/abs/S8390003.html
9. D. Olego and M. Cardona Phys. Rev. B **22**, 886(1980).
10. L. Wang, B. J. Aitchison, N. M. Haegel Appl Phys Lett. **60** 1111(1992).
11. G. Borghs, K. Bhattacharyya, K. Deneffe, P. Van Mieghem, R. Mertens J. Appl. Phys. **66**, 4381(1989).
12. D. E. Aspnes and A. A. Studna, Phys. Rev. B **27,** 985(1983).
13. B. P. Zakharchenya, V. I. Zemskiĭ, and D. N. Mirlin, Sov. Phys. JETP **43**, 569(1976).
14. R. A. Abram, G. J. Rees and B. L. H. Wilson, Advance n Physics **27**, 799(1978).
15. R. K. Ahrenkiel, Ellingson, W. Metzger, D. I . Lubyshev, and W. K. Liu, Appl. Phys. Lett. **78**, 1879 (2001).

16. W. Songprakob, R. Zallen, W. K. Liu, and K. L. Bacher, Phys. Rev. B **62**, 4501(2000)

17. W. Songprakob, R. Zallen, D. V. Tsu, and W. K. Liu, J. Appl. Phys. **91,** 171(2002).

18. T. Furuta, and M. Tomizawa, Appl. Phys. Lett. **56**, 824 (1990).

19. J. A. Silberman, T. J. de Lyon, and J. M. Woodall, Appl. Phys. Lett. **58**, 2160 (1991).

20. F. W. Smith, A. R. Calawa, C. L. Chen, M. J. Manfra, L. J. Mahoney, IEEE Electron Dev. Lett. **9**, 77 (1988).

21. S. K. Metha, T. Srinivasan, and R. K. Jain, in *Physics of Semiconductor Devices*, Edited by V. Kumar and S. K. Agarwal, (Narosa Publishing house, New Delhi 1998), p. 333.

22. T. M. Cheng, C. Y. Chang, and J. H. Huang, Appl. Phys. Lett. **66**, 2095 (1995).

23. B. A. Wilson, Phys. Rev. B **23**, 3102 (1981).

Table 8-1 Results of the photoluminescence experiments on GaAs:C

Sample	p (10^{19} cm^{-3})	E_{laser} (eV)	E_g (eV)	E'_F (eV)	E_v-E_F (eV)	η	$F(\eta)$
Back side	-	2.541	1.410	1.380	-0.030	-1.14	0.29
10981.02	0.014	2.541	1.410	1.399	-0.011	-0.42	0.54
10983.02	0.39	2.541	1.397	1.427	0.030	1.15	1.73
10985.02	3.3	2.541	1.362	1.458	0.096	3.69	5.84
10512.02	14	2.541	1.336	1.533	0.197	7.58	16.0
10514.02	0.52	2.410	1.387	1.446	0.059	2.27	3.17
10977.02	6.6	2.410	1.350	1.478	0.128	4.92	8.64
10986.02	9.1	2.410	1.349	1.501	0.152	5.85	11.0
10511.02	10.5	2.410	1.344	1.504	0.160	6.15	11.9
Back side	-	1.959	1.411	1.396	-0.015	-0.58	0.47
10514.02	0.52	1.959	1.390	1.434	0.044	1.69	2.38
10977.02	6.6	1.959	1.348	1.475	0.127	4.88	8.54
10986.02	9.1	1.959	1.338	1.508	0.170	6.54	12.7
10511.02	10.5	1.959	1.332	1.498	0.166	6.38	12.3

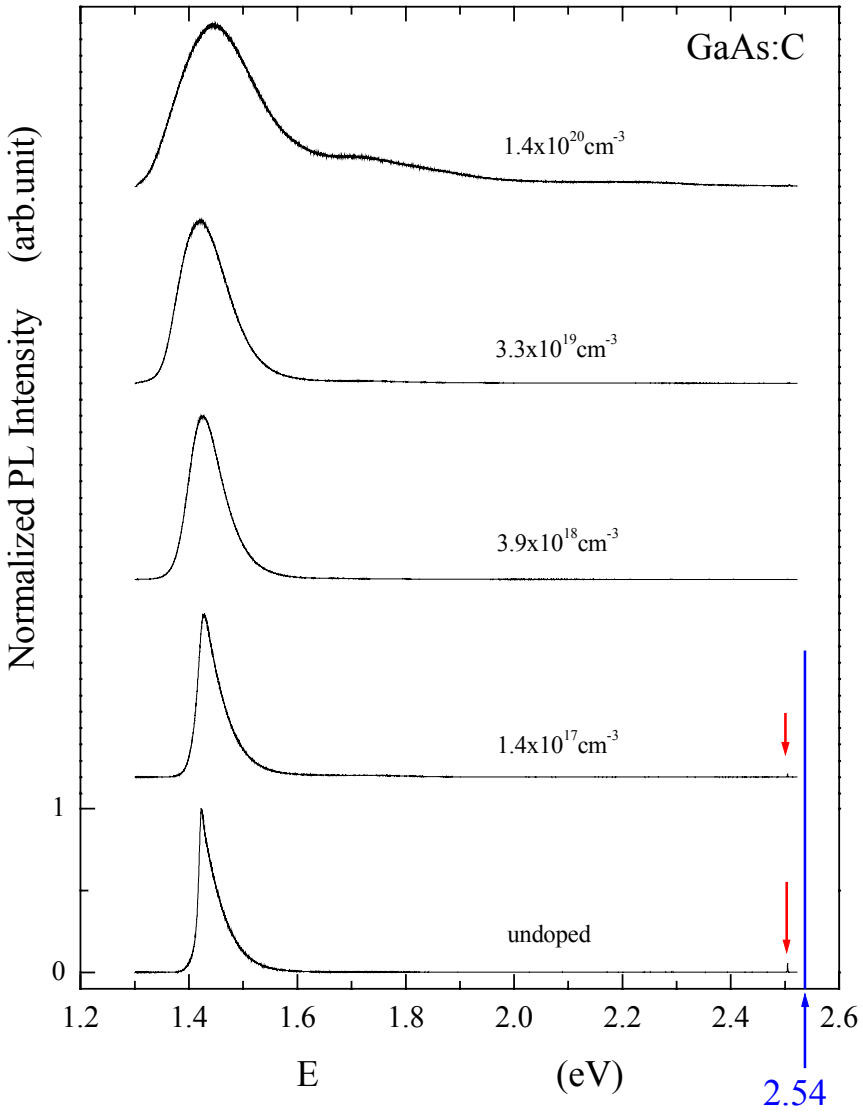

Figure 8-1. Photoluminescence spectra of MBE-grown GaAs:C films as a function of carbon concentration. The position of the laser photon energy (2.54 eV) is marked by the long vertical line at the right. The small sharp peak marked by an arrow, for the two low-doping spectra, is a Raman-scattering feature (the LO line). The PL spectra are normalized with respect to the peak intensity and are displaced vertically for clarity.

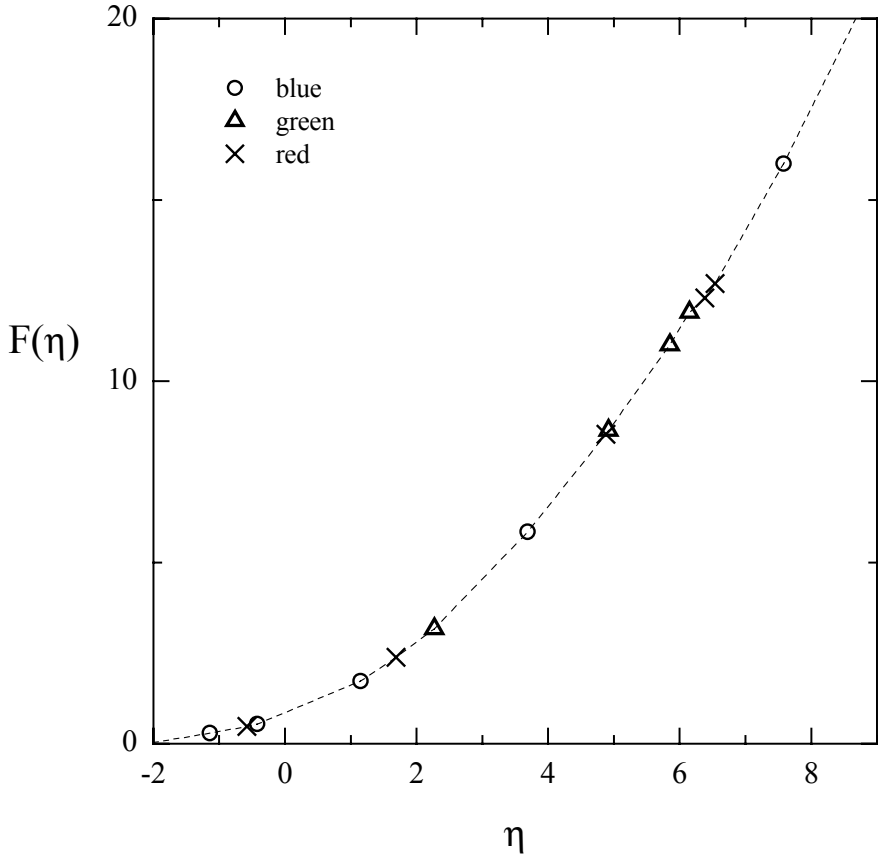

Figure 8-2. The Fermi integral F(η), evaluated numerically for various values of the degree of degeneracy η. The points are the calculated F(η) values; the dashed curve is a polynomial (quadratic) fit to the points presented to provide a graphic representation of F(η). For the range of the degree of degeneracy shown in the graph, the dashed line corresponds to $F(\eta) = 0.80+0.72\eta+0.17\eta^2$. The η values at which F(η) was determined came out of our photoluminescence measurements made using the blue, green, and red laser lines listed in Table 8-1.

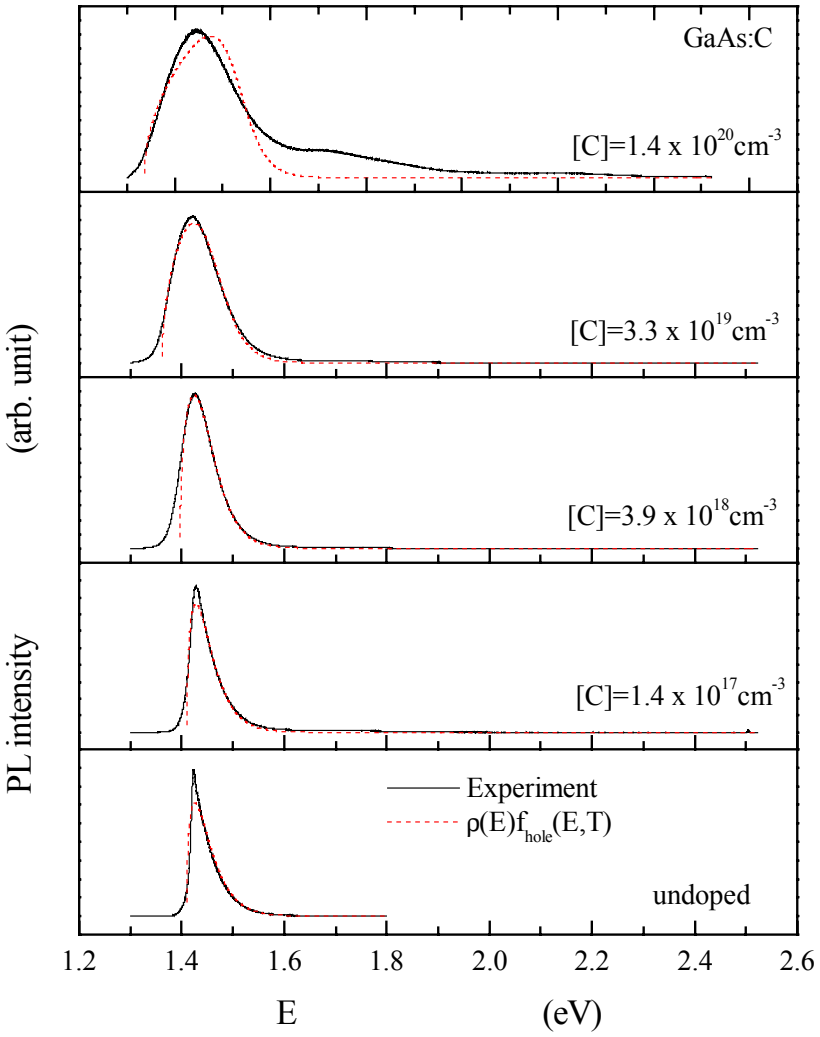

Figure 8-3. Comparison of the experimental photoluminescence spectra of Fig. 8-1 to fits based on the simple model expressed in equation (8-9)

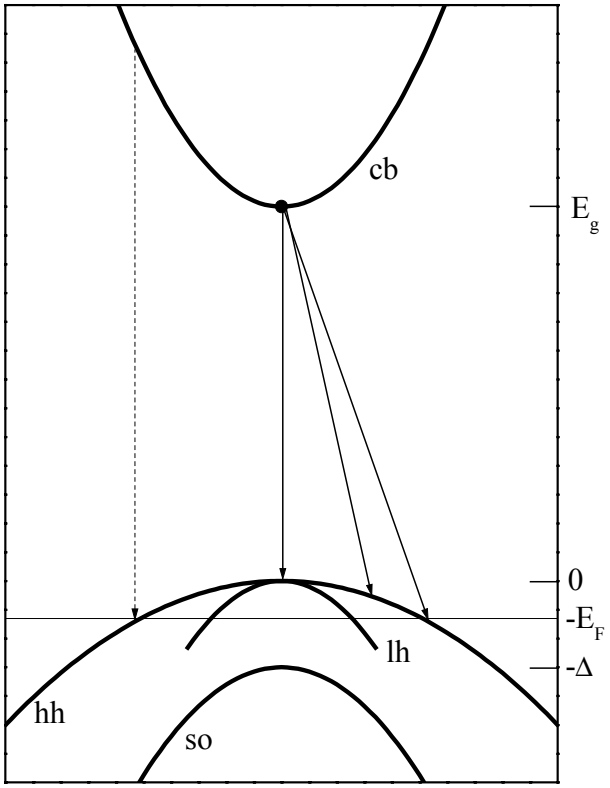

Figure 8-4. Band-structure illustration of the model underlying equation (8-9) for the photoluminescence lineshape I(E). From top down, the curves represent E(k) for the conduction band (cb), the heavy-hole (hh) valence band, the light-hole (lh) valence band, and the split-off (so) valence band. The three cb→hh lines originating from the bottom of the conduction band represent emission processes included in our I(E). Although the band structure shown is schematic, the relative curvatures near k=0 qualitatively respect the relative sizes of m_c^*, m^*_{hh}, m^*_{lh}, and m^*_{so} effective masses for GaAs. Similarly for the bandgap E_g and the spin-orbit splitting Δ (1.42 and 0.34 eV, respectively, at room temperature). However the nonparabolicity of the bands (most notably, the lh band) is not included. The E_F value shown (about 0.14 eV) corresponds to a hole concentration of about 8×10^{19} cm^{-3}. The dashed line represents a direct transition involving a nonthermalized electron high in the conduction band; such high-photon-energy process are not observed in the measured PL spectrum.

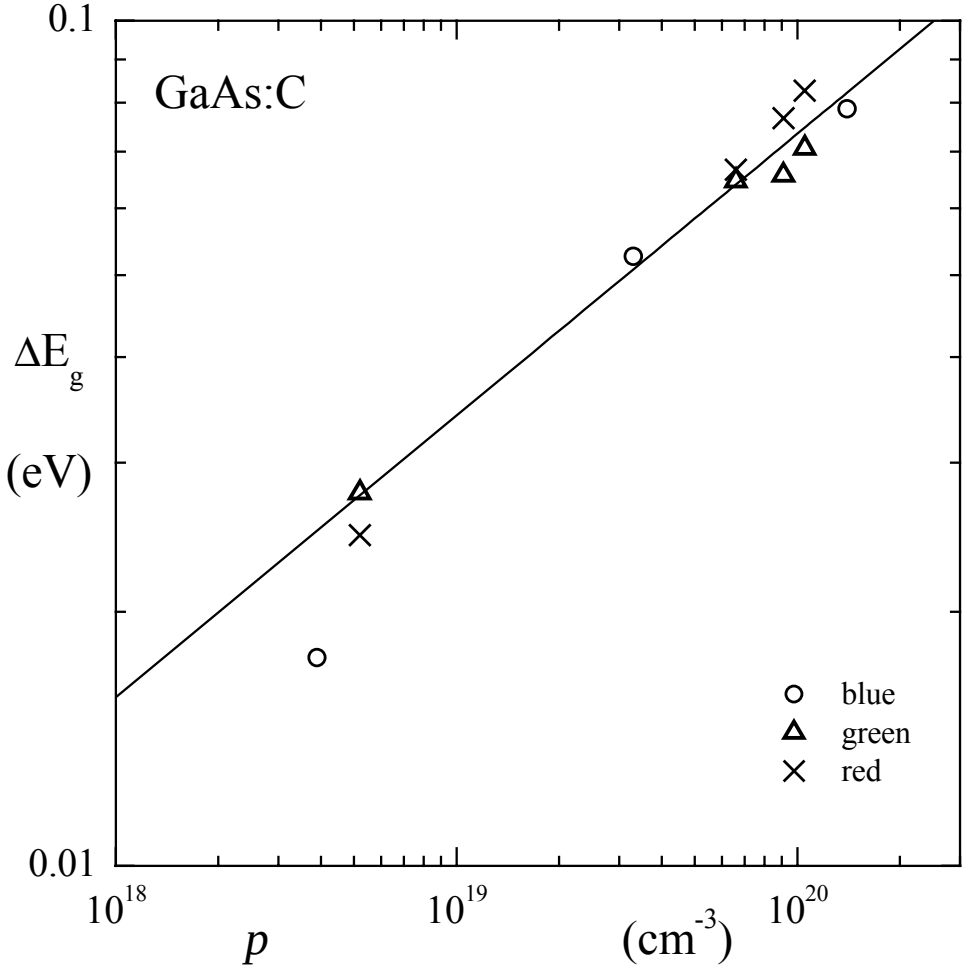

Figure 8-5 The concentration dependence of the photoluminescence-derived bandgap reduction at high doping, shown on the log-log plot. The straight line has a slope of $\frac{1}{3}$ and corresponds to $E_g(p) = E_g(0) - Ap^{\frac{1}{3}}$ using the best-fit values of $E_g(0)$ and A given by 1.415 eV and 1.58×10^{-8} eV.cm.

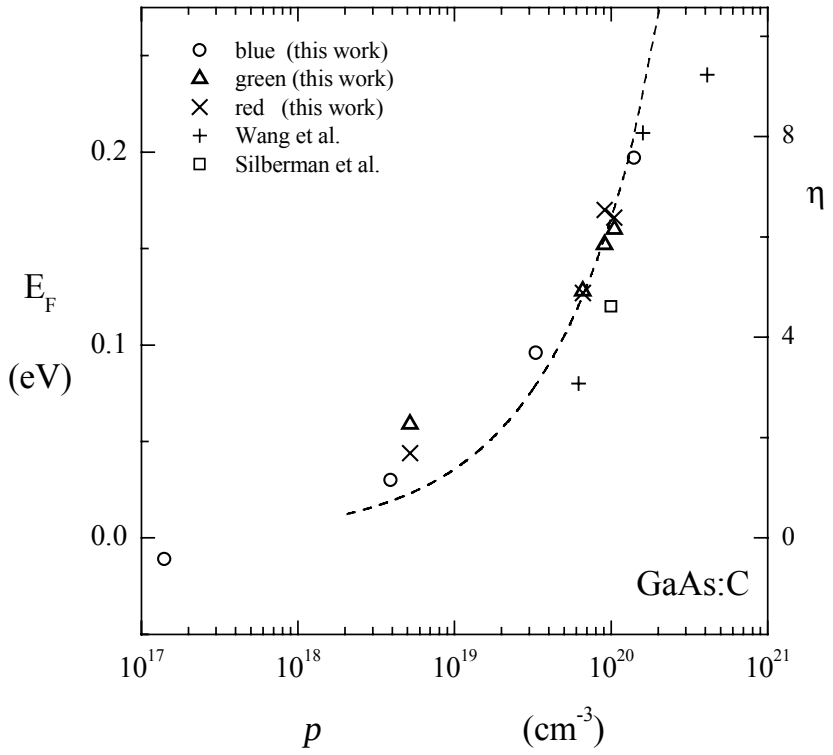

Figure 8-6. The concentration dependence, for our MBE GaAs:C films, of the photoluminescence-derived depth of the Fermi level (labeled E_F in Fig. 8-4) below the top of the valence band. Different symbols (as indicated at the top left) are used for the PL results obtained with the three different laser lines. Also included are the results of Wang et al. [10] and Silberman et al. [19]. The dashed curve is a fit assuming (at high doping) a two-thirds power law, and is given by $E_F = (7.7\times10^{-15}\,\mathrm{eV.cm^2})p^{\frac{2}{3}}$. The scale at the right border gives the degree of degeneracy η. In terms of the E_F plotted here, η is E_F/kT.

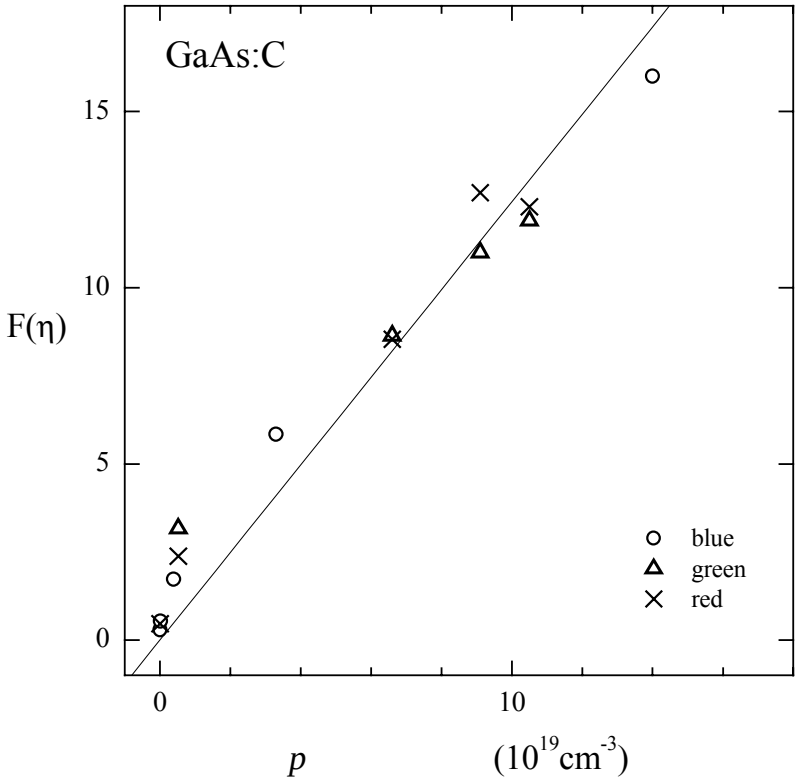

Figure 8-7. The concentration dependence of F(η), where F denotes the Fermi-Dirac integral and η is the photoluminescence-derived degree of degeneracy $(E_V-E_F)/kT$. (In terms of E_F of Fig. 8-4 and 8-6, η is E_F/kT.) The line is a fit which assumes that F(η) is proportional to p. Its slope yields (via equation 8-7) an effective density of states N_v of 8.1×10^{18} cm^{-3} and (via equation 8-8) a density-of-states hole mass of $0.47m_e$.

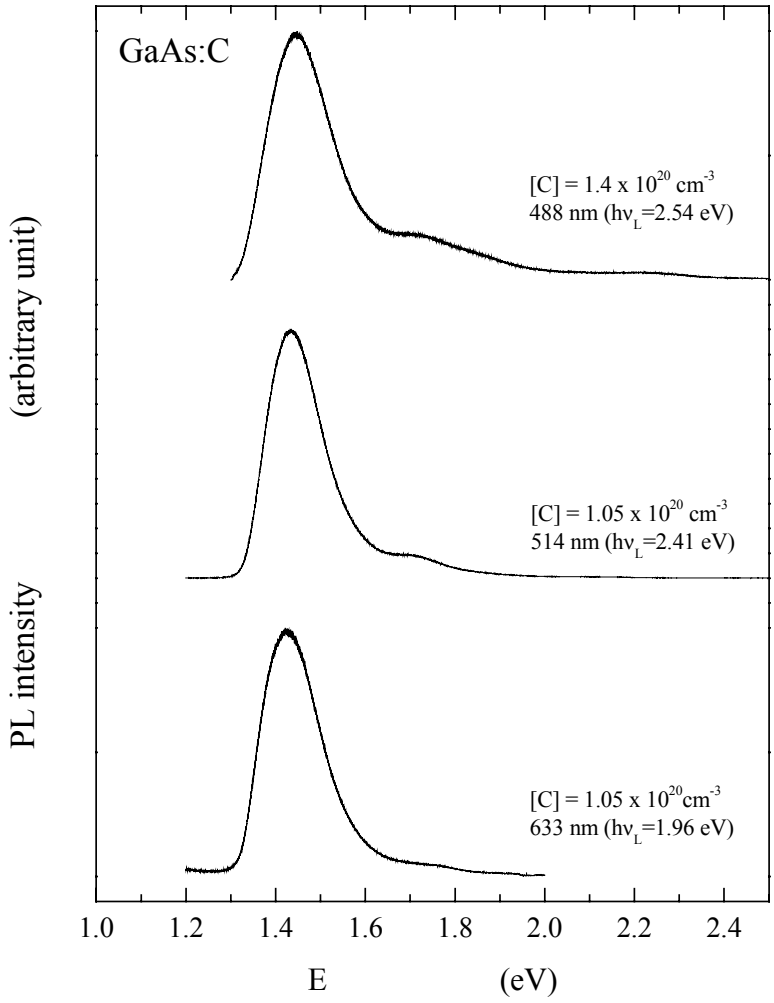

Figure 8-8. Comparison of photoluminescence spectra obtained using different laser lines: blue (2.54 eV), green (2.41 eV), and red (1.96 eV). For the 1.05×10^{20} cm^{-3} sample, the bandgap emission band near 1.4 eV is the same with green and red excitation (lower two curves), while the weak band near 1.7 eV associated with the split-off valence band (corresponding to cb→so transitions in Fig. 8-4) is stronger with the green line. The cb→so band is most prominent in the top spectrum, taken with the blue line for our most highly doped film.

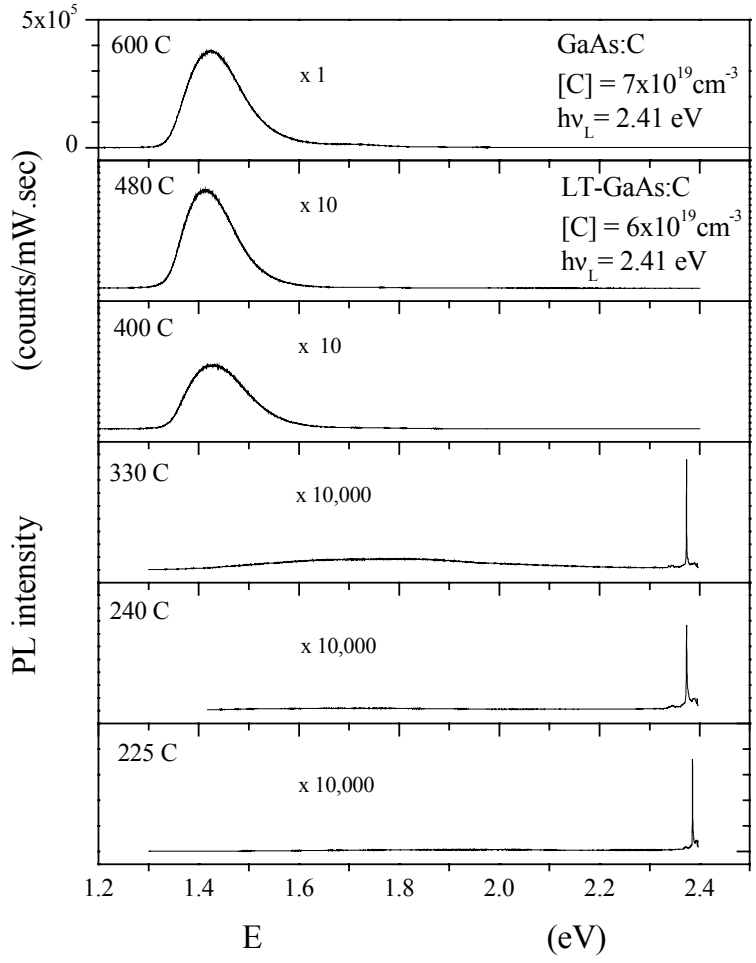

Figure 8-9. The photoluminescence of LT-GaAs:C films prepared at different growth temperatures, obtained using laser excitation at 2.41 eV, for a series of samples doped to the same carbon concentration of 6×10^{19} cm^{-3}. The top spectrum, for a film grown at 600 C with carbon concentration of 7×10^{19} cm^{-3}, is the PL spectrum of normal GaAs:C. The spectra for T_{growth} = 480 C and 400 C are similar, but weaker by about a factor of 10. The three lowest spectra are shown magnified, relative to the top spectrum, by a factor of 10^4. At this sensitivity, the LO Raman line is seen (at the right) just below the laser photon energy.

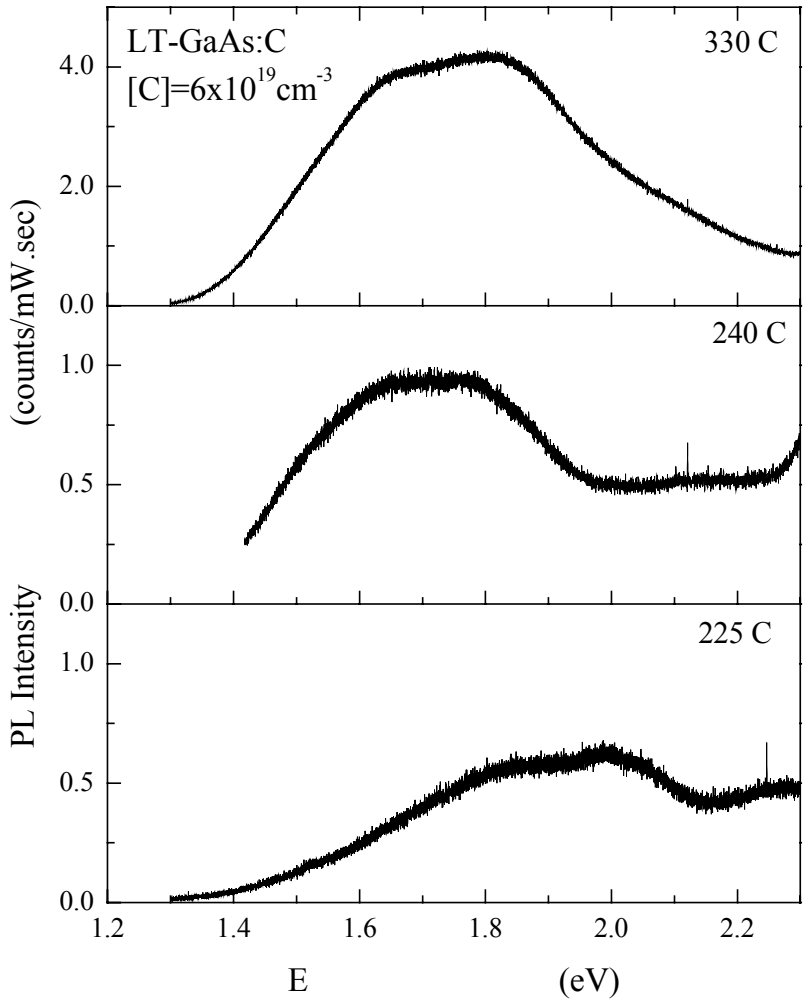

Figure 8-10. Photoluminescence for three growth temperatures of LT-GaAs:C.

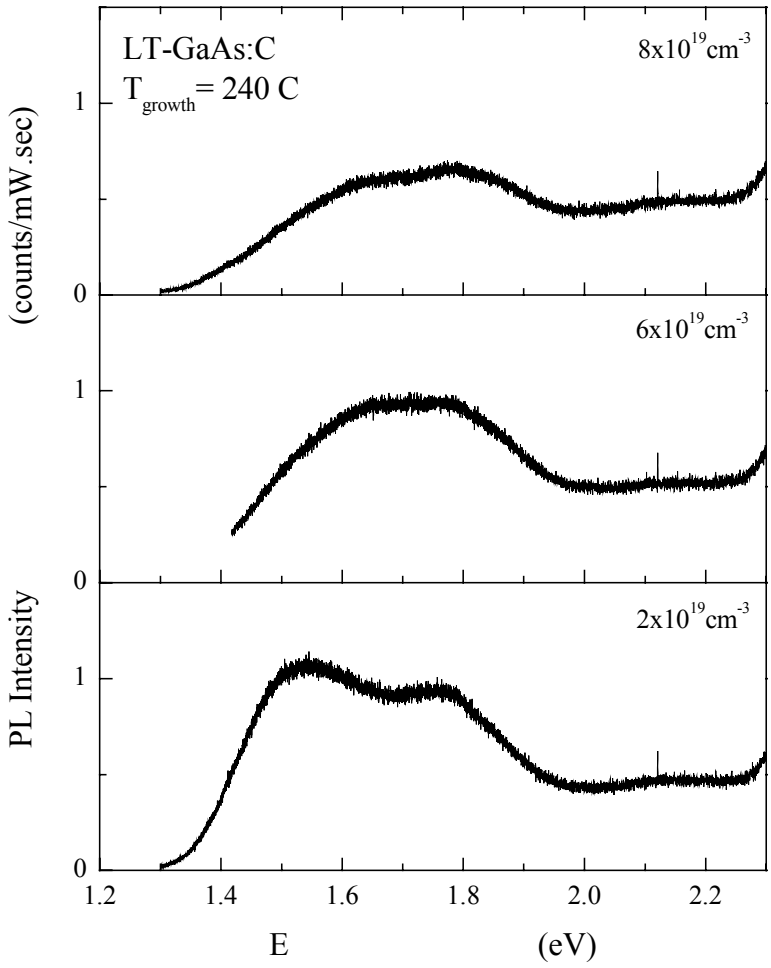

Figure 8-11. Doping dependence of the apparent PL spectra of LT-GaAs:C films grown at 240 C.

Chapter 9. Optical studies of annealed carbon-doped GaAs grown at low growth temperature

9.1 Introduction

LT-GaAs, GaAs grown by molecular beam epitaxy at low substrate temperature (about 300 C), has properties that are quite different from MBE GaAs grown at the standard growth temperature (about 600 C). LT-GaAs shows high resistivity and short photoexcited carrier lifetimes [1]. After LT-GaAs has been prepared, post-growth thermal annealing has been reported to increase photocarrier lifetime [2] and to actually increase its resistivity [3]. Berylliun has been used as a dopant to help maintain short carrier lifetimes in LT-GaAs after annealing [4]. However, LT-GaAs:Be is not stable after high-temperature annealing. The resistivity of LT-GaAs:Be drops by six orders of magnitude after a proximity anneal at 700 C in a nitrogen atmosphere for 30 minutes [5]. (a proximity anneal is one in which the GaAs surface is kept in close contact with another GaAs sample to prevent arsenic depletion of the near-surface region.). Carbon is an alternative to beryllium for p-type doping and shows promise for maintaining stability after high-temperature annealing [6]. Hall measurements on heavily doped (6.6×10^{19} cm^{-3}) LT-GaAs:C shows high resistivity (1×10^{4} Ωcm) after 700°C anneal [6]. This is much higher than that of LT-GaAs:Be annealed to this temperature.

We have carried out Raman-scattering, photoluminescence, and infrared measurements on LT-GaAs:C annealed in air. The results show that LT-GaAs:C remains stable after a 600 C anneal, maintaining the LT properties. However, annealing in air causes damage to the surface of the sample, making some of our results difficult to interpret.

9.2 Samples and Experiments

A 1000-nm LT-GaAs:C film, prepared at a growth temperature of 240 C with a doping concentration 6×10^{19} cm^{-3} was annealed in air in a 3-zone tube furnace at 600 C for 20 minutes. The sample was covered on both sides with sacrificial GaAs wafers in a proximity anneal. Annealing changed the mirror-like sample surfaces from colorless to a golden color. On the side of the sample containing the MBE LT-GaAs:C film, small black spots appeared. The spots were absent on the back side (GaAs substrate) of the sample and on the surfaces of the undoped-GaAs proximity wafers.

Raman-scattering measurements on the sample were done with a SPEX 1403 Raman system using an Ar^+ ion laser operating at 488 nm(2.54 eV). The laser power was set at 300 milliwatts at the laser head, corresponding to about 20 milliwatts at the sample. The slit width used was 300 microns, corresponding to a resolution of 3.4 cm^{-1}. Also, in order to study small areas on the surface, Raman measurements were made by Jing Ling of Virginia Tech Geology Department, using a Dilor XY Raman microprobe and an Ar^+ ion laser operating at 514 nm (2.41 eV). With the Dilor the diameter of the laser beam at the sample was under 200 microns.

Infrared transmission and reflection measurements were carried out with a Bomem DA3.01 spectrometer. Photoluminescence measurements were carried out by Ming-Ling Hsieh at Imperial College, London using a Renishaw microprobe and excitation from an Ar^+ ion laser at 2.41 eV.

9.3 Results and Discussion

Photoluminescence

Figure 9-1 presents photoluminescence spectra for GaAas:C, LT-GaAs:C, and anneal LT-GaAs:C. The bottom panel shows the LT-GaAs:C spectrum for a film grown at 240 C with a carbon doping of 6×10^{19} cm^{-3}. The middle panel shows the spectrum of the same LT-GaAs:C film after it was annealed for 20 minutes at 600 C. The bandgap emission of standardly grown GaAs:C is absent in both lower panels, showing that photoluminescence is quenched in LT-GaAs:C both before and after annealing. MBE GaAs:C grown at about 600 C (standard GaAS:C) is p-type conducting and luminescent. LT-GaAs:C is nonconducting and nonluminescent. LT-GaAs:C annealed at 600 C is also nonluminescent, showing that it retains its LT properties. This is evidence that, once formed, LT-GaAs:C (unlike LT-GaAs:Be) is stable against post-growth high-temperature anneal. PL spectra for the annealed LT-GaAs:C sample, taken with three different excitation energies (1.59, 1.96, and 2.41 eV), are shown in Fig. 9-2. A sharp bandgap emission line (peak at 1.42 eV) is seen with 1.59 eV excitation. But this bandgap emission does not originate from the LT- GaAs:C film, it originates from the undoped GaAs substrate. The MBE LT-GaAs:C film is 1000 nm (=10^{-4} cm) thick. At 1.59 eV, 1.96 eV, and 2.41 eV), the absorption coefficient α of GaAs is 1.5×10^4 cm^{-1}, 4×10^4 cm^{-1}, and 9×10^4 cm^{-1}, respectively [7]. The light intensity reaching the substrate is proportional to $e^{-\alpha d}$. Assuming that $\alpha(h\nu)$ for LT-GaAs:C is not drastically different from that for GaAs, The fraction of light (relative to that just inside the front surface of the film) reaching the substrate is roughly 22%, 2%, and 0.01% at 1.59 eV, 1.96 eV, and

2.41 eV. The PL signature of the substrate shows up clearly in spectrum taken with 1.59 eV excitation.

Raman scattering

Raman lines are seen close to the laser photon energy in several of the spectra of Figs. 9-1 and 9-2. The single strong Raman line seen for the as-grown LT-GaAs:C film in the bottom panel of Fig. 9-1 is the GaAs zone-center longitudinal optical (LO) phonon line. But the Raman spectrum observed for the annealed film (Fig. 9-2, middle panel of Fig. 9-1) is significantly different.

Fig. 9-3 shows a Raman spectrum obtained with our conventional SPEX system on the annealed LT-GaAs:C film. Raman lines are seen at 199, 257, 267, and 290 cm^{-1}. The 290 cm^{-1} line is the GaAs LO line and the 267 cm^{-1} line is the GaAs TO line (corresponding to the zone-center transverse- optical phonon). The lines at 199 and 257 cm^{-1} are identified as phonon lines of crystalline arsenic [8]. These lines also appear on the back (substrate) side of the sample, (which is also golden in color after annealing). We believe that these lines come from a crystalline arsenic film formed by the oxidation of GaAs [8],

$$4GaAs + 3O_2 \rightarrow 2Ga_2O_3 + 4As \qquad (9\text{-}1)$$

The spectrum of Fig. 9-3 was obtained from a region of the surface which included some small dark spots. Figure 9-4 shows Raman spectra from several of these spots as well as one from the off-spot region. The off-spot spectrum is dominated by the two arsenic lines, but these are absent from the spectra of the spots which show only the GaAs To and LO lines. The spots thus appear to be pinholes in the crystalline arsenic film which provide a window to the underlying GaAs. After annealing, spots are also

seen (under a microscope) on the substrate side, but these spots differ in that Raman shows them to be (like the surrounding area) covered by arsenic, not bare as they are on the MBE-film side.

The strong-LO/weak-TO GaAs Raman spectra seen in the upper three spectra of Fig. 9-4 are representative of undoped GaAs. In highly conducting p-type GaAs:C, the TO line is replaced by a much stronger plasmon-phonon line. This is evidence that the LT-GaAs:C film remains resistive after annealing at 600 C, in agreement with the resistivity results obtained from Hall-effect measurements by Liu et al.[6].

Infrared measurements

There are two parts to the infrared work. First, we studied the effect of annealing on the localized-vibrational-mode (LVM) infrared absorption of carbon in LT-GaAs:C. Second, we studied the infrared reflectivity of as-grown and annealed LT-GaAs:C in the mid-infrared plasmon region. Infrared transmission spectra of the as-grown and the subsequently annealed LT-GaAs:C sample were carefully measured in the range 550-600 cm^{-1} which contains the carbon LVM absorption line at 580 cm^{-1}. The absorption contribution α_{LVM} corresponding to the LVM line was extracted from the transmission spectra by the procedure described in chapter 4.

After anneal, the large full-width-of-half-maximum (FWHM) linewidth of the LVM line in LT-GaAs:C decreases by about a factor of 2 and becomes closer to the FWHM of GaAs:C (5.5 cm^{-1}). We interpret this narrowing as an indication of annealing-induced reduction in the disorder and defect concentration of LT-GaAs:C. The integrated absorption of the LVM absorption line also decreases with annealing, approaching the integrated absorption of GaAs:C at the same concentration (chapter 4).

The infrared reflectance of the as-grown and the annealed LT-GaAs:C film are shown in Fig. 9-6 which span a spectral region in which heavily doped GaAs:C exhibits a broad plasmon like reflectivity and the absence of a hole plasmon. After annealing, a weak reflectivity dip appears which has the appearance of a shallow version of the reflectivity dip seen in conducting GaAs:C. This results suggests that every thin (≈10 nm [10]) surface layer of the annealed LT-GaAs:C film has been transformed to GaAs:C.

9.4 Summary

An MBE-grown LT-GaAs:C film was annealed in air at 600 C and then investigated by Raman scattering, photoluminescence, infrared absorption, and infrared reflectivity. After the anneal, both the MBE-film and the undoped-GaAs substrate sides of the sample develop a golden color which Raman scattering reveals to be caused by a film of crystalline arsenic. Dark spots on the LT-GaAs:C side correspond to exposed material not covered by arsenic, and micro-Raman spectra from these spots are dominated by the GaAs LO phonon line (as in nonconducting LT-GaAs:C) rather than by the coupled plasmon-phonon line (as in p-type-conducting GaAs:C). This indicates that the annealed film has retained its high-resistivity LT properties. The annealed film (like the as-grown LT-GaAs:C film) exhibits no bandgap luminescence, which is also consistent with the idea that it remains LT-GaAs:C. However, infrared measurements show that annealing does cause a significant narrowing of the carbon localized-vibrational- mode infrared absorption band, which indicates a significant reduction in defect concentration. Also, the infrared reflectivity of the annealed film exhibits a broad shallow dip which is much weaker than, but has a resemblance to, the hole-plasmon

feature seen in GaAs:C. This suggests that a very thin near-surface layer of the annealed LT-GaAs:C film has been converted to GaAs:C. More experiments are need to clarify the complex changes that occur in LT-GaAs:C upon annealing.

References

1. Frank W. Smith, Mater. Res. Soc. Symp. Proc. **241**, 3 (1992)
2. E. S. Harmon, M. R. Melloch, J. M. Woodall, D. D. Nolte, N. Otsuka, C. L. Chang, Appl. Phys. Lett. **63**, 2248 (1993).
3. Gerald L. Witt, in *Semiconductor Materials for Optoelectronics and LTMBE materials*, E-MRS Symposia proceedings, edited by J.P. Hirtz, C. Whitehouse, H.P. Meier, H. J. Von Bardeleben, M. O. Manasreh (Strasbourg, France 1993) p. 9.
4. P. Specht, S. Jeong, H. Sohn, M. Luysberg, A. Prasad, J. Gebauer, R. Krause-Rehberg, and E. R. Weber, Mater. Sci. Forum **951**, 258 (1997).
5. P. Specht, R. C. Lutz, R. Zhao, E. R. Weber, W. K. Liu, K. Bacher, F. J. Towner, T. R. Stewart, and M. Luysberg, J. Vac. Sci. Technol. B. **17**, 1200 (1999).
6. W. K. Liu, K. Bacher, F. J. Towner, T. R. Stewart, C. Reed, P. Specht, R. C. Lutz, R. Zhao, and E. R. Weber, J. Cryst. Growth **201/202**, 217 (1999).
7. D. E. Aspnes and A. A. Studna, Phys. Rev. B. **27**, 985 (1983).
8. Neil T. McDevitt, James S. Solomon, J. Electrochem. Soc. **133**, 1913 (1986).
9. W. Songprakob, R. Zallen, W. K. Liu, and K. L. Bacher, Phys. Rev. B. **62**, 4501 (2000); W. Songprakob, R. Zallen, D. V. Tsu, and W. K. Liu, J. Appl. Phys. **91**, 171 (2002).
10. W. Songprakob, private communication. This estimate is based on an effective-plasmon film-on-substrate fit to the annealed LT-GaAs:C reflectivity spectrum of Fig. 9-6.

Table 9-1. Localized-vibrational-mode infrared absorption results for as-grown and annealed LT-GaAs:C. The as-grown film was grown by MBE at 240°C with a carbon concentration of 6×10^{19} cm^{-3}. The annealed sample was the same film annealed at 600°C for 20 minutes.

Sample	IA [cm^{-2}]	α_{max} [cm^{-1}]	FWHM [cm^{-1}]
As-grown	8200	580	14
Annealed	6500	820	7.7

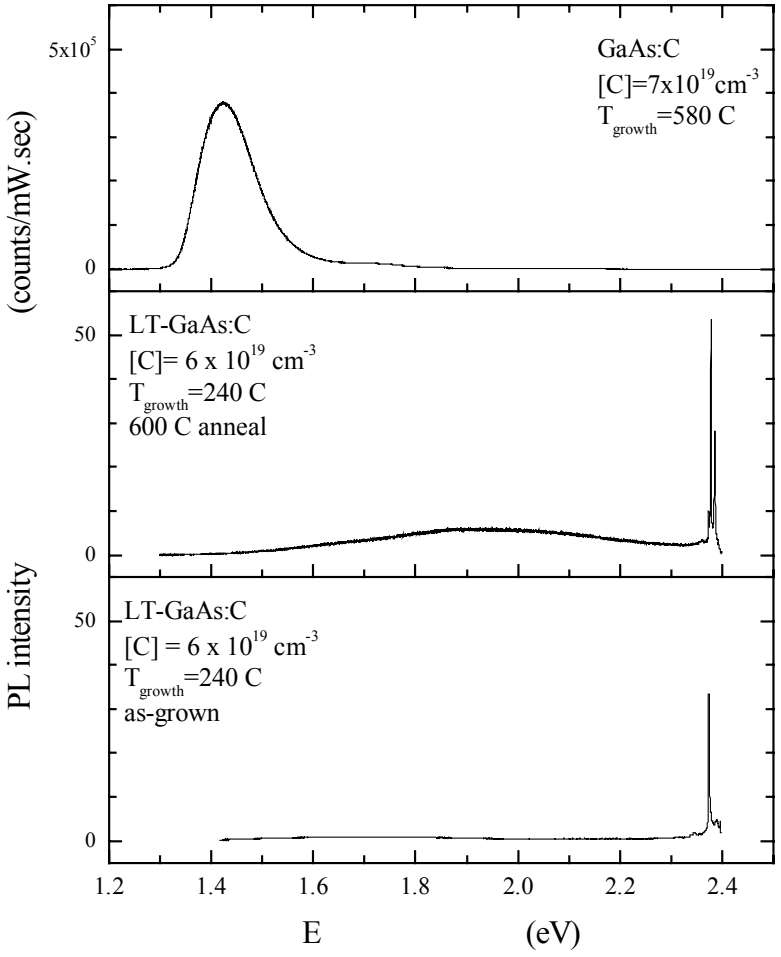

Figure 9.1. Photoluminescence spectra of GaAs:C, annealed LT-GaAs:C, and as-grown LT-GaAs:C. The GaAs:C spectrum (top panel) is the 7×10^{19} cm^{-3} spectrum of Fig. 8-9, taken with 2.41 eV excitation. The other two spectra were also taken with 2.41 eV excitation and higher sensitivity; Raman lines are visible at the right. The bottom panel is for an as-grown LT-GaAs:C film grown at 240 C with carbon doping of 6×10^{19} cm^{-3}. The middle panel is for the same film after annealing at 600 C for 20 minutes.

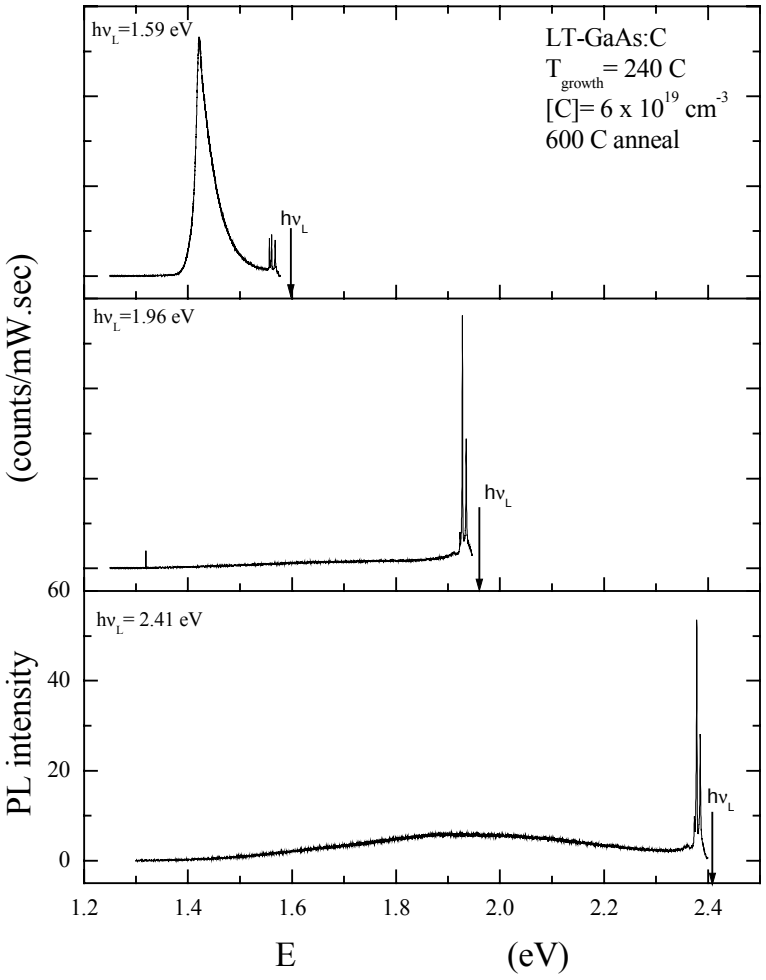

Figure 9-2. Photoluminescence of the annealed LT-GaAs:C sample taken with three different excitation energies: 1.59 eV (diode laser), 1.96 eV (He-Ne laser), and 2.41 eV (Ar^+ laser). The sharp bandgap PL band seen with 1.59-eV excitation arises from the underlying undoped-GaAs substrate. Raman lines from the LT-GaAs:C film are seen close to each laser line position (marked by $h\nu_L$).

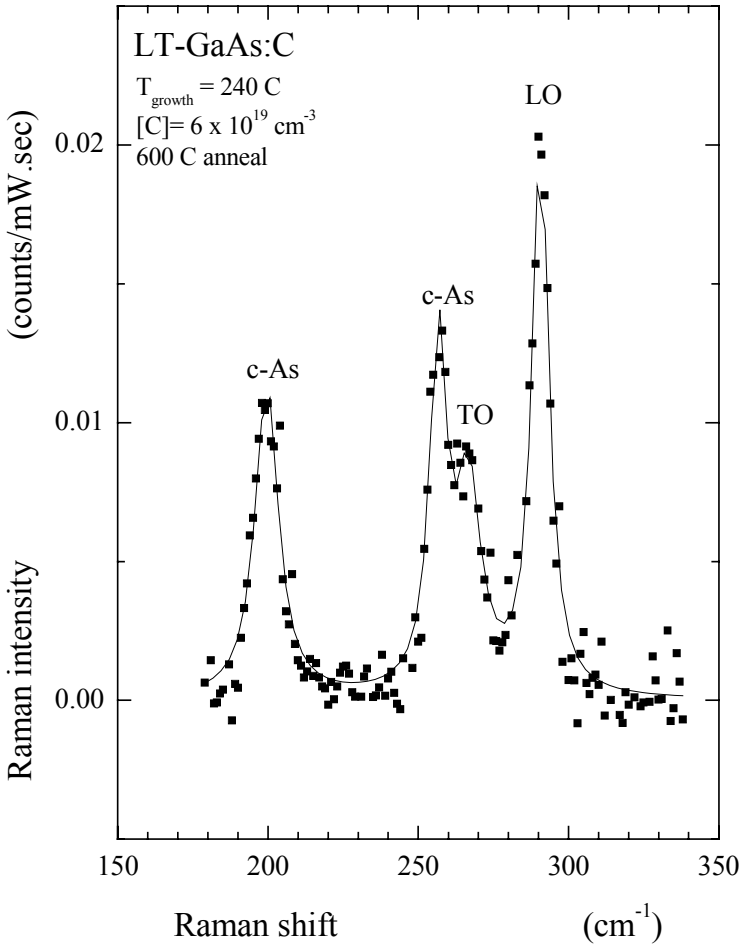

Figure 9-3. Raman scattering observed from the annealed LT-GaAs:C film, using the SPEX 1403 spectrometer and 2.54 eV excitation. Data points are shown as solid squares; the continuous curves correspond to a sum of four Lorentzians. The peaks labeled LO and TO correspond to GaAs. The peaks labeled c-As correspond to crystalline arsenic.

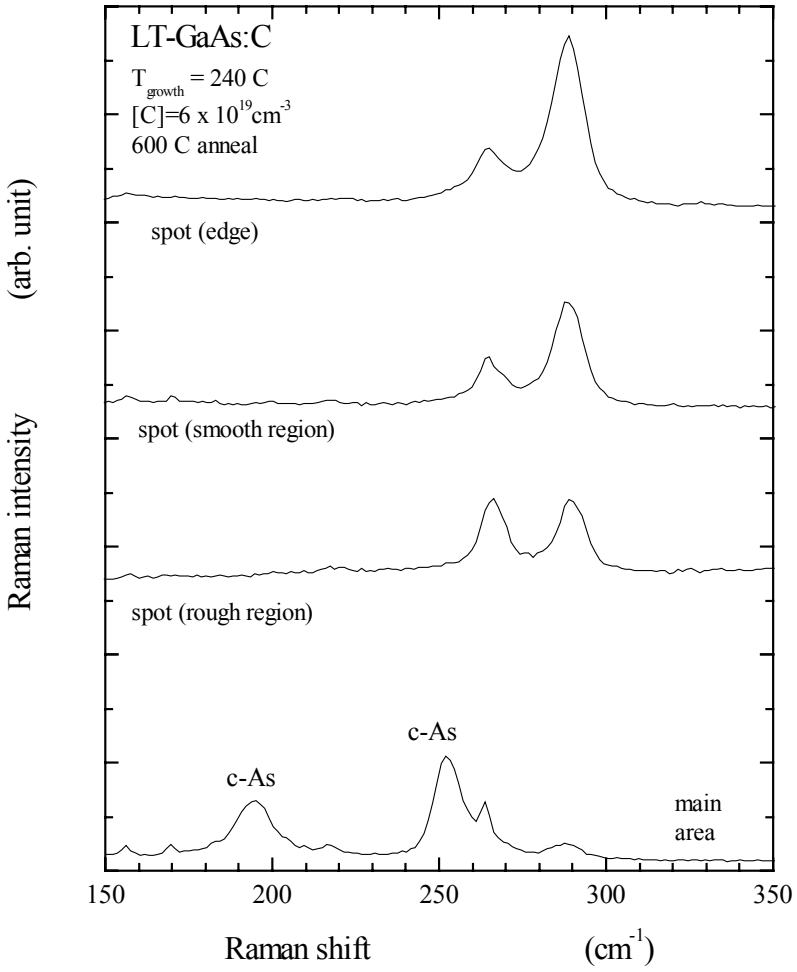

Figure 9-4. Raman scattering of the annealed LT-GaAs:C film, taken at several locations using the small beam size (200 micron) of a Dilor Raman microprobe. Laser excitation was at 2.41 eV. The three upper spectra are from dark spots on the annealed film; the bottom spectrum is from the main gold-colored area.

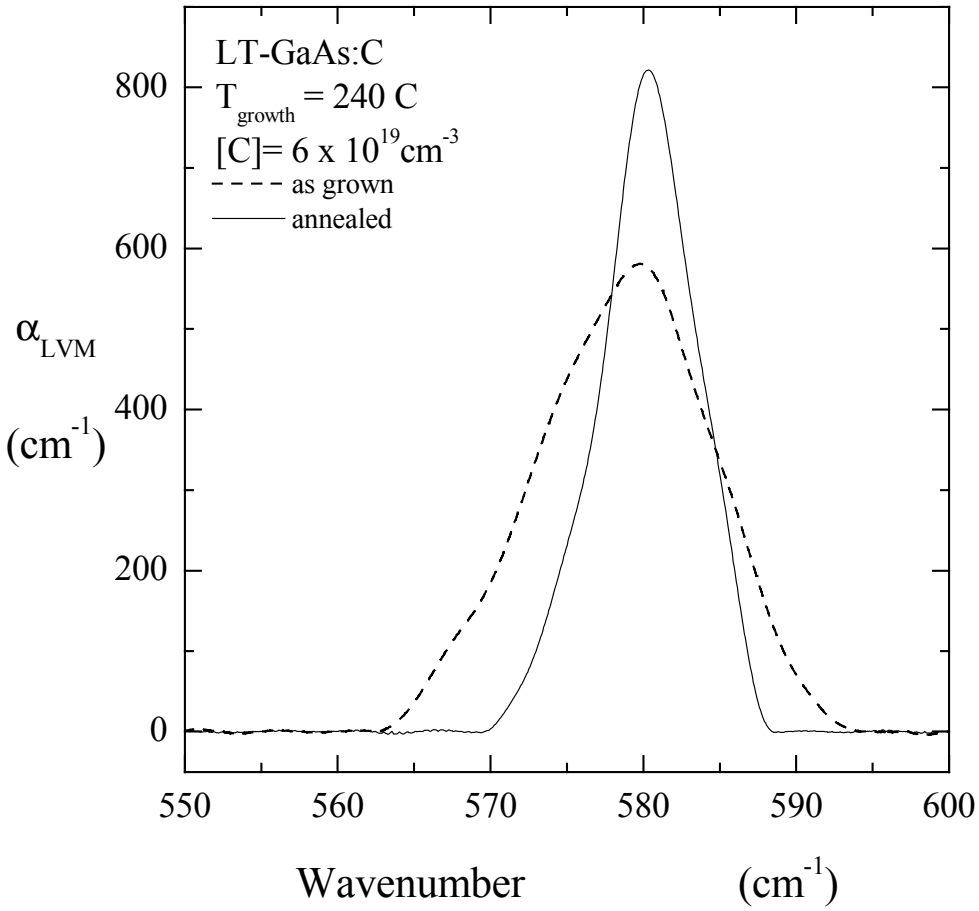

Figure 9-5. Infrared absorption band of the C_{As} localized vibrational mode in LT-GaAs:C before (dashed line) and after (solid line) annealing at 600 C.

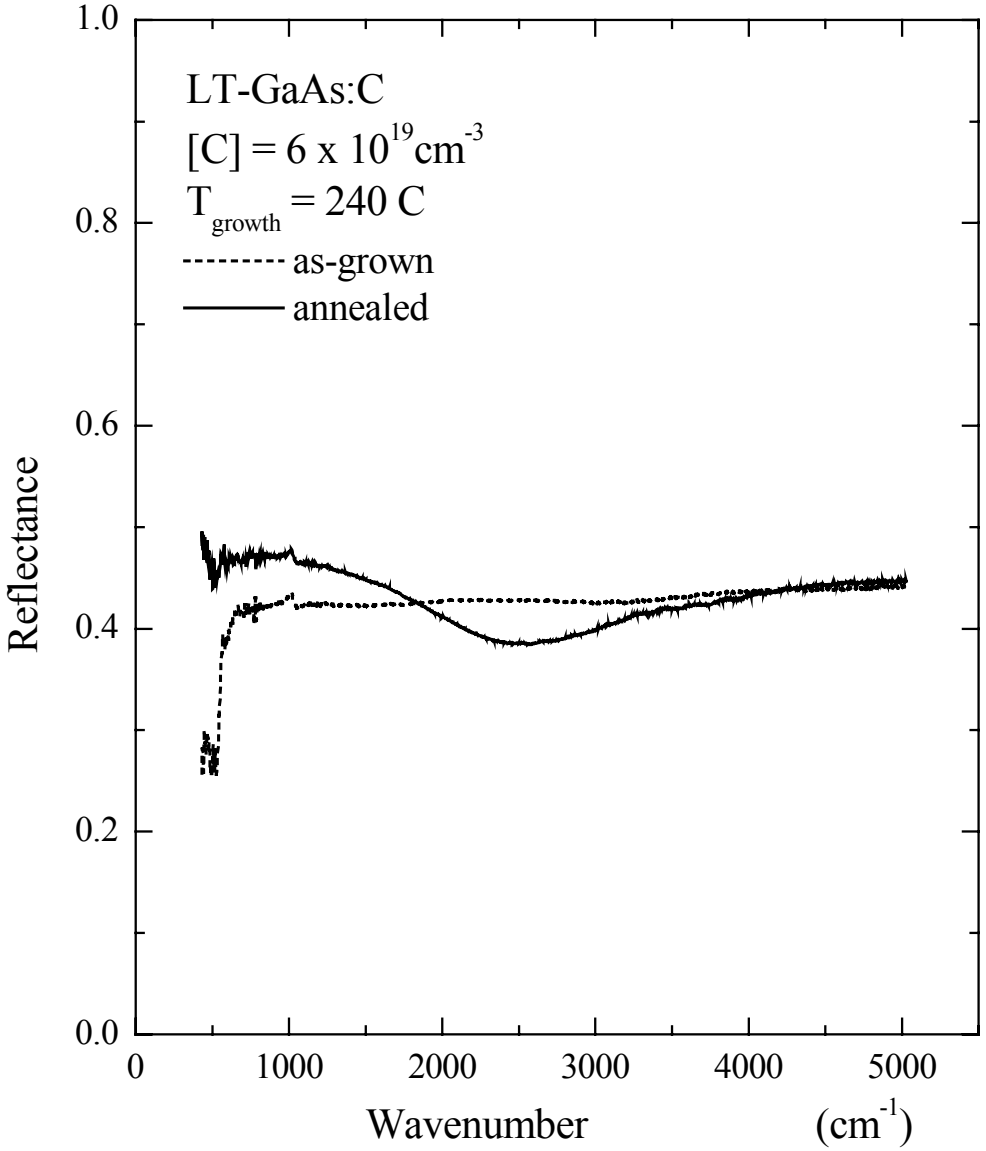

Figure 9-6. Mid-infrared reflectivity of the LT-GaAs:C film before (dashed line) and after (solid line) annealing at 600 C.

Chapter 10. Further studies

As part of the research reported in this dissertation, infrared transmission measurements were used to investigate the localized vibrational mode of carbon atoms occupying arsenic sites in GaAs:C films. The results show that the integrated absorption, the integral of the absorption coefficient over the LVM absorption band, is proportional to the carbon concentration for concentrations up to 5×10^{19} cm^{-3}. At higher carbon concentrations, the integrated absorption saturates and remains constant. This behavior limits the use of infrared transmission as a method for determining carbon concentration in highly doped material. We propose that the formation of C_{As}-Ga-C_{As} carbon clusters causes a reduction in the per-carbon oscillator strength of the LVM mode. However, the actual vibrational modes of this cluster are not understood. Further experimental (including low-temperature) studies, as well as theoretical calculations, are needed to clarify the role of carbon clusters in GaAs:C.

For carbon-doped MBE-grown GaAs deposited at low substrate temperature (LT-GaAs:C), the infrared studies show that the fraction of carbon atoms occupying arsenic sites is significantly smaller than in standardly grown MBE GaAs:C. At a growth temperature of 240 C, we estimate that about 37% of carbon atoms are C_{As} substitutional impurities occupying arsenic sites, the rest being at interstitial sites. The increased disorder in LT-GaAs:C causes the broadening of the LVM spectral line. Also, our Raman-scattering studies show that the longitudinal-optical-phonon Raman line in LT-GaAs:C is shifted to higher frequency, broader and more asymmetric than in GaAs. These effects appear to be correlated with the amount of interstitial carbon, but more

work is needed to determine the mechanisms responsible. These disorder-type effects in LT-GaAs:C are not the same as the finite size effects seen in nanocrystalline GaAs.

Photoluminescence studies of anneal LT-GaAs:C confirm that LT-GaAs:C is stable to high-temperature annealing; it is able to maintain the characteristics of LT-GaAs after 600 C anneal for 20 minutes. However, our annealing study was carried out in air, which results in a layer of crystalline arsenic (and probably also of GaAs:C) on top of the LT-GaAs:C film. To clearly investigate air annealed LT-GaAs:C films with Raman scattering and infrared absorption, the arsenic layer need to be removed. Several acidic etched were tried, but without success. If a successful etching technique was found, it might be possible to use these optical methods to obtain a more detailed picture of the effect of annealing.

In the photoluminescence experiments on our most highly doped p-type GaAs:C films, the above-bandgap emission peak corresponding to the split-off valence band was clearly seen, especially with laser excitation at high photon energy. Further PL experiments on these films (Low temperatures, excitation-energy dependence) might yield new information on the behavior of deep-hole scattering processes in GaAs.

Vita

Sathon Vijarnwannaluk was born on November 9, 1964. He received the degree of B.Sc. (2^{nd} class honors) in Physics in 1986 and the degree of M.Sc (Physics) in 1989 from Chulalongkorn University in Bangkok. In 1995 he received a Royal Thai Scholarship for existing instructors at Chulalongkorn University to continue his studies for the Ph. D. in Physics in the area of semiconductor physics. He arrived at Virginia Tech on June 7, 1995 and began his studies in the Department of Physics. In 1998 he received the Tipsword Graduate Scholarship from the Virginia Tech Department of Physics for excellence in research in experimental condensed-matter physics, and in 2000 he received the Dunn Award from the same department for collegial spirit and enthusiasm for physics. He currently is an instructor at the Physics Department, Faculty of Science, Chulalongkorn University.